The application of remote sensing technology to marine fisheries: an introductory manual

FAO
FISHERIES
TECHNICAL
PAPER

295

FOOD
AND
AGRICULTURE
ORGANIZATION
OF THE
UNITED NATIONS

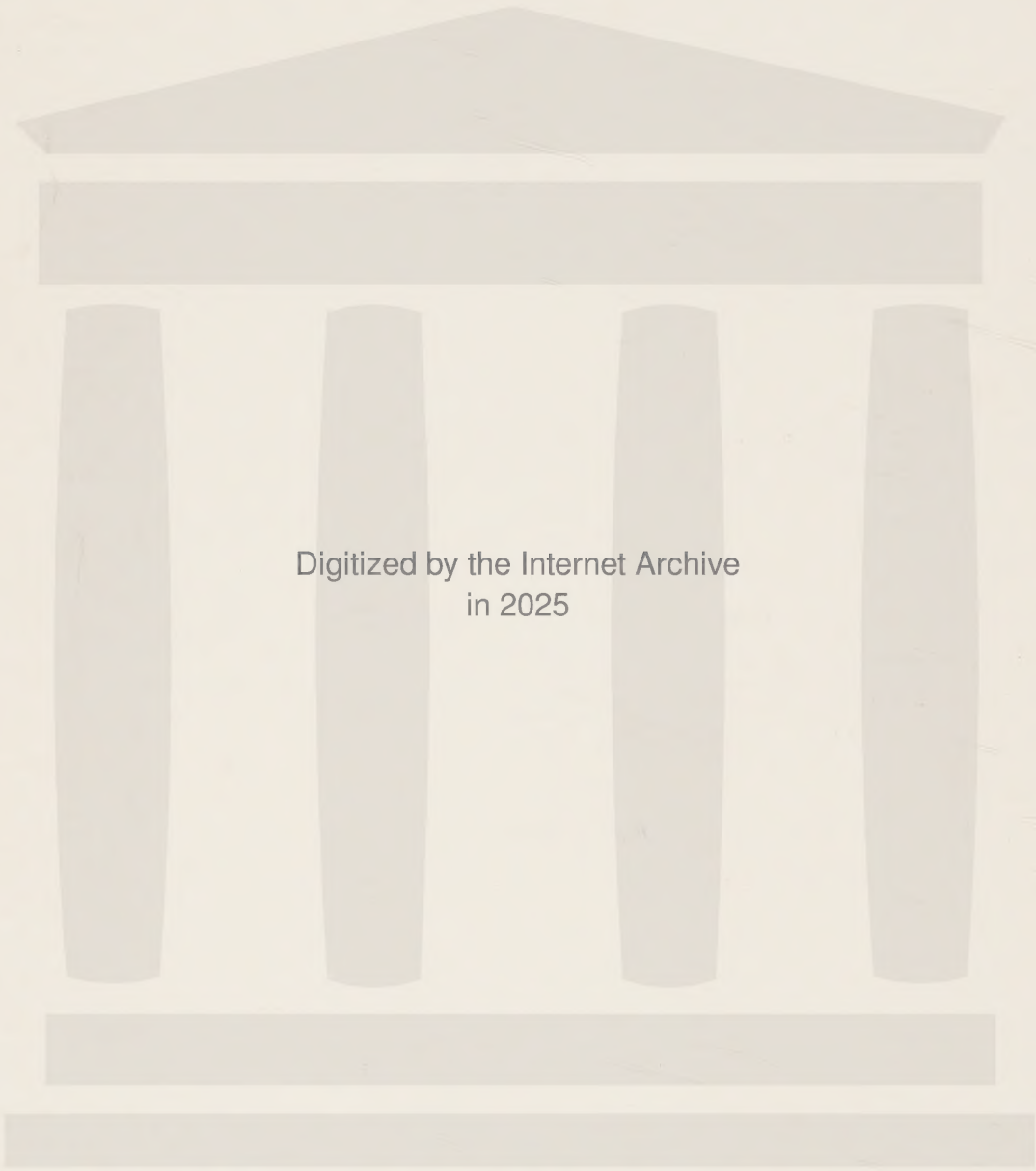

Digitized by the Internet Archive
in 2025

https://archive.org/details/fao-fisheries-and-aquaculture-technical-paper_1988_295

The application of remote sensing technology to marine fisheries: an introductory manual

FAO
FISHERIES
TECHNICAL
PAPER

295

Authors:
M.J.A. Butler
Maritime Resource Management Service (MRMS) Inc.
Amherst, Nova Scotia, Canada
M.-C. Mouchot
Canada Centre for Remote Sensing (CCRS)
Ottawa, Ontario, Canada
V. Barale
TASK Research and Development
Via Verbano 2, 21027 Ispra (VA), Italy
C. LeBlanc
Maritime Resource Management Service (MRMS) Inc.
Amherst, Nova Scotia, Canada

FOOD
AND
AGRICULTURE
ORGANIZATION
OF THE
UNITED NATIONS
Rome, 1988

The designations employed and the presentation of material in this publication do not imply the expression of any opinion whatsoever on the part of the Food and Agriculture Organization of the United Nations concerning the legal status of any country, territory, city or area or of its authorities, or concerning the delimitation of its frontiers or boundaries.

M-40
ISBN 92-5-102694-7

All rights reserved. No part of this publication may be reproduced, stored in a retrieval system, or transmitted in any form or by any means, electronic, mechanical, photocopying or otherwise, without the prior permission of the copyright owner. Applications for such permission, with a statement of the purpose and extent of the reproduction, should be addressed to the Director, Publications Division, Food and Agriculture Organization of the United Nations, Via delle Terme di Caracalla, 00100 Rome, Italy.

© FAO 1988

PREPARATION OF THIS DOCUMENT

The economic welfare of a nation or region is directly dependent on the resources available to it and on the ability of the people to use these resources to their benefit. The declaration of Exclusive Economic Zones (EEZ) by coastal states underlines the economic significance of fisheries resources. At one time the success of a fishing trip was dependent on a fishermen's keen sense of sight, smell and hearing. The modern science of remote sensing has expanded man's perceptions far beyond the limits of those human senses. This manual is intended to be an introduction to the rapidly developing field of remote sensing for persons involved in the study, management or utilization of fisheries resources, particularly in developing countries.

ACKNOWLEDGEMENT

The authors and editors would like to acknowledge the role of Dr. J.F. Caddy (Senior Fishery Resources Officer, Fisheries Department, FAO) and Mr. D. Kalensky, (Senior Officer, Technical Support Group, Remote Sensing Centre, FAO) who initated and supported this project.

T.T. Alföldi of the Canada Centre for Remote Sensing (CCRS) provided professional advice and assistance on the content of the manual. N.M. Butler was responsible for the overall editing, particulary in terms of syntax, comprehension and continuity. We thank them for their efforts.

Dr. D. Jayasinghe and T. Perrott made significant contributions to the initial drafts of this manual. We also wish to acknowledge the assistance provided by G. Landi of FAO and by MRMS employees, namely: C.A. Speight, B.R. Rowley and M.L. McCourt for technical advice; M.E. Campbell for bibliographic research assistance; and M. Jones, M.P. Donovan and M. Stewart for the word processing. Also acknowledged for their constructive comments are the participants of the 12th UN/FAO International Training Course in Co-operation with the Government of Italy: Contribution of Remote Sensing to Marine Fisheries, Rome, Italy, 11-30 May 1987. Dr. R. Sudarshana of the Indian Institute of Remote Sensing provided valuable information concerning India's space programme. The cover of the manual was modified from an original design by K. Coldwell, a former student of cartography at the College of Geographic Sciences, Lawrencetown, Nova Scotia.

The production of this training manual was, in a very real sense, the result of a team effort by the authors, editors, advisors and word processing operators. We would like to recognize their collective endeavours.

Distribution:

FAO Fisheries Department
FAO Regional Fishery Officers
Authors
Marine Sciences (General)

For bibliographic purposes this document should be cited as follows:

Butler, M.J.A. *et al.*, 1988 The application of remote sensing technology to marine fisheries: an introductory manual. FAO Fish. Tech.Pap., (295):165 p.

ABSTRACT

The science and technology of remote sensing is introduced in terms of its history, concepts and language, and its application to the exploitation and management of marine fisheries. The physics of electromagnetic radiation is reviewed with reference to atmospheric and target interactions. The variety of sensor platforms and sensor types are described, the latter in the context of either global or sequential acquisition systems. Environmental satellites, their associated sensors and the techniques of digital image processing also are reviewed. Direct and indirect applications of remote sensing technology to fisheries are described in general, followed by a series of specific case studies. Recommended reference material, a glossary of terms and acronyms, sources of oceanographic satellite data and a selected list of training institutions conclude this manual.

PREFACE

This manual is designed for personnel from departments of fisheries and other agencies who are responsible for the development and management of marine resources. The manual does not presume that the reader has extensive knowledge of either fisheries or the science of remote sensing.

The importance of the fishery sector to the economy of most nations is now widely recognized. Because of the increasing demand for fishery products and the need to exploit marine resources in a cost effective manner, the introduction and application of modern techniques have become important considerations. The rapidly developing science of remote sensing is but one of these technologies. It is not a panacea but, as this manual indicates, it does have considerable potential for assisting fishermen, fishery scientists and managers, air-sea rescue authorities, and many other personnel with responsibilities in this natural resource sector. To date, fisheries applications for remotely sensed information have been the prerogative of the fishing fleets of industrialized nations. This situation will change, however, with the increasing awareness of remote sensing applications, the increasing availability of remotely sensed data, the increasing demand and provision for training, and the belated recognition that one of the first and most widely used remote sensing techniques, that of aerial photography, is readily available to all nations.

The manual is designed to introduce the reader to some of the fundamental concepts of remote sensing and its application to fisheries. In addition it will provide a basic understanding of the language of remote sensing, including the plethora of acronyms.

The introduction, Section 1, provides a historical overview, introduces the reader to basic remote sensing terminology and indicates the types of fisheries-related studies to which remote sensing technology can be applied. Section 2 reviews the properties of electromagnetic radiation and its interaction with the atmosphere and oceans. Sections 3 and 4 consider the variety of sensor platforms and systems, respectively, which have applications to oceanography in general and fisheries in particular. The major environmental satellites and their marine-related sensors are reviewed in terms of their technical specifications in Section 5. The tasks and techniques associated with processing digital images and analyzing remotely acquired data are considered in Section 6. The applications of remote sensing to fisheries are further developed in Section 7 in terms of direct and indirect methods of fish detection and fishery assessment, and of aids to fishing operations. Section 8 considers twenty-two case studies which collectively cover the majority of applications of remote sensing to fisheries from a theoretical and a practical perspective. The Bibliography, Section 9, identifies a selection of topical remote sensing texts and scientific papers which should be used to supplement this manual. The two volume "Manual of Remote Sensing" edited by R.N. Colwell and published by the American Society of Photogrammetry provides a particularly detailed coverage of the subject.

Four appendices comprise, respectively, a Glossary of Terms and Acronyms; Sources of Oceanographic Satellite Data; a Selected List of National and International Institutions which provide training in remote sensing technology and, finally, Conversion Tables for units of measurement commonly used in remote sensing.

In conclusion, the manual is not intended to be all-inclusive. Reference to specialized texts should be made whenever supplementary information is required. With the knowledge gained from reviewing this manual, the reader should feel confident to assess remote sensing applications in relation to the problems of fisheries exploitation and management, and to communicate with remote sensing specialists.

TABLE OF CONTENTS

	Page
1. INTRODUCTION	1
1.1 Historical Overview	1
1.2 Basic Terms and Concepts	3
1.3 Fisheries Applications	5
2. ENERGY SOURCES AND INTERACTIONS	8
2.1 Electromagnetic Radiation and its Properties	8
2.2 Atmospheric Interactions	12
2.3 Target Interactions	13
3. SENSOR PLATFORMS	19
3.1 Boats	19
3.2 Balloons	19
3.3 Aircraft	19
3.4 Satellites	20
3.4.1 Orbital parameters	20
3.4.1.1 Geosynchronous orbit	20
3.4.1.2 Sun-synchronous (Heliosynchronous) orbit	22
4. SENSOR SYSTEMS	23
4.1 Global Acquisition Systems	23
4.1.1 Aerial cameras	23
4.1.1.1 Focal length (f)	23
4.1.1.2 Angle of view (d)	24
4.1.1.3 Scale (s)	24
4.1.1.4 Contrast	25
4.1.1.5 Resolution	25
4.1.1.6 Film speed	25
4.1.2 The Return Beam Vidicon camera	26
4.2 Sequential Acquisition Systems	26
4.2.1 Passive sensors	26
4.2.1.1 Spatial characteristics of passive sensors	27
4.2.1.2 Spectral and radiometric characteristics of passive sensors	31
4.2.2 Active sensors	31
4.2.2.1 Echo-sounders and sonars	31
4.2.2.2 Radars	31
4.2.2.3 Lidars	35

Page

5. ENVIRONMENTAL SATELLITES 38

5.1 The LANDSAT Series 38

5.1.1 The first generation: LANDSAT-1, 2, 3 38

5.1.1.1 MultiSpectral Scanner (MSS) 38

5.1.2 The second generation: LANDSAT-4, 5 41

5.1.2.1 Thematic Mapper (TM) 41

5.2 The NOAA Series 42

5.2.1 The first generation: NOAA-2 to 5 42
5.2.2 The second generation: TIROS-N, NOAA-6 to 9 43

5.2.2.1 Advanced Very High Resolution Radiometer (AVHRR) 43

5.3 Heat Capacity Mapping Mission (HCMM) 44

5.3.1 Heat Capacity Mapping Radiometer (HCMR) 44

5.4 NIMBUS Series 44

5.4.1 Coastal Zone Colour Scanner (CZCS) 45

5.5 SEASAT-A 46

5.5.1 Scanning Multichannel Microwave Radiometer (SMMR) 46
5.5.2 Radar Altimeter (Alt) 47
5.5.3 SEASAT-A Satellite Scatterometer (SASS) 47
5.5.4 Synthetic Aperture Radar (SAR) 48
5.5.5 Visible and Infrared Radiometer (VIRR) 48

5.6 GOES/METEOSAT Series 48
5.7 SPOT 50

5.7.1 Haute Résolution Visible (HVR) radiometer 50

5.8 Space Shuttle and Space Stations 52
5.9 Bhaskara Series 52
5.10 MOS-1 52
5.11 Satellites of the Future 52

5.11.1 IRS-1 52
5.11.2 ERS-1 52
5.11.3 TOPEX 53
5.11.4 NROSS 53
5.11.5 OCI 54
5.11.6 RADARSAT 54
5.11.7 The Sea Wide Field Sensor (Sea WIFS) Program 54
5.11.8 Earth Observing System (EOS) 54

Page

6. DIGITAL IMAGE PROCESSING 55

6.1 Digital Images 55

6.1.1 Image display 57

6.2 Image Processing 58

6.2.1 Radiometric corrections 58
6.2.2 Geometric corrections 59
6.2.3 Image enhancement 59

6.2.3.1 Contrast enhancement 59
6.2.3.2 Edge enhancement 59
6.2.3.3 Colour enhancement 59
6.2.3.4 Multi-image enhancement 60
6.2.3.5 Density slicing 60

6.2.4 Image interpretation 60

6.2.4.1 Image classification 60
6.2.4.2 Pattern recognition 60

7. APPLICATION OF REMOTE SENSING TO FISHERIES 61

7.1 Direct Methods of Fish Detection 61
7.2 Indirect Methods of Fishery Assessment 62

7.2.1 Surface optical properties 62

7.2.1.1 Diffuse attenuation coefficient 62
7.2.1.2 Total suspended matter (seston) 62
7.2.1.3 Yellow substance 62
7.2.1.4 Chlorophyll pigments 63
7.2.1.5 Macrophytes 63

7.2.2 Surface temperature 63
7.2.3 Circulation features 68
7.2.4 Salinity 68
7.2.5 Oil pollution 68
7.2.6 Sea state 68

7.3 General Aids to Fishing Operations 69

8. REMOTE SENSING CASE STUDIES 72

8.1 Case Study No. 1 73

Hara, I., 1985,
Moving direction of Japanese sardine school on the basis of aerial surveys. Bull.Japan.Soc.Sci.Fish., 51(12):1939-45

8.2 Case Study No. 2 77

Bazigos, G.P. et al., 1979,
Aerial frame survey along the southwest coast of India. Rome, FAO, UNDP/FAO Pelagic fishery investigation project on the southwest coast of India. FIRM-IND/75/038:104 p.

Page

8.3 Case Study No. 3 80

Blindheim, J., G.H.P. de Bruin and G. Saetersdal, 1979, A survey of the coastal fish resources of Sri Lanka. Report No. 2, April - June 1979. Reports on surveys with R/V DR. FRIDTJOF NANSEN. Bergen, Institute of Marine Research, 63 p.

8.4 Case Study No. 4 84

Roithmayr, C.M., 1970, Airborne low-light sensor detects luminescing fish schools at night. Commer.Fish.Rev., 32(12):42-51

8.5 Case Study No. 5 86

Cram, D.L., 1979, A role for the NIMBUS-9 coastal zone colour scanner in the management of a pelagic fishery. Fish.Bull./Visserij-Bull., Cape Town, (11):1-9

8.6 Case Study No. 6 88

Caraux, D. and R.W. Austin, 1983, Delineation of seasonal changes of chlorophyll frontal boundaries in Mediterranean coastal waters with NIMBUS-7 coastal zone colour scanner data. Remote Sensing Environ., 13(3):239-49

8.7 Case Study No. 7 90

Kemmerer, A.J., 1980, Environmental preferences and behaviour patterns of Gulf menhaden (Brevoortia patronus) inferred from fishing and remotely sensed data. ICLARM Conf. Proc., (5):345-70

8.8 Case Study No. 8 92

Lasker, R. et al., 1981, The use of satellite infrared imagery for describing ocean processes in relation to spawning of the northern anchovy (Engraulis mordax). Remote Sensing Environ., 11:439-53

8.9 Case Study No. 9 94

Cornillon, P. et al., 1986, Sea surface temperature charts for the southern New England fishing community. Marine Technology Society Journal, 20(2):57-65

8.10 Case Study No. 10 98

Laurs, R.M. et al., 1984, Albacore tuna catch distributions relative to environmental features observed from satellites. Deep-Sea Res., 31(9):1085-99

Page

8.11 Case Study No. 11 102

Montgomery, D.R. et al., 1986,
The applications of satellite-derived ocean color products to commercial fishing operations. Marine Technology Society Journal, 20(2):72-86

8.12 Case Study No. 12 105

Feldman, G.C., 1986,
Variability of the productive habitat in the Eastern Equatorial Pacific. EOS, Transactions, American Geophysical Union, 67(9):106-8

8.13 Case Study No. 13 110

Barale, V. et al., 1986,
Space and time variability of the surface color field in the Northern Adriatic Sea. J.Geophys.Res.,91(C11):12957-74

8.14 Case Study No. 14 114

Pringle, J.D. and R.E. Duggan, 1983,
A remote sensing technique for quantifying lobster fishing effort. Can.Tech.Rep.Fish.Aquat.Sci., 1217:16 p.

8.15 Case Study No. 15 116

Bour, W., L. Loubersac and P. Rual, 1986,
Thematic mapping of reefs by processing of simulated SPOT satellite data: application to the Trochus niloticus biotope on Tetembia Reef (New Caledonia). Mar.Ecol.Prog.Ser., 34:243-9

8.16 Case Study No. 16 120

Jensen, J.R. et al., 1980,
Remote sensing techniques for kelp surveys.
Photogramm.Eng.Remote Sensing, 46(6):743-55.

8.17 Case Study No. 17 123

Belsher, T. and M. Viollier, 1984,
Thematic study of the 1982 SPOT simulation of Roscoff and the west coast of the Contentin peninsula (France). In Proceedings of the Eighteenth International Symposium on remote sensing of environment, Paris, France. Ann Arbor, Environment Research Institute, pp.1161-6

8.18 Case Study No. 18 126

Armstrong, R.A., 1983,
Marine environments of Puerto Rico and the Virgin Islands: automated mapping and inventory using LANDSAT data.
Caribbean Fishery Management Council, 37p.

Page

8.19 Case Study No. 19 129

Middleton, E.M. and J.L. Barker, 1976,
Hydrographic charting from LANDSAT satellite: a comparison with aircraft imagery. In Oceans '76. Second combined conference, Marine Technology Society/Institute of Electrical and Electronics Engineers. New York, IEEE Inc. and Washington, D.C., MTS, (CH 1118-90 EC):6 p.

8.20 Case Study No. 20 131

Roy, S.E., 1978,
Sea surface temperature and related measurements of the South Caribbean Sea, utilizing GOES, NOAA and GOSSTCOMP data for locating structures. In Proceedings of the Seventh annual remote sensing of earth resources conference. Tullahoma, Tennessee, University of Tennessee, Space Institute, pp.261-87.

8.21 Case Study No. 21 133

Mattie, M.G. and D.E. Lichy, 1980,
SEASAT detection of waves, currents and inlet discharge. Int.J.Remote Sensing, 1(4):377-98.

8.22 Case Study No. 22 135

Tanaka, S. et al., 1983,
Accuracy of direct measurement of mean surface water velocity of the Kuroshio using multi-temporal NOAA-6 imageries. In Proceedings of the Seventeenth International Symposium on remote sensing of environment, Ann Arbor, 1983. Ann Arbor, Michigan, Environment Research Institute, pp. 933-44.

9. BIBLIOGRAPHY 137

APPENDIX A GLOSSARY OF TERMS AND ACRONYMS 143

APPENDIX B SOURCES OF OCEANOGRAPHIC SATELLITE DATA 158

APPENDIX C SELECTED LIST OF NATIONAL AND INTERNATIONAL INSTITUTIONS WHICH PROVIDE TRAINING IN REMOTE SENSING TECHNOLOGY 161

APPENDIX D CONVERSION TABLES 165

LIST OF FIGURES

		Page
2.1	An electromagnetic wave and its components	9
2.2	Electromagnetic spectrum showing bands employed in remote sensing	10
2.3	Plot of radiance from a blackbody against wavelength, with temperature as a variable	11
2.4	Transmission of energy through the atmosphere as a function of wavelength	13
2.5	Specular and diffuse radar reflection	14
2.6	Spectral reflectance of ocean water and a thin layer of crude oil	15
2.7	Effect of emissivity differences on radiant temperature	16
2.8a	Light absorption by 10 m of pure water as a function of wavelength	17
2.8b	Variation of light transmission as a function of depth for various sea waters	17
3.1	Orbits of satellites	21
4.1	Principal components of a single-lens frame camera	24
4.2	Components of a passive microwave signal	27
4.3	Thermal IR scanning system	28
4.4	LANDSAT MSS orientation	29
4.5	General characteristics of a push-broom radiometer	30
4.6	The concept of Angular Field of View (AFOV) or scanning angle and Instantaneous Field of View (IFOV)	30
4.7a	Principle of operation of side looking radar	32
4.7b	Propagation of one radar pulse	32
4.7c	Resulting antenna return	32
4.8	A synthetic aperture radar system	34
4.9	Scatterometer output from iceberg as a function of time for different angles of incidence	34
4.10	Principle of operation of airborne lidar bathymetric system	36
4.11	Principle of operation of airborne fluorescence lidar	37

		Page
5.1a	LANDSAT configuration	39
5.1b	Typical daytime LANDSAT orbit paths for a single day	40
5.1c	LANDSAT orbits over the United States on successive days	40
5.2	SEASAT-A configuration	46
5.3	Positions of the five geo-synchronous meteorological satellites that provide global weather watch capabilities	49
5.4	METEOSAT data collecting system	49
5.5	Attributes of the SPOT system	51
5.6	ERS-1 configuration	53
7.1	Suspended sediment concentrations in the Bay of Fundy, Canada, as derived from LANDSAT MSS data	64
7.2	Chlorophyll concentration off the West coast of France, derived from a CZCS image (July 1981)	65
7.3	Colour infrared aerial photograph (1:10,000) of the Chausey Islands, France, taken on April 24, 1982, at low tide	66
7.4	Sea surface temperature image of the Northwest Atlantic Ocean recorded by IR radiometer aboard NOAA-9	67
7.5	SEASAT image of the Strait of Juan de Fuca taken on August 13, 1978, at an altitude of 805 km	70
7.6	Visible band image from GOES West taken at 18:00 on November 15,1984	71
8.1	Flight line for visual observation on September 22, 1984	74
8.2	Flight line for visual observation on September 23, 1984	74
8.3	Changes in oval-shape school sketched from vertical or oblique photography	75
8.4	The changes of the elongate and the intermediate-shape schools expressed in the same manner as Figure 8.3	76
8.5	Pictorial chart of the distribution of the marine fishing boats covered by the AFS in the project area by one degree of latitude	79
8.6	Dimensions of the sound beam from the echo sounder at 20 m echo depth in relation to the distance between trawl doors and wind ends of the trawl net	82

		Page
8.7	Example of "Type A" echo recordings of demersal and semi-demersal fish	82
8.8	Example of "Type B" echo recordings of dispersed pelagic fish	83
8.9	Example of "Type C" echo recordings of schooling small pelagic fish among recordings of dispersed larger pelagic fish (Type B)	83
8.10	A large luminescing school of thread herring, 160 m (500 ft.) in diameter, amplified by airborne low-light sensor	85
8.11	Plankton distribution and observed positions of pilchard shoal (school) groups - cumulative over 10 days	87
8.12	Monitoring of chlorophyll frontal boundaries in the Golfe de Lion throughout 1979	89
8.13	Classification of LANDSAT MSS data from May 20, 1975 into high and low probability menhaden fishing areas for the eastern half of the Mississippi Sound	91
8.14	Distribution of anchovy eggs superimposed on the thermal image of the Southern California Bight	93
8.15	NOAA/NESDIS (National Environmental Satellite Data and Information Service) oceanographic analysis chart for June 18, 1984	95
8.16	Subsection of the NOAA/NESDIS chart shown in Figure 8.15, modified by NMFS (National Marine Fisheries Service)	96
8.17	Enlargement of the region east of Long Island, mailed to fishermen	97
8.18	Satellite data collection and processing network utilized by National Marine Fisheries Service (Southwest Fisheries Centre)	99
8.19	Central California daily albacore catches, 27 September to 2 October, 1981, superimposed on the NOAA-7 AVHRR sea surface temperature, 30 September, 1981, 14:02 PST	100
8.20	Central California daily albacore catches, 27 September to 2 October, 1981, superimposed on the NIMBUS-7 CZCS blue-green colour ratio and phytoplankton pigment concentration, 29 September, 1981, 11:30 PST	101
8.21	Chart forwarded by telecopier to radio facsimile broadcast stations for subsequent transmission to participating fishing vessels	103
8.22	Representative chart generated as part of fisheries demonstration effort	104

		Page
8.23	Map of the eastern equatorial Pacific Ocean, showing the major features of the submarine bathymetry	107
8.24	Cumulative frequency distributions of satellite-derived phytoplankton pigment concentrations (in milligrams per cubic metre) versus the percentage of total cloud-free surface area covered by each concentration range for the eastern equatorial Pacific, as observed by the CZCS	108
8.25	Frequency distributions of satellite-derived phytoplankton pigment concentrations (in milligrams per cubic metre) versus the percentage of total cloud-free surface area covered by each concentration range for the region 0°-10°S, 87°-78°W, as observed by the CZCS	109
8.26	Average conditions of the surface colour field in the Northern Adriatic Sea: 1979 yearly (a) mean and (b) standard deviation of phytoplankton pigment concentration; 1980 yearly (c) mean and (d) standard deviation of phytoplankton pigment concentration	112
8.27	Comparison of monthly averaged Po river outflow (in cubic metres per second) with Po river plume scale and western coastal layer scale (in kilometres) for the period from August 1978 to December 1980	113
8.28	Map of buoy locations - actual fishery	115
8.29	Tetembia reef: general themes	118
8.30	Tetembia reef: hard bottom themes	119
8.31	Example of high altitude CIR photography (original scale 1:125,000) and manually interpreted kelp acreage surveys on four dates	122
8.32	Kelp acreage surveys derived from four dates of LANDSAT image processing	122
8.33	Digital processing of SPOT image	125
8.34	Classified image of St. John, US Virgin Islands	128
8.35	The charted depth contour (5 m) in the study site in comparison with the binary print of the OCS-4 radiance-value distribution pattern for a single grey level in this depth range	130
8.36	SEASAT SAR image	134
8.37	"Sea Mark" chase method for current vector measurement	136

LIST OF TABLES

		Page
1.1	Representative fish types observable from low-level aircraft	6
4.1	Radar wavelengths and frequencies used in remote sensing	33
5.1	LANDSAT-2 MSS characteristics	41
5.2	LANDSAT TM characteristics	42
5.3	NOAA-7 - AVHRR characteristics	43
5.4	HCMM - HCMR characteristics	44
5.5	NIMBUS-7 CZCS characteristics	45
5.6	NIMBUS-7/SEASAT - SMMR characteristics	47
5.7	SEASAT - Radar Altimeter characteristics	47
5.8	SEASAT - Radar Scatterometer characteristics	48
5.9	SEASAT - SAR characteristics	48
5.10	METEOSAT - Scanning Radiometer characteristics	50
5.11	SPOT - HRV characteristics	51

SECTION 1

1. INTRODUCTION

At one time, the success of a fishing trip often depended on a fisherman's keen sense of sight, smell and hearing. To that end the value of a high vantage point, the crow's nest, to scan for fish was appreciated. Modern aircraft and satellites have raised mankind's vantage point to a level undreamed of by earlier generations; at the same time, devices have been developed which have expanded man's perceptions far beyond the limits of the human senses. The combination of these technologies has resulted in the modern science known as remote sensing which may be defined as the acquisition of information about an object or event without being in physical contact. We are just starting to discover some of the ways in which remote sensing can be applied to man's centuries-old quest to harvest food from the sea.

This manual is intended to be an introduction to the field of remote sensing for persons involved in the study, management or utilization of fisheries resources, particularly in developing countries. Although some forms of remote sensing have been in existence for many years and are generally well understood, extraordinary advances have taken place during the past two or three decades, both in the technology and in its application. The sheer volume of literature now available in this field and of technical knowledge needed to understand it makes an introductory manual of this kind essential. It is beyond the scope of this text to attempt a complete or comprehensive description of modern remote sensing or even to document all of the ongoing research programs and their application to the locating and capture of fish. Rather it is intended to provide the reader with a basic understanding of some of the terms, concepts and specific systems used in remote sensing and, through case studies, to illustrate some applications of importance to fisheries personnel.

1.1 Historical Overview

The term "remote sensing" was coined in 1960 by Evelyn Pruitt of the U.S. Office of Naval Research. The history of remote sensing, however, is considerably older. The first aerial photographs were taken from a captive balloon near Paris in 1858. During the next fifty years significant advances were made in camera design and film emulsions. Photographs were taken from such diverse platforms as kites, rockets and even carrier pigeons. The first photograph taken from an airplane was a motion picture shot over Centocelli, Italy, in 1909, in a plane piloted by Wilbur Wright. Most of this early photography provided an oblique rather than a vertical view of the ground. Popular illustrative pictures of a number of large cities and other scenic attractions were also produced using this means. Scientists, however, recognized the potential of aerial photography as a mapping tool and gradually the science of photogrammetry was developed.

It was not until the First World War that aerial photography was acquired and utilized on a large-scale, systematic basis. Cameras were specifically designed for aerial reconnaissance and associated processing facilities were developed to produce thousands of photographs per day. Equally as important as the technological advances was the development of photo interpretation techniques to obtain intelligence information from the images. By observing the deployment of men and material over a period of time, it was possible for strategists to anticipate military manoeuvres. By the end of World War I, there had been substantial improvement in aircraft, cameras and processing equipment and a relatively

large number of people had gained experience in different aspects of airphoto acquisition and utilization.

As improved photogrammetric equipment was introduced in the 1920's and 1930's, vertical aerial photography became the standard information source for the compilation of topographic maps. Aerial photography was used to a limited extent by geologists, foresters and planners in Europe and North America and by cartographers and geographers for small-scale geographic studies in Africa and South America. Colour film was first developed during this period, although it saw little aerial application until the Second World War. Several areas of scientific research were also initiated which would later form the foundation of modern remote sensing techniques.

World War II provided another catalyst for rapid technological development in the field of remote sensing. Once again the acquisition of reconnaissance photography for military intelligence was the primary application. Photo interpretation techniques became highly sophisticated. One aspect of value to later coastal zone studies was the use of aerial photography in planning amphibious assaults. The water penetration capability of aerial film, particularly colour film, made it possible to obtain reliable information on bathymetry and bottom materials when navigational charts were inaccurate or non-existent. The first colour infrared films were also developed during the war for camouflage detection. Large radar networks were erected in the 1940's to provide an early warning system for aircraft detection. Advances in radar technology permitted the development of smaller transmitting and receiving equipment appropriate for airborne use. Included in this class were plan position indicator (PPI) radars which provided an image of the terrain below the aircraft, independent of weather conditions or light availability. The PPI radar, which was used mainly for target detection during nighttime bombing missions or high altitude bombing through cloud cover, also proved useful for coastal navigation.

In the 1950's thermal infrared imaging systems were developed which provided a "heat picture" of objects or terrain. As with radars, thermal infrared systems are not dependent on light availability but, unlike radar, they are unable to "see" through clouds. In the same period, Side Looking Airborne Radar (SLAR) was developed to improve upon the relatively crude imagery produced by PPI radar. Both of these systems were originally designed for military use and did not become available for civilian application for several years.

The launch of SPUTNIK-1 by the U.S.S.R. in 1957 marked the beginning of the "space age". In 1959 the U.S. satellite EXPLORER-6 transmitted the first image of the earth as seen from space. The world's first meteorological satellite, TIROS-1, was launched in 1960; this was the forerunner of the more advanced weather satellites which are in place today. Manned space flights were particularly important in creating an awareness of the potential for resource mapping and monitoring from space. The first pictures of the earth, taken by hand-held cameras in space, provided an amazing amount of detail of land and water features over a large area. Later missions by the U.S.A. and the U.S.S.R. carried more sophisticated camera and scanning equipment, specifically for the acquisition of imagery for resource evaluation.

While the manned missions were successful in demonstrating the value of space imagery, they were generally of short duration and did not provide uniform global coverage. These limitations were largely overcome by the development of earth resource satellites such as the U.S. LANDSAT series. Operating in a lower orbit than the meteorological satellites, LANDSAT, and later similar systems, provided greater spatial detail, although less frequent temporal coverage. Although the sensors were

chosen primarily for land-based applications, they have proved to be useful for several coastal and marine studies.

In addition to the operational satellites now in place, there have been a number of experimental systems launched which have further demonstrated the value of monitoring the marine environment from space. Prominent among these have been the NIMBUS-7 satellite which carried the Coastal Zone Colour Scanner (CZCS) and the short-lived SEASAT satellite which carried a number of specialized marine sensors. In recent years several nations in addition to the U.S.S.R. and the U.S.A. have launched their own remote sensing satellites.

It should be emphasized that aircraft continue to play a major role in remote sensing because of their flexibility in terms of altitude, scheduling and sensor complement. Depending upon the user's information requirements and available resources, aircraft suitable for remote sensing studies can range from single-engine light aircraft to high-altitude, multi-engine jets. Aircraft are often used as platforms to test sensor designs before the sensors are used onboard satellites.

The rapid advances in computer technology have affected all aspects of remote sensing. Of particular interest to users are the digital processing techniques developed for data analysis. Programs are available for geometric correction, image enhancement and quantitative data extraction. The speed of digital computers allows a single operator to perform data analysis for large geographic areas in a relatively short period of time.

While there continue to be advances in data collection and analysis techniques, the major challenge for remote sensing today is to provide usable information in a timely fashion to those who need it. This requires an infrastructure to access and distribute the data and a user community who can apply it to their programs. Meteorological remote sensing is perhaps the only area of application which can truly be considered operational in this sense, at least on a global basis. The Food and Agriculture Organization (FAO) of the United Nations provides a framework for international cooperation in remote sensing and, through its research programs, publications and training courses, is actively encouraging more widespread and effective use of this technology.

1.2 Basic Terms and Concepts

Before we proceed further, some of the terms and concepts which are used throughout this manual will be explained. Although they will be discussed in greater detail in subsequent sections, they are introduced briefly at this point to facilitate an understanding of the text.

Remote sensing may be defined as the acquisition of information about an object or event on the basis of measurements taken at some distance from it. In practice the term is normally used to describe the collection and analysis of data made by instruments carried in or above the earth's atmosphere.

A **sensor** is a device which detects and measures a physical parameter, such as radiation, and converts it into a form which can be stored or transmitted. In other words, it is the device which "sees" the objects or terrain towards which it is pointed. While devices which sense gravity, magnetic fields or sound waves can properly be classified as remote sensors, many authors restrict their use of the term remote sensing to describe measurements of electromagnetic radiation. That convention will be followed in this manual although a brief section is included on underwater acoustic devices such as sonars and echo sounders because of their importance to the fishing industry.

Electromagnetic radiation (EMR) is a type of energy which appears in such forms as X-rays, visible light, microwaves and radio waves. While these forms of EMR may initially seem to be separate phenomena, they are in fact part of a continuous spectrum. This can be understood best by considering how a prism separates white light into different colours; each colour represents a different wavelength of light. Visible light is the only segment of EMR which human vision can detect.

A given sensor can detect EMR only over a limited range of wavelengths: this range is referred to as a **spectral band.** The width of the spectral band, i.e. the extent of the limited range of wavelengths detected, is referred to as **spectral resolution.** Some sensors are comprised of a number of detectors, each of which is sensitive to a different spectral band. These are called **multispectral** or **multiband** sensors. By our looking at the earth in two or more bands simultaneously, it is possible to discriminate a wider range of features. The combination of typical responses coming from a specific target seen by a sensor in various spectral bands is called the **spectral signature** of that target.

Sensors may be classified according to a number of different criteria. For example, there are **imaging** and **non-imaging** sensors. As their name implies, imaging sensors produce a two-dimensional "picture" while non-imaging sensors produce point measurements or profiles. Sensors are also described as being either **active** or **passive.** Active sensors transmit radiation to "illuminate" the surface and to receive and measure the amount of radiation which is reflected back. Passive sensors, in contrast, measure naturally produced radiation which is either reflected solar energy or emitted terrestrial energy.

In order to provide a view of the earth's surface a sensor must be mounted on a **platform** which is simply the device or vehicle from which the sensor operates. Although stationary platforms, either attached or tethered to the ground, are sometimes used for specialized applications, aircraft and satellites are the most commonly used platforms for remote sensing. A general rule is that the higher the altitude of the platform, the larger the area that can be "seen" by the sensor; however, the ability to discriminate small objects will be reduced.

The level of spatial detail which can be observed or recorded by a sensor is referred to as its **spatial resolution.** For a given sensor/platform system, spatial resolution is usually described in terms of the smallest unit area which can be distinguished from its neighbours. In an imaging sensor system, the individual elements which make up the image are called **pixels**, a term derived from "picture elements". The area on the earth's surface represented by a pixel normally corresponds to the spatial resolution of the sensor, i.e. the ground resolution cell size.

Data from sensors may be stored in **analog** or **digital** formats. In an analog system variations in the strength of the original input signal (e.g., the brightness variation in an image) are represented by continuous variations in some other medium such as voltage or film density. A digital representation, in contrast, divides the original signal into discrete ranges, each of which is assigned a numerical value. The range of the original signal as represented by a single numerical value is termed the **radiometric resolution** of the sensor system. Digitally recorded data, unlike analog data, can be processed easily by computers and can be copied repeatedly without negatively affecting the original or copied data. For human interpretation, however, an analog display such as a photograph or television picture is more useful. With appropriate equipment, it is possible to convert data from one format to the other.

A final concept which should be mentioned is the timeliness of remotely sensed information. The term **real time** is used to describe data that is available for display or analysis at the same time and rate at which it is acquired. Most commonly, there is some delay between the time the sensor "observes" the surface and the time the data is available for use. If this delay is short, for example, a few hours, the data is said to be **near real time**. When the data has been collected considerably in advance of being analyzed, it is referred to as **historical** or **archival** data. Timeliness is a particularly important consideration for fisheries applications because of the dynamic nature of marine resources and ocean processes.

1.3 Fisheries Applications

The discussion has focussed thus far on the technology of remote sensing without reference to its application to fisheries management. The sections which immediately follow describe remote sensing principles, systems and analysis techniques in greater detail. Before we proceed with this examination of remote sensing, it is appropriate to outline the types of fisheries-related studies to which remote sensing may be applied. It should be emphasized that a number of the applications described are in the research stage and are not presently operational.

Although direct detection of fish stocks would appear to be the most obvious goal for remote sensing, it is in fact the most difficult to achieve. Visual fish spotting from aircraft is used successfully for locating a number of pelagic species such as anchovy, swordfish, menhaden and tuna. In this case, a trained observer is the "sensor" and direct radio communication is maintained with vessels in the area. If a camera is also carried onboard the aircraft, photographs can be taken for subsequent stock assessment. Different species can be distinguished on the basis of their colour, behaviour and schooling patterns. Table 1.1 lists a number of species which are directly observable from low-level aircraft. Fish spotting is limited by the range of the aircraft and is only feasible when the probability of fish detection is reasonably high and the economic return derived from the catch justifies the expense of aerial surveillance.

A modified type of fish spotting makes use of the phenomenon of **bioluminescence** which is the emission of light by certain types of plankton when they are disturbed by the movement of fish. This phenomenon has been recognized by fishermen for centuries and is regularly used to locate fish when bioluminescent organisms are abundant. Sensitive low-light level television (LLLTV) systems equipped with image intensifier tubes can be used to amplify the relatively small amount of biologically produced light. Information derived from aircraft-mounted LLLTV systems can be used to direct vessels towards schools of fish. Attempts also have been made to image bioluminescence from an orbiting satellite while scanning the night side of the earth.

While the direct detection of fish is not always feasible, their indirect detection may be possible by observation of sea surface phenomena associated with species distribution. This may simply involve mapping the distribution of fishing activities within a given area. Changes in ocean colour from blue to green may also serve as an indicator of increasing plankton abundance. The green colour is associated with the presence of chlorophyll, the light retaining pigment of phytoplankton. While ocean colour has long been used locally by fishermen to locate fish species, aircraft and satellite imagery can record colour variations over a much wider area in a more precise manner. Techniques have been developed to quantify biological productivity on the basis of chlorophyll distribution and abundance.

TABLE 1.1

REPRESENTATIVE FISH TYPES OBSERVABLE FROM LOW-LEVEL AIRCRAFT
(After W.H. Stevenson and E.J. Pastula, 1971)

ATLANTIC OCEAN AND MEDITERRANEAN SEA

Eastern

Fish:
- Spanish sardine (*Sardinella aurita*)
- herring (*Sardinella eba*)
- Spanish mackerel (*Scomberomorus maculatus*)
- yellowfin tuna (*Thunnus albacares*)
- skipjack tuna (*Katsuwonus pelanis*)
- pilchard (*Sardinops trachurus*)

Northern

Fish:
- thread herring (*Opisthonema oglinum*)
- Spanish mackerel (*Scomberomorus maculatus*)
- bluefish (*Pomatomus saltatrix*)
- gulf menhaden (*Brevoortia patronus*)

Northern (Continued)

Fish:
- ladyfish (*Elops saurus*)
- blue runner (*Caranx crysos*)
- tarpon (*Megalops atlantica*)
- herring (*Clupea harengus*)
- Atlantic mackerel (*Scomber scombrus*)
- butterfish (*Poronotus triacanthus*)
- Atlantic menhaden (*Brevoortia tyrannus*)

Mediterranean Sea

Fish:
- Spanish sardine (*Sardinella aurita*)
- Atlantic mackerel (*Scomber scombrus*)

PACIFIC OCEAN AND INDIAN OCEAN

Eastern

Fish:
- basking shark (*Cetorhinus maximus*)
- white shark (*Carcharodon carcharias*)
- northern anchovy (*Engraulis mordax*)
- Pacific sardine (*Sardinops sagax*)
- Pacific bonito (*Sarda chiliensis*)
- jack mackerel (*Trachurus symmetricus*)
- Pacific mackerel (*Scomber japonicus*)
- Pacific barracuda (*Sphyraena argentea*)
- yellowtail (*Seriola dorsalis*)
- white seabass (*Cynoscion nobilis*)
- bluefin tuna (*Thunnus thynnus*)
- albacore tuna (*Thunnus alalunga*)
- yellowfin tuna (*Thunnus albacares*)
- skipjack tuna (*Katsuwonus pelamis*)
- jacksmelt (*Atherinopsis californiensis*)

Eastern (Continued)

Fish:
- ocean sunfish (*Mola mola*)
- striped bass (*Morone saxatilis*)
- Pacific saury (*Cololabis saira*)
- swordfish (*Xiphias gladius*)
- striped marlin (*Tetrapturus audax*)

Mammals:
- gray whale
- pilot whale
- Blackfish (killer whale)
- Porpoise and dolphin
- Seals and sea lions

Invertebrates:
- Squid
- Jellyfish

Western and Indian Oceans

Fish:
- pilchard (*Sardinops pilchardus*)
- sardine (*Sardinella fimbriata*)
- mackerel (*Rastrelliger kanagurta*)

Water temperature is another important factor in determining species distribution and thermal sensors can be used to produce maps of the sea surface temperature (SST). Such mapping can be used to identify cold water upwellings of nutrient-rich water and to locate boundary areas between warm and cold waters where certain species are known to congregate.

In addition to resource detection, remote sensing can be valuable in characterizing the marine and coastal environments. This may involve such activities as updating navigational charts with coastline and bathymetric data; mapping the distribution and types of coastal wetlands; identifying marine plants and sediment types in the intertidal zone and in shallow waters; and monitoring the condition of coral reefs. While the above applications are related to relatively static or slowly changing conditions, remote sensing can also be used to observe more dynamic phenomena on a regular, repetitive basis. Examples in this category include turbidity patterns (due to both organic and inorganic materials), currents, freshwater and saltwater mixing, and wind and wave regions. Long term monitoring of these phenomena can provide a better understanding of the physical environment which supports biological activity and establishes a baseline against which divergent or unusual events can be measured.

Improved weather forecasting, aided in part by remote sensing, can mean greater safety for fishermen at sea. Pollution from coastal or offshore sources which can negatively affect fishing grounds can be monitored by remote sensing. The intensity and type of fishing activity also can be remotely sensed. This information can be used to determine the rate of resource exploitation and to assist in the enforcement of fishing regulations.

The examples cited above illustrate some of the remote sensing applications which may be of interest to fisheries personnel. It must be stressed, however, that remote sensing can seldom be used in isolation; it must be integrated with other sources of information. The sections which follow explain how remotely sensed data is acquired, processed and analyzed and they demonstrate, through a series of case studies, how it is currently being utilized to facilitate fisheries exploitation and management.

SECTION 2

2. ENERGY SOURCES AND INTERACTIONS

To understand how remote sensing operates it is necessary to understand some of the physical principles which make it possible. This requires knowledge of electromagnetic radiation (EMR) and its interactions with various components of the environment. The elements involved in obtaining a remotely sensed signal are: the energy source, the atmosphere, the target and the sensor. This section deals with the first three of these elements. Sensors and the processing and interpretation of the signal will be explored in later sections.

2.1 Electromagnetic Radiation and its Properties

Electromagnetic radiation is a form of energy which can only be observed by its interaction with matter. EMR is made up of both electric and magnetic components and is affected by the electric and magnetic properties of the matter with which it comes in contact. Two hypotheses are generally used to describe the behaviour of EMR: the wave model and the particle model. Both models are valid and both are important for remote sensing; for application specialists, however, the wave model is generally favoured.

Figure 2.1 illustrates a series of electromagnetic waves travelling through space. The electric and magnetic components are in phase and are always perpendicular to each other as well as perpendicular to the direction of travel. For this reason, it is simpler to think of the wave as a single entity without distinguishing between the two components. The orientation of the wave (i.e. the plane along which it travels) is referred to as the polarization. Naturally produced EMR contains waves which are randomly polarized; polarizing filters may be used to select those waves which have a particular orientation. Manmade sources of EMR such as radar systems sometimes produce waves with a single polarization, usually vertical or horizontal with respect to the surface. Certain types of materials can be distinguished by their tendency to "depolarize" these waves.

The physical distance from one wave crest to the next is termed the wavelength and is usually designated by the Greek letter lambda (λ). The number of wavelengths passing a given point in space in a specified period of time is called the frequency and is designated by the letters f or ν . Since each wavelength represents one complete cycle of the wave, frequency is generally expressed as a number of cycles per second or Hertz (Hz). One Hertz equals 1 cycle per second.

Regardless of its wavelength, all EMR travels at the same velocity (c) which in a vacuum is approximately 300 million metres per second. The relationship between velocity, wavelength and frequency is given by:

$$c = \lambda f$$

It is thus possible to determine either the frequency or the wavelength of an electromagnetic wave, providing that the other value is known. The change in velocity of EMR as it passes from one medium to another is defined as refraction. For most purposes, however, the velocity (c) may be regarded as a constant.

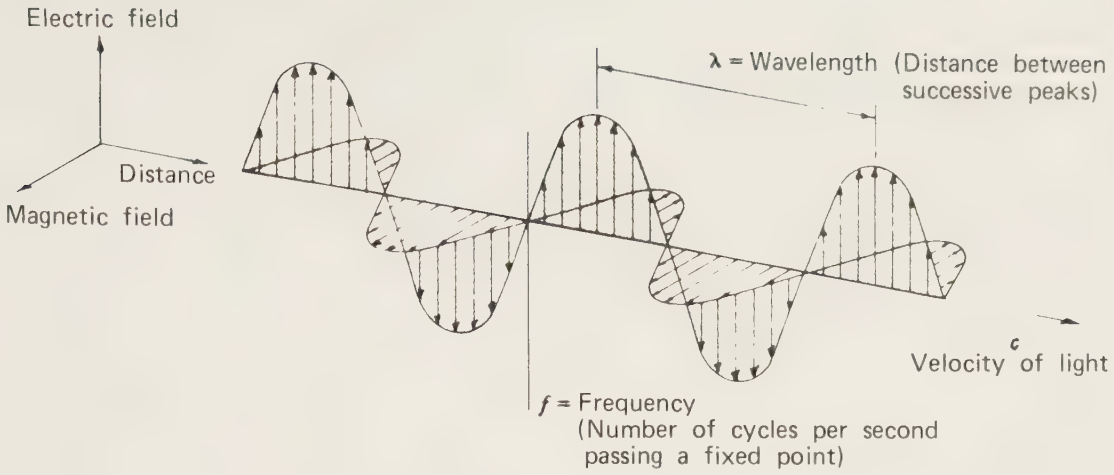

Figure 2.1 An electromagnetic wave and its components.

With the exception of some radar systems, wavelength rather than frequency is more commonly used to describe EMR. Figure 2.2 illustrates how different portions of the electromagnetic spectrum are designated in terms of wavelength bands. The bands of interest to remote sensing are as follows:

i) the photographic ultraviolet, with wavelengths between 0.3 and 0.4 micrometres (μm) (300 - 400 nanometres); shorter wavelength ultraviolet radiation is absorbed by ozone in the upper atmosphere;

ii) the visible, with wavelengths between 0.4 and 0.7 μm; this region contains all the colours of light which can be perceived by the human eye;

iii) the near infrared, with wavelengths between 0.7 and 3 μm; although not visible, this radiation can be detected by films with infrared sensitive emulsions in the range of 0.7 to 1.3 μm;

iv) the middle infrared, with wavelengths between 3 μm and 8 μm; as with the shorter wavelength bands, energy in this region is primarily from reflected solar radiation and does not contain information on the thermal properties of materials;

v) the far (thermal) infrared, with wavelengths from 8 to 1000 μm; this region includes terrestrial radiation related to thermal emission;

vi) the microwave, with wavelengths between 1 millimetre and 100 centimetres; this region can be used to measure terrestrial emission but is also important for active sensors such as radar systems.

It should be understood that these divisions are arbitrary and that the electromagnetic spectrum, by definition, is the continuum of energy ranging from kilometres to nanometres in wavelength. The waves travel at 3×10^8 metres per second and are capable of propagation through a vacuum such as outer space. The broad categories listed above may be further

subdivided. Within the visible band, for example, wavelengths between 0.4 and 0.5 μm correspond approximately to blue light, those between 0.5 and 0.6 μm to green light, and between 0.6 and 0.7 μm to red light. Much finer discrimination is also possible depending upon the spectral resolution of a particular sensor.

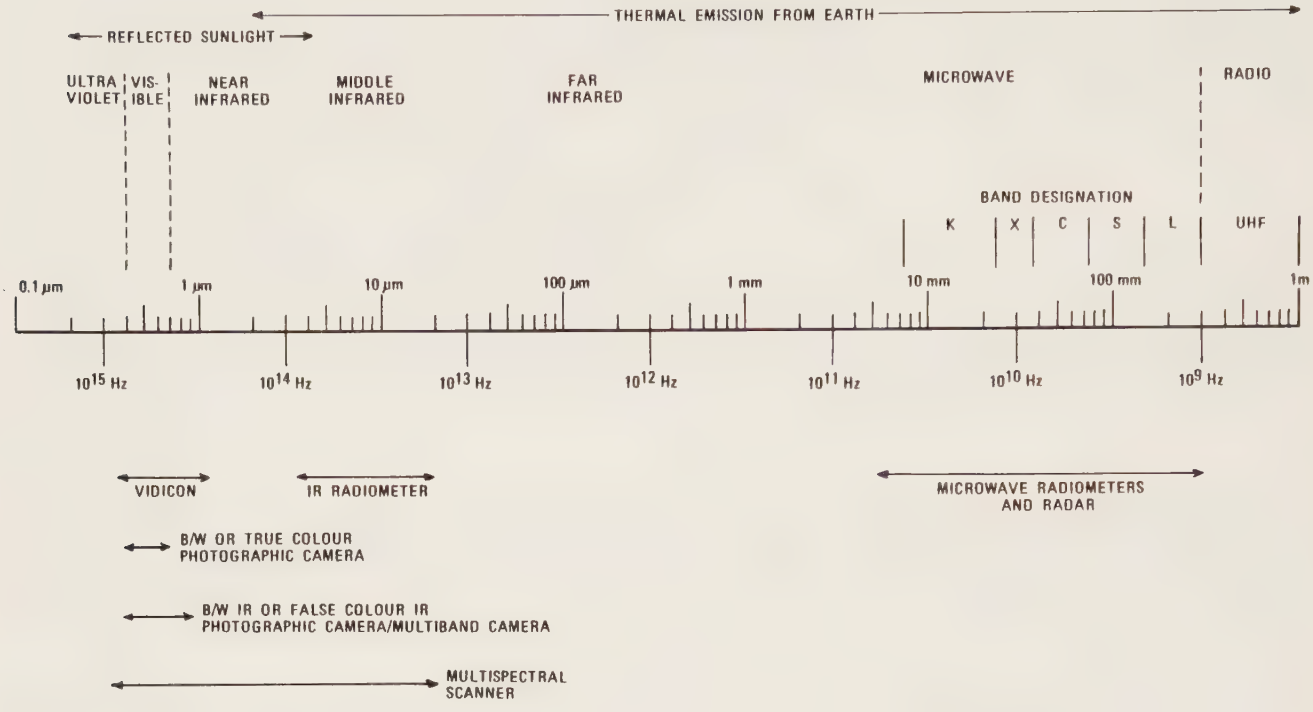

Figure 2.2 Electromagnetic spectrum showing bands employed in remote sensing.

While the wave model is the more appropriate for describing how EMR travels through space, the particle model is better for explaining how it is detected and measured. In accordance with the particle model, EMR is emitted in discrete units called quanta or photons. When a photon emitted from an object reaches a sensor it causes a physical reaction which can be amplified and measured. This may be the exposure of a silver halide grain in a film emulsion or a voltage signal in an electronic system. Planck's quantum theory states that the energy of a photon can be described by:

$$E = hf$$

where E = the amount of energy in Joules,

h = Planck's constant of 6.626×10^{-34} Joules-seconds, and

f = the frequency of the radiation.

Thus it is clear that the higher the frequency of EMR the more energy there is available, which facilitates its detection. In addition, the relationship between velocity, wavelength and frequency ($c = \lambda f$) indicates that the shorter the wavelength, the greater the amount of available energy. Since there is less energy in the longer wavelength bands, sensors operating in these regions generally have a coarser spatial

resolution because they must collect photons from a wider area in order to receive a measurable signal.

With the exception of active sensor systems, which provide their own illumination, remote sensing relies on radiation from natural sources. Whether dealing with reflected solar radiation or with radiation emitted directly from the earth's surface and atmosphere, it is important to understand certain fundamentals. All matter which is at a temperature greater than absolute zero (273°C or 0° Kelvin) constantly emits electromagnetic radiation. The amount of EMR which is emitted by an object and its spectral distribution (i.e. the range of wavelengths) can be graphically described by a spectral emittance curve as shown in Figure 2.3. This curve is for an idealized, hypothetical object called a blackbody which is capable of absorbing and re-emitting all of the energy which it receives, regardless of the wavelength.

There are two relationships which describe the amount and spectral characteristics of EMR emitted by a blackbody as a function of temperature. The Stefan Boltzmann Law states that the radiant emittance increases as the fourth power of the temperature increase, while Wein's Displacement Law states that as the temperature increases the emission reaches a peak at progressively shorter wavelengths. The shift of wavelengths with temperature can be seen when a piece of metal is heated: when cool, it emits no visible light but as it becomes hotter it begins to glow a dark red, then orange, then yellow and finally white at high temperatures.

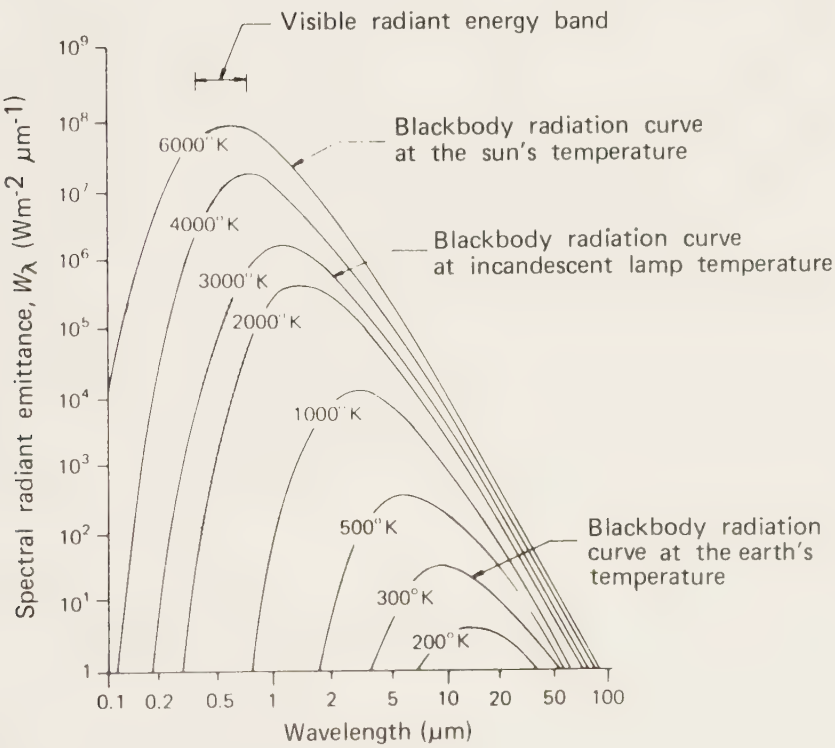

Figure 2.3 Plot of radiance from a blackbody against wavelength, with temperature as a variable. (After T.M. Lillesand and R.W. Kiefer, 1979)

Although blackbodies are hypothetical, actual materials generally exhibit a similar pattern of emission, at least within certain wavelength ranges. These materials, however, emit less EMR than would be emitted by a blackbody at the same temperature. The ratio between the actual and theoretical emission is referred to as the emissivity of the material. Because of differences in emissivity, it is sometimes possible to distinguish between two materials which have the same surface temperature, due to the difference in the amount of radiation which they emit.

Radiation from the sun can be approximated by the spectral emission curve for a blackbody at 6000° Kelvin, while terrestrial radiation (considered as a whole) resembles that of a 300° K blackbody. Solar radiation peaks at around 0.5 micrometres (500 nm) in the visible portion of the spectrum while the earth's energy peak is approximately 9.7 micrometres in the thermal infrared. Thus, if one is interested in studying phenomena which can be observed only at short wavelengths, data collection is generally restricted to daylight hours (the detection of bioluminescence being an exception) or to using an active sensor.

2.2 Atmospheric Interactions

The energy which a sensor receives from a target of interest must pass through the atmosphere. The gaseous components and particulate matter within the atmosphere can affect the intensity and spectral distribution of the energy and may impair or prevent observations of surface features. The magnitude of atmospheric effects depends upon such factors as the path length, the wavelengths being observed and the day-to-day variation in atmospheric conditions. In the case of reflected energy, the atmosphere intervenes between the source of illumination and the target, as well as between the target and the sensor. For emitted wavelengths the situation is simpler since the target is the source of illumination.

The most easily discernible effect of the atmosphere at visible wavelengths is that of scattering. Scattering is simply the reflection of energy by particles in the atmosphere; while the individual particles are small, their net effect can be quite significant if they are present in appreciable quantities. Rayleigh scattering is caused by atmospheric molecules and minute particles which are considerably smaller than the wavelengths of radiation which they affect. This type of scattering primarily occurs in the ultraviolet and blue portions of the spectrum and, in fact, is responsible for the blue appearance of the daytime sky. It is also one of the major causes of haze in imagery. Mie scattering is caused by spherical particles such as dust or water vapour which are approximately the same size as the wavelengths which they affect. Although Mie scattering occurs throughout the photographic spectrum (ultraviolet to near infrared), it tends to affect longer wavelengths than does Rayleigh scattering. When EMR encounters particles which are several times larger than the affected wavelength, nonselective scattering occurs. The term nonselective means that all of the reflected solar wavelengths are affected more or less equally. Water droplets in clouds or fog banks are nonselective scatterers; they appear to be white because all of the visible wavelengths are reflected. Due to their long wavelengths, microwave sensors are not affected by atmospheric scattering and are therefore able to "see" through clouds.

Because of scattering, the energy which is received by the sensor includes reflections from the atmosphere as well as the reflection from the target. The atmospheric reflection component is referred to as the path radiance and complex algorithms are needed to correct this effect. In the case of nonselective scatterers, such as clouds, no radiation from the target reaches the sensor, at least in the visible and infrared bands. In the case of Rayleigh and Mie scatterers, it is possible to measure the influence of path radiance by looking at very dark objects, which reflect

relatively little energy, in several bands acquired at the same time. Visually, the effect of scattering is a more diffuse image with lower overall contrast.

Unlike scattering which redirects EMR and causes a loss of detail, atmospheric absorption actually reduces the amount of energy in certain wavelength bands. Although the atmosphere is essentially transparent in the visible portion of the spectrum, there are several regions in which it is partially or totally opaque. Various component gases in the atmosphere absorb or 'take in' energy at these wavelengths which are called absorption bands. Figure 2.4 illustrates the percentage of EMR which can pass through the atmosphere as a function of wavelength. Sensor systems are only designed to operate in atmospheric windows, nonabsorption regions of the spectrum where transmission is high.

When gas molecules absorb EMR, their energy level is raised; this energy is subsequently re-emitted as heat which is thermal infrared radiation. Atmospheric emissions can degrade the signal which reaches a sensor from a target in much the same way that scattering affects reflected energy. Again, it is possible to correct for this effect by comparing measurements made simultaneously in different bands.

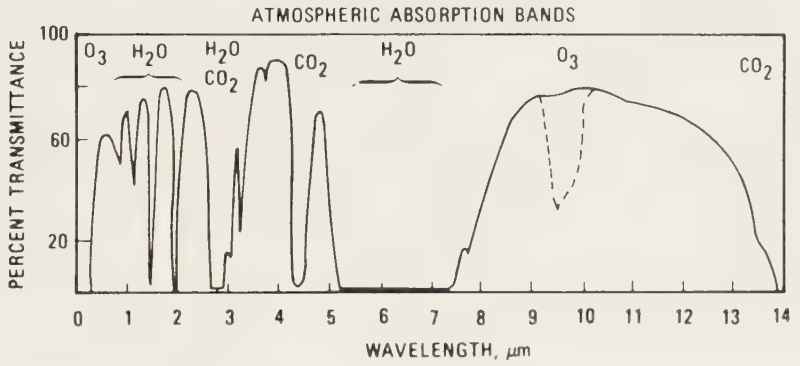

Figure 2.4 Transmission of energy through the atmosphere as a function of wavelength. Wavelength regions of high transmittance are atmospheric windows. Gases responsible for absorption are noted. (After F.F. Sabins, Jr., 1978)

2.3 Target Interactions

When EMR interacts with matter it may be reflected, absorbed or transmitted. In the previous section these interactions were discussed with reference to the atmosphere. Remote sensing, however, is primarily concerned with how EMR is modified by the terrestrial and marine environments. In some respects, terrestrial interactions are easier to describe since, in most cases, these take place at the earth surface where transmission is not a significant factor. In the marine environment, on the other hand, certain wavelengths are transmitted; the energy which reaches the sensor may come from the water surface, from substances in the water column or from bottom materials.

The reflection of energy from a surface is generally described as being specular or diffuse (refer to Figure 2.5). Specular reflection occurs when the energy which is reflected by the surface continues to travel in one direction and the angle of reflection is equal to the angle of incidence. This is the type of reflection which is seen in mirrors or from a smooth sea surface, at visible wavelengths. In diffuse reflection the reflected energy, in contrast, is broken up or scattered in all directions. In reality, most surfaces are neither perfectly specular nor perfectly diffuse reflectors but fall somewhere between these two extremes.

For remote sensing purposes, it is the spectral content of diffuse reflection which generally provides the most information, at least with regards to the composition of surface materials. Specular reflection, however, can be useful in characterizing the surface roughness and geometry of different areas. In fact, it is the characteristic of surface roughness relative to the wavelength of the incident energy which, together with the incidence angle, determines whether a surface is a specular or diffuse reflector. The bright glint of sunlight reflected from calm (i.e. smooth) water is an example of specular reflectance; as the water surface becomes rougher, the reflectance becomes more diffuse unless the sun is low on the horizon. By measuring the relative roughness of the water, it may in turn be possible to infer the wind speed. Moreover, surfaces which are diffuse reflectors at one wavelength may be specular reflectors at a longer wavelength. Simultaneous measurements made at two or more wavelengths can thus be used to differentiate, for example, between sand and gravel beaches or between smooth ice and rough ice.

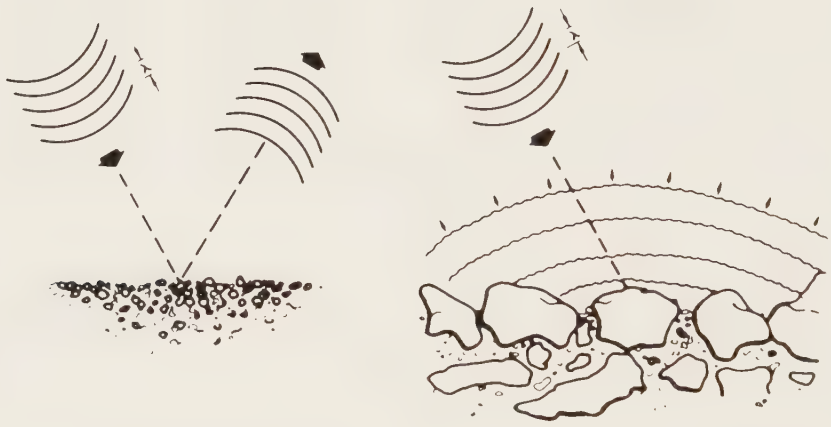

Figure 2.5 Specular and diffuse radar reflection. (After T.E. Avery and G.L. Berlin, 1986)

In most applications, however, specular reflectance is a hindrance rather than an asset. It is the pattern of spectral reflection rather than surface roughness which usually permits a determination of the chemical or biological processes which are active at the surface. When EMR strikes an object, some of the wavelengths are reflected while others are absorbed or transmitted. In the visible spectrum this selective reflectance of certain wavelengths is perceived as colour. The amount of

energy which is reflected by an object in different wavelengths (relative to the energy which it receives) is termed the spectral reflectance and is an intrinsic property of each material. The reflectance characteristics of different materials can be illustrated graphically on a spectral reflectance curve as shown in Figure 2.6. In this figure, typical reflectance values are given for ocean water and crude oil. As can be seen, at certain wavelengths some materials can be readily distinguished while at others they may appear quite similar. Ideally it would be desirable to find a single band which would allow all of the features of interest to be separated. In practice this is not always possible. It is therefore necessary to have simultaneous measurements from several bands. When it is necessary to distinguish two or more features with similar spectral reflectance curves, such as different plant species, it may be possible to acquire data from a very narrow band where the reflectance differences are maximized. Alternatively, it may be possible to use a sensor system which is sensitive to small changes in reflectance values, i.e. has a fine radiometric resolution. These techniques may also be used to detect variations or changes within a given type of material.

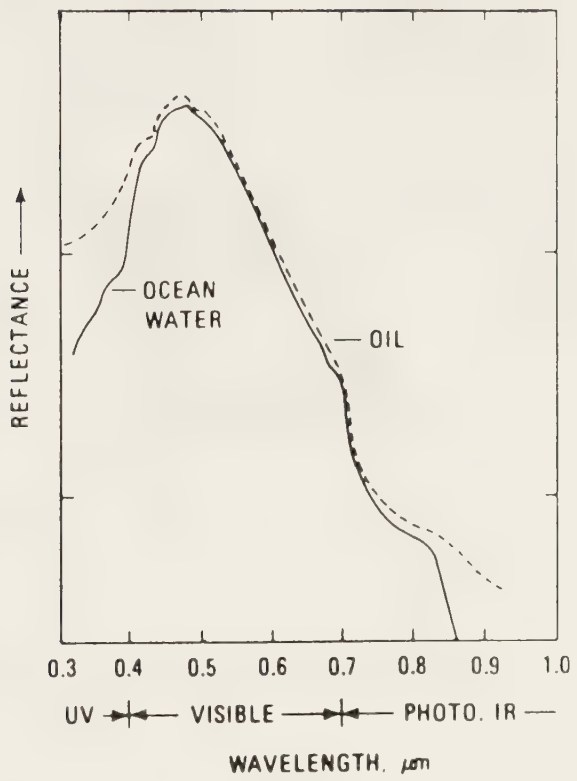

Figure 2.6 Spectral reflectance of ocean water and a thin layer of crude oil. (After F.F. Sabins, Jr., 1978)

For materials which do not transmit EMR the incident energy which is not reflected is absorbed. As with the atmosphere, the absorbed energy is subsequently re-emitted usually as heat. As previously described, the amount of energy which is emitted is a function of the temperature and emissivity of the material (refer to Figure 2.7). Since the earth emits most strongly in the thermal infrared region and because the emissivity of

water is essentially constant within this range, infrared measurements can be used to determine surface water temperatures with a reasonable degree of accuracy, if the measurements are calibrated. While such measurements can also be made for terrestrial materials, the variations in emissivity from one material to another make absolute rather than relative temperature determination much more difficult. It should be noted that energy is only emitted from the surface and that subsurface conditions may be quite different. For example, a film of oil on the surface of water will appear to be cooler than oil-free water at the same temperature since oil has a lower emissivity. This characteristic can be utilized to detect unauthorized discharges or to direct cleanup operations.

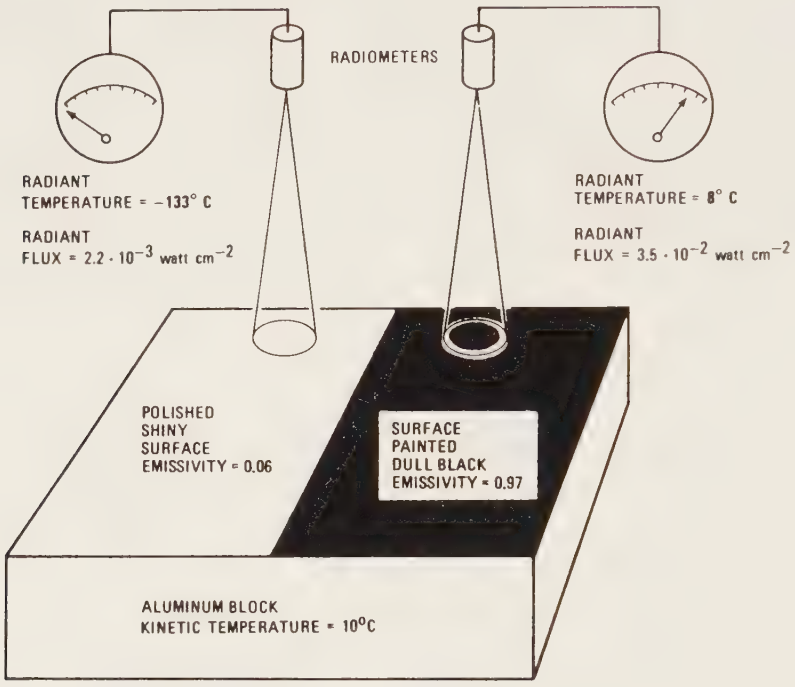

Figure 2.7 Effect of emissivity differences on radiant temperature. (After F.F. Sabins, Jr., 1978)

There is another type of emission, called fluorescence, in which absorbed radiation is re-emitted at a longer wavelength without first being converted into thermal energy. Many minerals fluoresce in the visible spectrum when exposed to ultraviolet radiation. The wavelengths emitted by fluorescent materials are generally in a number of very narrow well-defined bands which are characteristic of specific materials. For marine applications fluorescence may be used to identify chlorophyll, algae and various types of pollutants. Special fluorescent dyes also may be used to trace water masses. Fluorescence occurs naturally due to solar radiation or it can be induced by active sensors equipped with lasers. In order to detect fluorescence, however, it is necessary to have a sensor with sufficiently fine spectral resolution.

The transmission of EMR through water is important when information is needed on conditions or phenomena below the surface. Transmission, however, is essentially limited to the visible spectrum and is greatest at the blue and green wavelengths (refer to Figure 2.8a). As might be expected, there is greater transmittance through clear water than through turbid water (refer to Figure 2.8b). It is perhaps less obvious that the peak transmittance shifts to slightly longer wavelengths as the water becomes more turbid. Transmittance can be altered by certain dissolved organic materials, both natural and man-made.

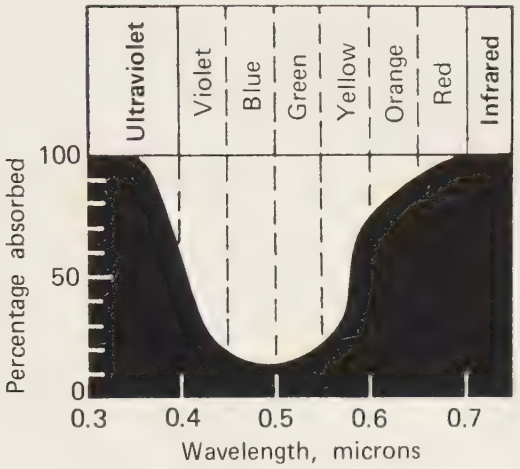

Figure 2.8a Light absorption by 10 m of pure water as a function of wavelength. (After P.K. Weyl, 1970)

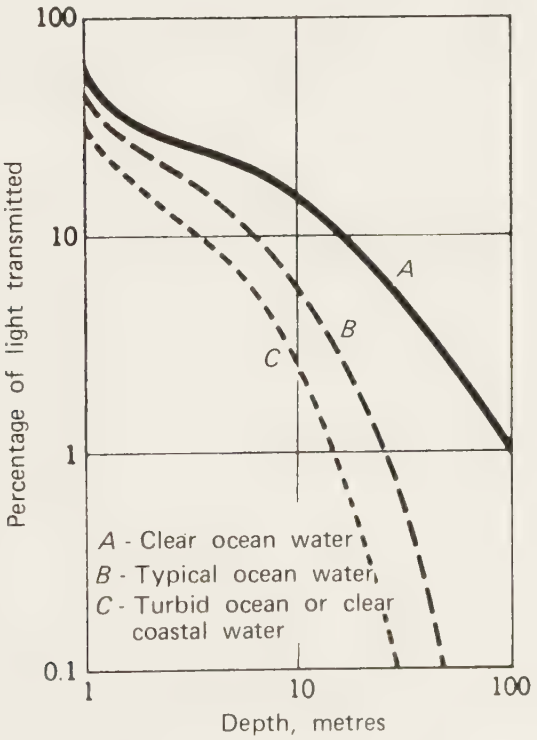

Figure 2.8b Variation of light transmission as a function of depth for various sea waters. (After P.K. Weyl, 1970)

The energy which is detected by a sensor may be reflected by the water surface, by particles suspended in the water column or by bottom materials. As the percentage of light which is transmitted decreases, the ability to "see" into the water is also decreased because the energy is attenuated both approaching and leaving the reflector. Suspended particles produce a volume scattering effect which is analogous to that caused by atmospheric aerosols; if the concentration is relatively low, their reflectance is super-imposed on top of the reflectance from bottom materials. At higher concentrations, suspended particles can effectively block out transmission to and from lower depths. In the absence of bottom reflections, the reflectance from water can be used to measure the concentration of suspended materials. The presence of chlorophyll is of particular interest for fisheries management as it is an index of primary productivity. As the level of chlorophyll increases, there is a decrease in reflectance between 0.4 and 0.5 μm and, at higher concentrations, there is an increased reflectance in the 0.5 to 0.6 μm range. Suspended sediments discharged by rivers are particularly strong reflectors. Mapping these sediment plumes is a means of studying water mixing and circulation patterns. Measurements in the 0.6 and 0.7 μm band show a high degree of correlation with suspended sediment concentrations. Because they reflect so strongly over a wide range of wavelengths, however, high sediment concentrations can interfere with or prevent chlorophyll measurements.

Different investigators have different targets of interest; what may constitute "noise" in one study may be the "signal" in another. The energy which eventually reaches a sensor is reflected or emitted by a variety of environmental components. By knowing the spectral response patterns of these components it is possible to determine the optimum spectral regions for observation. The marine environment presents particular opportunities and challenges because of its spectral characteristics and its dynamic nature. In the next few chapters, we will examine the instrumentation which is available for its study.

SECTION 3

3. SENSOR PLATFORMS

Remote sensing of the aquatic environment can be carried out from a variety of observation platforms. Depending on the distance between the sensor and the target, four categories of platforms can be identified: boats, balloons, aircraft and satellites.

3.1 Boats

Boats, buoys and submarines and other submersibles have been in use as remote sensing platforms for fifty years, primarily in conjunction with echo sounders and sonar. Sonar was developed in 1918 and was first used for fishery applications in the 1930's. Most modern fishing boats are equipped with echo sounders which utilize paper strip charts or cathode ray tubes (CRT) as display units. Now, however, sonar with audio systems is becoming popular as it is a quick and effective method of transmitting information.

The use of buoys and submarines for visual or echo detection of fish has been mainly experimental. Echo sounders or sonar have been installed in submersibles towed at a distance from the mother ship to minimize the noise interference of the ship's engine on the target species. Submersibles such as RUFAS (Remote Underwater Fishery Assessment System), equipped with underwater TV cameras, have been used successfully in assessing scallop resources.

3.2 Balloons

Free floating or anchored balloons have been used to a limited extent for the aerial photography of water bodies such as bays and lakes to trace water circulation, sedimentation, etc.

Balloons are of limited use for the remote sensing of vast ocean surfaces due to their instability and slow speed.

3.3 Aircraft

Aircraft have been used extensively as remote sensing platforms for land and coastal mapping, oceanographic studies and the spotting of fish schools. This is one of the most efficient methods of remote sensing the earth's surface at larger scales. Aircraft have the advantage of optimizing data acquisition by providing operator access to the remote sensing instrumentation and by allowing a wide choice of acquisition parameters. A remote sensing mission can be performed over a particular area at a specified time (weather permitting) and may be repeated under controlled conditions. A suitable altitude can be chosen to optimize resolution and coverage area. Commercially available aircraft can reach an altitude of 15 km. Aircraft can be equipped with black and white, colour or colour infrared (CIR) photographic equipment, multispectral scanners or active sensors such as radar.

The main disadvantages of remote sensing from aircraft are the instability of the platform, the limited geographic coverage (due to the relatively low altitude of the aircraft), the high cost and the dependence on weather conditions. This method, therefore, is used mainly for time-critical missions. When the mission requires repetitive imaging of the same area, the significantly lower access cost of satellite data generally is preferred.

3.4 Satellites

With the use of satellites as remote sensing platforms it has been possible to overcome some of the difficulties encountered in remote sensing with aircraft. Satellites can monitor the entire earth surface on a periodic basis, covering a sizeable section on each revolution. Satellites designed for remote sensing on an operational basis are generally unmanned. Nevertheless, some manned satellites have provided valuable information despite the short duration of their mission, e.g., SKYLAB, SOYUZ and space shuttles.

3.4.1 Orbital parameters

The theoretical orbit of a satellite is an ellipse. In the case of environmental satellites, however, this ellipse is generally considered as a circle having the earth as its centre. The orbits of satellites are described as follows (refer to Figure 3.1):

i) equatorial - having an orbit within the plane of the equator;

ii) polar - having an orbit within the plane of the earth's axis;

iii) near-polar - having an orbit oblique to the axis of the earth.

Most of the communication satellites have equatorial orbits, while the earth observation satellite series such as TIROS, NOAA and NIMBUS have polar or near-polar orbits. The polar orbits are preferred for viewing longitudinal zones in full daylight or during nighttime.

The orbital inclination "i" may be defined as the angle formed by the orbital plane and the equatorial plane (refer to Figure 3.1).

The near-polar orbiting satellites can be of two types:

i) prograde - which move in the same direction as the earth's rotation, i.e. "i" is less than 90^{o};

ii) retrograde - which move in the opposite direction to the earth's rotation, "i" is between 90^{o} and 180^{o}.

The track of the satellite crosses the equator at the nodal points. The ascending node is the nodal point at which the northbound track of the satellite crosses the equatorial plane and the descending node is the nodal point at which the southbound track crosses the equatorial plane. Two particular orbits are described by the near complete earth coverage of environmental satellites: the geosynchronous orbit and the sun-synchronous (heliosynchronous) orbit.

3.4.1.1 Geosynchronous orbit: Geosynchronous orbits have altitudes up to 3600 km. Satellites in these orbits move in the same direction as the rotation of the earth (prograde) and their velocities are adjusted to maintain the satellites position over a designated point on the earth's surface. When a geosynchronous satellite "hovers" in the equatorial plane (i.e. the orbital inclination "i" equals zero), it is called a geostationary satellite, e.g., the GEOS/METEOSAT meteorological satellite series. Geostationary satellites cannot image the earth's surface at latitudes higher than 80^{o}. They are generally able to image and read out their whole viewable area (1/3 of the earth's surface) every 30 minutes. The large viewable area and the repetitiveness of data acquisition have made this type of satellite popular for meteorological and oceanographic studies.

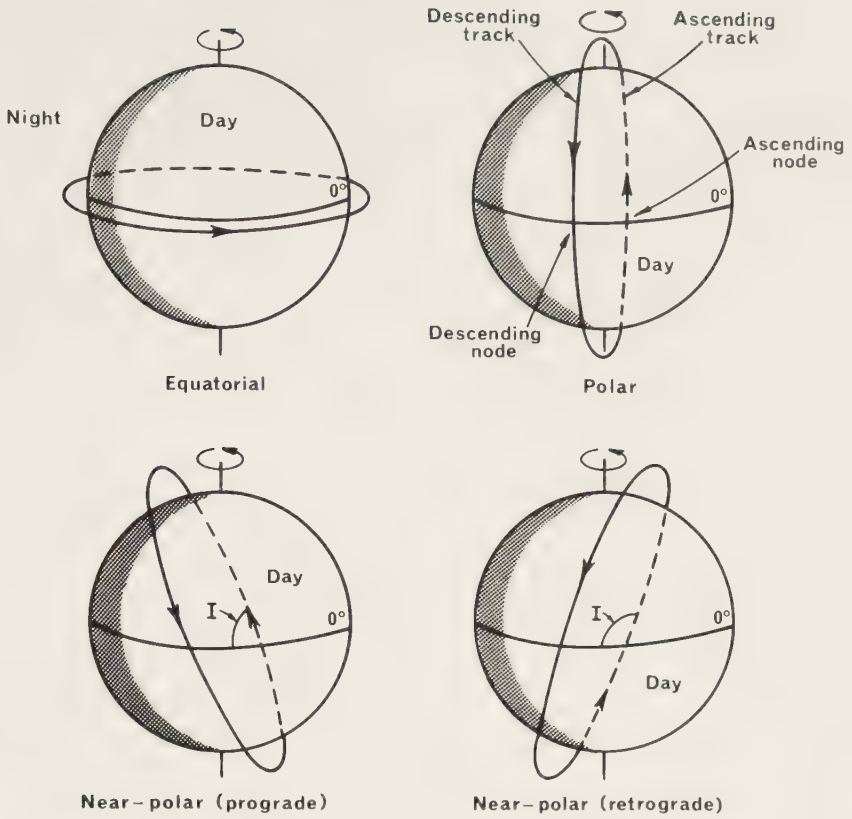

Figure 3.1 Orbits of satellites. (After E.C. Barrett and L.F. Curtis, 1982)

The main advantages of a geosynchronous satellite are:

i) the most frequent observation of the illuminated region of the earth possible from an orbital system;

ii) the possibility of scanning the same point on the earth repetitively, generating a series of spatially coregistered images;

iii) the largest area coverage possible from an orbital system;

iv) the effective use of telecommunications.

The main disadvantages of a geosynchronous satellite are:

i) the economical and technological difficulties of placing the system in such a high orbit and of obtaining an adequate performance from the sensors carried onboard (e.g., an adequate spatial resolution);

ii) the poor polar coverage.

3.4.1.2 Sun-synchronous (Heliosynchronous) orbit: This is a much lower orbit (about 900 km) than the geosynchronous orbit. The inclination of the orbit, relative to the equator, is near to 90° (polar or near-polar) and the satellite (e.g., LANDSAT, NOAA, SPOT, etc.) crosses the equator at the same sun time each day. This means that a particular point on the earth is seen regularly (depending on the period of the satellite) at the same hour, which is useful for comparative analysis of multi-temporal data. By selecting a particular orbit it is possible not only to obtain a repeated coverage of the whole surface of the earth, but also to select the interval between observations at a particular location. This is achieved with low level satellites in a polar or near polar sun-synchronous orbit. For example, LANDSAT-4 has an inclination angle of 98.3° and an altitude of 687 km. It crosses the equator every 98.5 minutes and, during that interval of time, the earth has rotated "s":

$$s = \frac{2\pi R}{T} \times 98.5 = 2752 \text{ km}$$

R = radius of the earth = 6400 km
T = period of the earth = 24 hours = 1440 minutes

The number of rotations per day is given by the ratio:

$$\frac{98.5 \text{ minutes}}{1440 \text{ minutes}}$$; yielding 14 or 15 revolutions per day.

The satellite overflies a given location every 233 revolutions (i.e. 16 days).

The main advantages of a sun-synchronous satellite are:

i) the economical and technological ease of placing the system in a low orbit and of obtaining an adequate performance from the sensors carried onboard (e.g., high spatial resolution in the order of tens of metres);

ii) the possibility of servicing the orbital system with manned space missions.

The main disadvantages of a sun-synchronous satellite are:

i) the low repetitiveness in coverage (e.g., in the order of weeks) this problem, however, can be overcome with the proper combination of orbital parameters and sensor imaging characteristics. The same location can thus be imaged as frequently as every 1 to 3 days, depending on latitude even though corrections are then required to compensate for the variable incidence angle;

ii) the lost imaging opportunities due to cloud cover, small area coverage and low repetitiveness.

SECTION 4

4. SENSOR SYSTEMS

A sensor is a device which detects emitted or reflected electromagnetic radiation and converts it to a physical value that can be recorded and processed. Sensor systems may be divided into two major categories:

i) global acquisition systems, e.g., photographic or T.V. cameras, which record an entire scene instantaneously;

ii) sequential acquisition systems, e.g., radiometers, radars, lidars and sonars, which acquire line-by-line information of the scene. This second category is generally divided into:

   a) passive sensors, which record reflected or emitted EMR from natural sources;

   b) active sensors, which illuminate an object with their own source of radiation and record the "echo".

4.1 Global Acquisition Systems

The global acquisition sensors commonly used for oceanographic studies are aerial, vidicon and underwater cameras. Underwater cameras are not considered in this manual.

4.1.1 Aerial cameras

These are one of the simplest forms of imaging system used in fisheries and ocean studies (refer to Figure 4.1). The detector is a photographic emulsion (film) which is sensitive to the visible or near-infrared parts of the electromagnetic spectrum. Cameras, films and photo interpretation are discussed in more detail in a companion training manual "Marine Resource Mapping: an Introductory Manual" (FAO Technical Paper 274).

Cameras have been in use for a long time and a great deal of knowledge has accumulated regarding techniques of image recording, image interpretation and data extraction. Cameras are less expensive and less cumbersome than other sensors and photographic materials are available world-wide. In addition, photography still produces superior resolution in comparison to electronic sensors.

One of the major disadvantages in the use of aerial cameras is the constraint imposed by adverse weather conditions. Also, photography is only operative within a narrow band of EMR (0.38 to 1.3 micrometres).

The quality of a photograph will depend on several interrelated factors: focal length; angle of view; scale; contrast; resolution; and film speed.

4.1.1.1 Focal length (f): The distance between the centre of the lens and the focus is called the focal length and determines the size of the camera and the scale of the photograph. The focus of a convex lens is the point through which all refracted rays will pass. The image of a distant object is formed at the focus; the film has to be placed at that location, which is referred to as the focal plane.

4.1.1.2 **Angle of view (d):** The angle of view of a lens is the angle between the rays that go to opposite corners of the film. The angle of view is also referred to as view angle, angle of field and covering power. The lens collects the light rays from an angle of view ranging from 45° to 60° (normal range of angle of view) and projects them onto the film within the same angle.

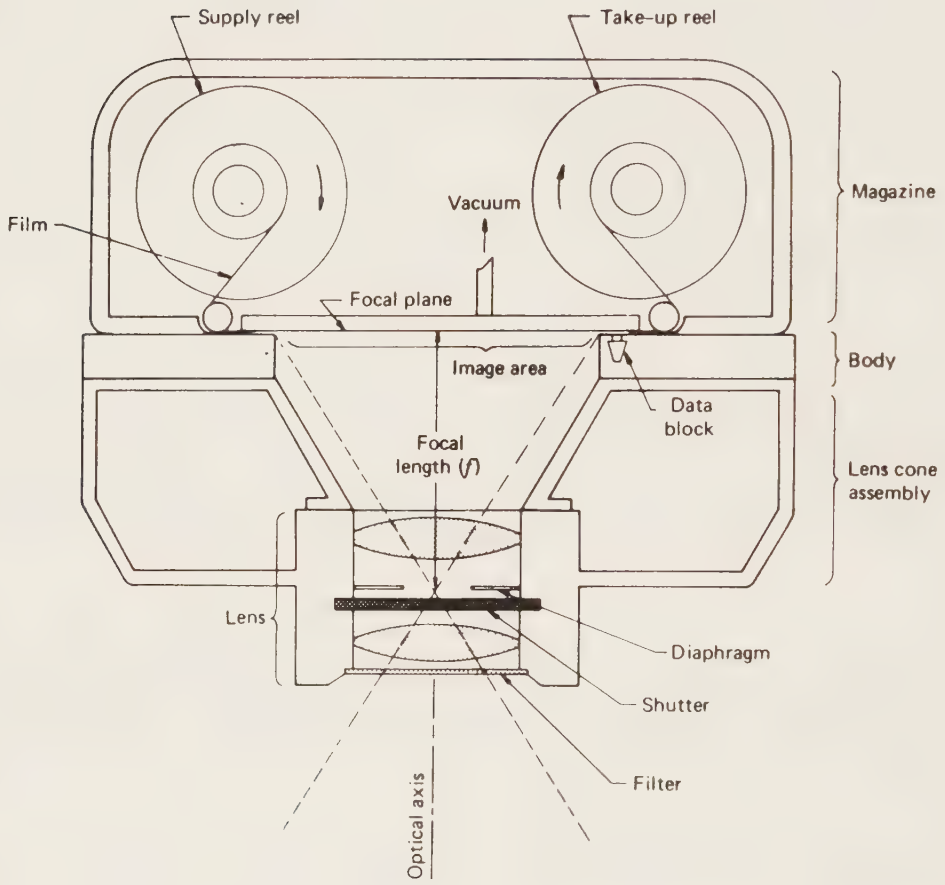

Figure 4.1 Principal components of a single-lens frame camera. (After T.M. Lillesand and R.W. Kiefer, 1979)

4.1.1.3 **Scale (s):** The scale of an aerial photograph, or of a map, can be expressed in terms of the ratio of the distance between two points, as seen in the photograph, to the actual distance between those points on the ground. Due to the difficulties that arise in accurately measuring distances on a photograph, however, the scale of an aerial photograph is

expressed as the ratio of focal length to the altitude at which the photograph was taken. The scale (s) is equal to the focal length (f) divided by the height of the camera above the ground. The latter is determined by subtracting the height of the terrain above sea level (h) from the altitude of the aircraft (camera) above sea level (H). Hence, scale (s) = $\frac{f}{H-h}$

e.g., focal length (f) = 15 cm, altitude (H-h) = 1,500 m;

therefore scale = $\frac{15}{1500 \times 100}$ = 1:10,000

4.1.1.4 **Contrast**: Contrast is a measure of the relationship between the lowest and highest brightness levels (E_{min} and E_{max} respectively) of the photograph. The contrast of a photographic image may be referred to qualitatively as being "high" or "low", or in terms of its contrast ratio (E_{max}/E_{min}). Images with low contrast are often referred to as "washed out" with monotonous, nearly uniform tones of grey. Low contrast may result from the following causes:

i) the object and its background having nearly uniform electromagnetic response;

ii) scattering of EMR by the atmosphere. This effect is more pronounced in the shorter wavelength (violet) portion of visible light;

iii) the camera or film lacking sufficient sensitivity to record the contrast of the scene.

4.1.1.5 **Resolution**: The quality of an aerial photograph is in part described in terms of its resolution or resolving power. This may be defined as the ability of an optical or photographic system to reproduce fine detail, expressed in terms of the greatest number of lines or cycles per mm which can be separated visually in an image or recorded on photographic material. The resolving power or resolution of a photograph is dependent on several factors:

i) lens resolution (optical quality): the ability of the lens to separate visually the greatest number of lines or cycles per mm;

ii) film resolution: the ability of the film to separate visually the greatest number of lines or cycles per mm;

iii) film flatness: the degree of flatness of the film held at the focal plane of the lens;

iv) rotational movement of platform: yaw, pitch and roll of the platform (i.e. the steadier the platform the higher the resolution);

v) optical quality of filters: parallelism of the filter surface, cleanliness of the filter.

The resolving power is usually measured by imaging a standard target pattern and by determining the spatial frequency in lines per unit length at which the image is no longer distinguishable.

4.1.1.6 **Film speed**: Film speed is directly related to the light sensitivity of the film. It may be defined as being inversely proportional to the exposure required to produce some desired response. Speed values can be quoted in terms of photometric or radiometric units.

Some of the standards used in measuring speed values are American Standards Association (ASA); Deutsche Industrie Norm (DIN); British Standards Institute (BSI).

4.1.2 The Return Beam Vidicon camera

As a remote sensor, the vidicon camera stands second best to the aerial camera which serves as the standard against which all global acquisition systems are compared. The Return Beam Vidicon (RBV) camera is able to produce synoptic images (i.e. all parts of the scanned area are seen by the detector at the same time) as does an aerial camera. The basic operating principle of a vidicon camera is similar to that of a television camera. A distant object is focused by a converging lens onto a photoconductive target. The image produced at the photo conductive target is held electrically until an electron beam scans the "frozen" image to read off the elements line by line. Having scanned the image the target is cleared to receive a new image.

This type of sensor was present on the earlier LANDSAT satellites. It recorded an image of 185 km square every 25 seconds using three cameras on LANDSAT-1 and 2 and an image of 90 km square using two cameras on LANDSAT-3.

The RBV camera produces images with a very high spatial resolution compared to those of other electronic sensors and the image data can be transmitted to earth via radio signals.

4.2 Sequential Acquisition Systems

4.2.1 Passive sensors

The sensors in this category are called radiometers. They receive and record, line-by-line, the EMR reflected or emitted by the earth and the atmosphere (refer to Figure 4.2). Depending on the type of detector used, passive sensors can record different parts of the EMR within the ultraviolet to microwave wavelengths.

The following radiometers are commonly used in fisheries and ocean studies. They are described in Section 5.

Sensor		Platform
MSS	MultiSpectral Scanner	LANDSAT
TM	Thematic Mapper	LANDSAT
AVHRR	Advanced Very High Resolution Radiometer	NOAA
HCMR	Heat Capacity Mapping Radiometer	HCMM
CZCS	Coastal Zone Colour Scanner	NIMBUS-7
HRV	Haute Résolution Visible	SPOT

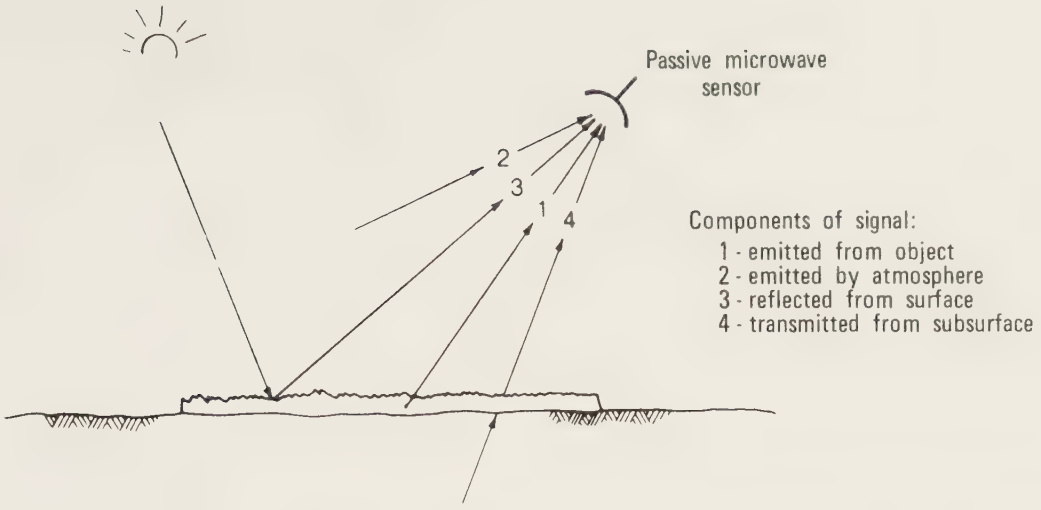

Figure 4.2 Components of a passive microwave signal. (After T.M. Lillesand and R.W. Kiefer, 1979)

Some categories of passive sensors include:

i) Scanning radiometers: These sensors collect a single line of data by using a rotating mirror to "scan" the view perpendicular to the line of flight, e.g., a thermal IR sensor and the MultiSpectral Scanner (MSS) of LANDSAT (refer to Figure 4.3 and 4.4 respectively). The forward movement of the satellite or aircraft produces subsequent lines of data.

ii) Push-broom radiometers: This type of sensor, e.g., the HRV of SPOT, has one or several arrays of detectors. A line of acquisition is seen instantaneously without any mechanical motion which is a significant improvement on scanning radiometers (refer to Figure 4.5).

4.2.1.1 Spatial characteristics of passive sensors: Passive sensors have two major spatial characteristics:

i) Instantaneous Field of View (IFOV) (refer to Figure 4.6): This is defined as the angle (radians or degrees) over which the detector is sensitive to radiation. The MSS of LANDSAT-2 has an IFOV of 0.086 milliradians. By knowing the altitude of the satellite to be 920 km, it can be calculated that the picture element (pixel) represents an area on the earth surface which has dimensions of 80 m by 80 m (ground resolution cell) at the nadir point.

ii) Swath width (refer to Figure 4.6): This is defined as the linear ground distance covered in the across-track direction. For a scanning radiometer this depends on the angular field of view (AFOV) or scanning angle; for example, the scanning angle of the LANDSAT-2 MSS is equal to 11.52° and, at an altitude of 920 km, results in a swath width of 185 km. For the push-broom radiometer, the field of observation is related to the size of the array; for example, the 6000 detectors of SPOT's HRV cover an angle of 4.13° and, at an altitude of 832 km, result in a swath width of 60 km.

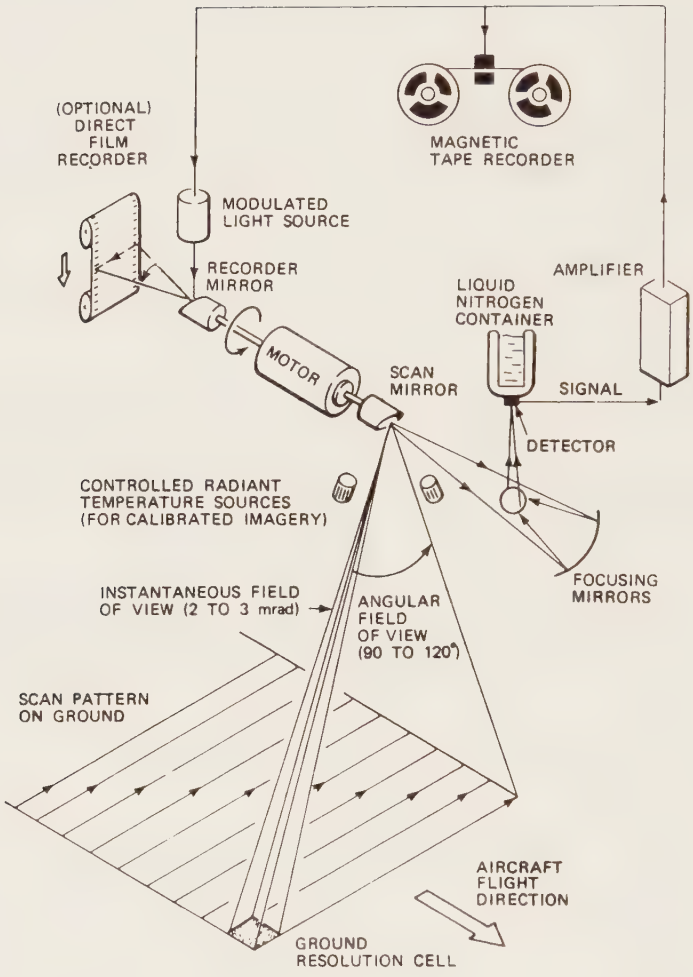

Figure 4.3 Thermal IR scanning system. (After F.F. Sabins, Jr., 1979)

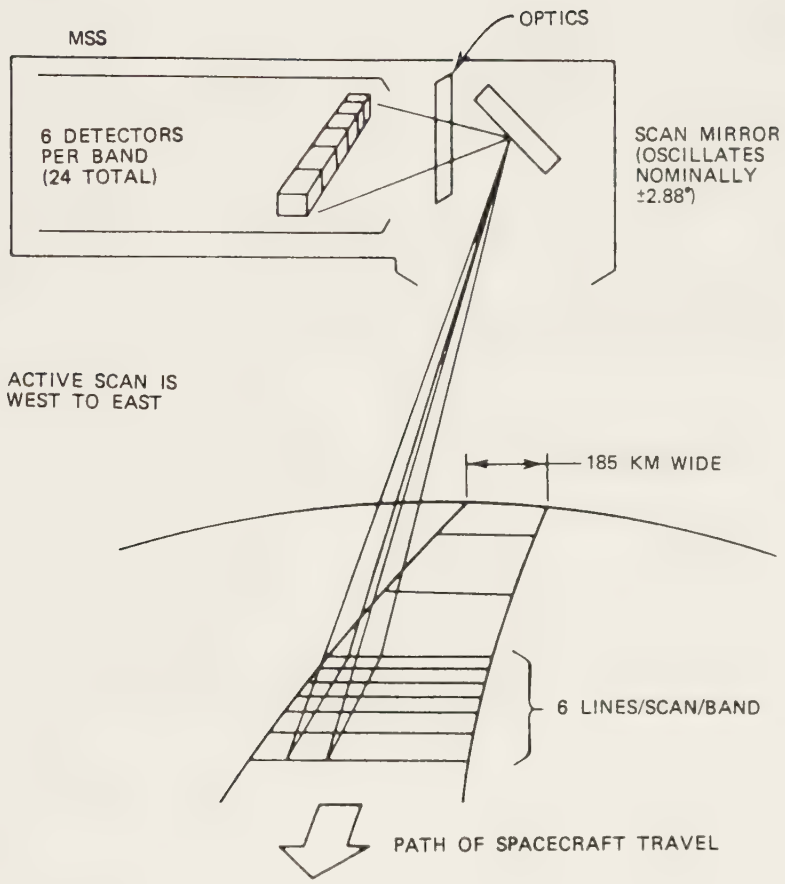

Figure 4.4 LANDSAT MSS orientation.

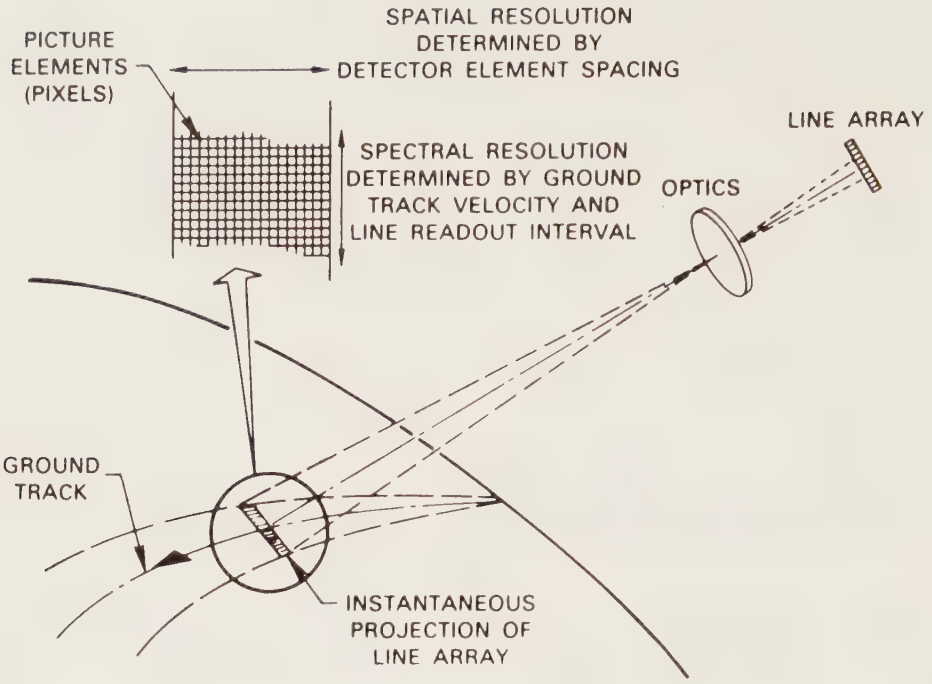
PICTURE ELEMENTS (PIXELS)
SPATIAL RESOLUTION DETERMINED BY DETECTOR ELEMENT SPACING
LINE ARRAY
SPECTRAL RESOLUTION DETERMINED BY GROUND TRACK VELOCITY AND LINE READOUT INTERVAL
OPTICS
GROUND TRACK
INSTANTANEOUS PROJECTION OF LINE ARRAY

Figure 4.5 General characteristics of a push-broom radiometer. (After T.E. Avery and G.L. Berlin, 1985)

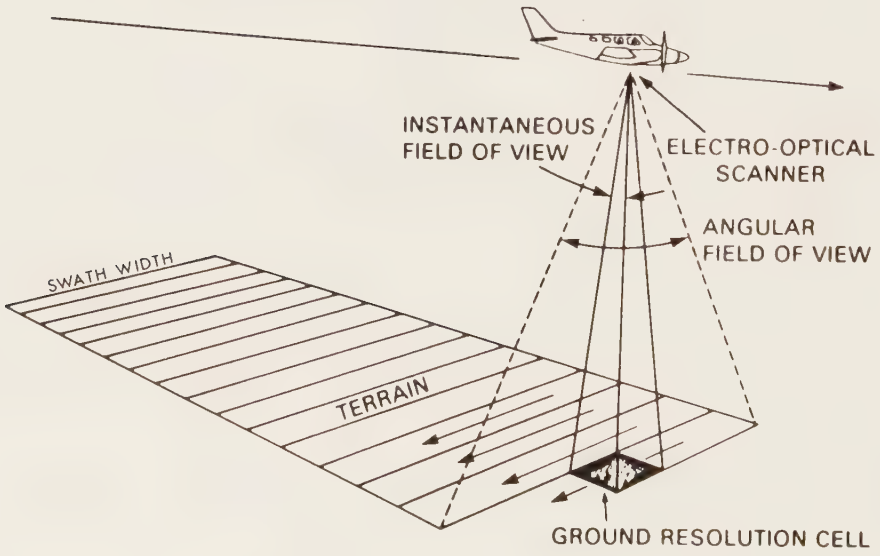

Figure 4.6 The concept of Angular Field of View (AFOV) or scanning angle and Instantaneous Field of View (IFOV). (After T.E. Avery and G.L. Berlin, 1985)

4.2.1.2 Spectral and radiometric characteristics of passive sensors: The spectral resolution of a sensor is its ability to differentiate the wavelengths of the electromagnetic spectrum. The radiometric resolution is its ability to distinguish different levels of intensity of EMR in a given spectral band.

4.2.2 Active sensors

Active sensors (e.g., radar, sonar) are able to illuminate an object with their own source of radiation. The illumination will either induce an object to emit radiation (fluorescence) or cause it to reflect the sensor-produced radiation. Active sensors often are used when natural radiation in a particular band of the spectrum is not sufficient to adequately illuminate the target, i.e. the natural radiation is below the signal-to-noise threshold.

4.2.2.1 **Echo-sounders and sonars**: Echo-sounders and sonars (Sound Navigation and Ranging) are based on the principle of directing acoustic waves at a target and receiving the reflected echo. The echo sounder transmits a fixed, vertical beam of sound whereas the sonar beam can be orientated. The main components of an echo-sounder and a sonar are: transmitter, transducer, receiver and display unit.

The function of the transmitter is to produce energy in the form of pulses of electrical oscillations. In the transducer, this electrical energy is converted to sound energy in the water and, conversely, the sound waves of the returning echoes are converted back to electrical energy. The receiver amplifies the weak electrical oscillations produced in the transducer by the echo so that they can be recorded on paper, displayed on a CRT (Cathode Ray Tube) or broadcast as an audible signal.

4.2.2.2 **Radars**: A radar is an active microwave sensor which uses radio waves to detect the presence of objects and to determine their range (position). This process entails transmitting short bursts or pulses of microwave energy in the direction of interest and recording the strength and origin of "echoes" or "reflections" received from objects within the system's field of view. The resolving power of the radar (its ability to differentiate between targets) is determined by the wavelength transmitted by the radar. Active microwave sensing is done in several wave bands which are designated by letters of the alphabet as indicated in Table 4.1. The transparency of the atmosphere to the microwaves or hyper-frequencies (refer to Section 2) allows a radar to acquire data regardless of the weather conditions. Microwaves penetrate clouds and are not scattered by haze or rain.

Radars can be either imaging or non-imaging:

i) imaging radars: Imaging radars display the radar backscatter characteristics of the earth's surface in the form of a strip map or a picture of a selected area. An example of an imaging radar includes the Side Looking Airborne Radar (SLAR) which is carried on aircraft. This sensor scans an area not directly below the aircraft but at an angle to the vertical, hence the term "Side Looking" (refer to Figure 4.7a, b and c).

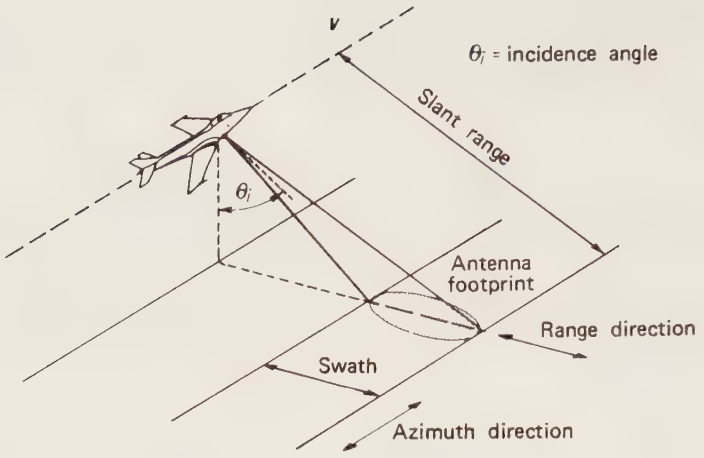

Figure 4.7a Principle of operation of side looking radar. (After J.A. Richards, 1986)

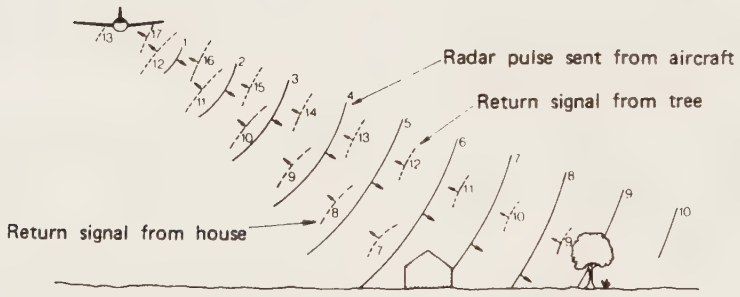

Figure 4.7b Propagation of one radar pulse (indicating the wavefront location at time intervals 1-17). (After T.M. Lillesand and R.W. Kiefer, 1979)

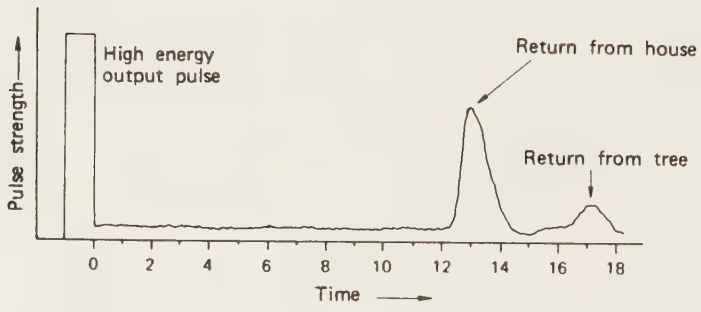

Figure 4.7c Resulting antenna return. (After T.M. Lillesand and R.W. Kiefer, 1979)

TABLE 4.1

RADAR WAVELENGTHS AND FREQUENCIES USED IN REMOTE SENSING
(After F.F. Sabins, Jr., 1978)

Band Designation	λ Wavelength cm	ν Frequency (megahertz) (10^6 cycle sec^{-1})
Ka (0.86 cm*)	0.8 to 1.1	40,000 to 26,500
K	1.1 to 1.7	26,500 to 18,000
Ku	1.7 to 2.4	18,000 to 12,500
X (3 and 3.2 cm*)	2.4 to 3.8	12,500 to 8,000
C	3.8 to 7.5	8,000 to 4,000
S	7.5 to 15.0	4,000 to 2,000
L (25 cm*)	15.0 to 30.0	2,000 to 1,000
P	30.0 to 100.0	1,000 to 300

* Indicates wavelengths commonly used in imaging radars.

To achieve a useful spatial resolution in an image of the ground from the altitude of a satellite would require an antenna with a length of several kilometres. Synthetic Aperture Radar (SAR) was developed to overcome this problem. SAR takes successive signals transmitted and received by a small real antenna and uses them to reconstruct (synthesize) the signal which would have been received had the antenna been several kilometres in length (refer to Figure 4.8). In addition, the reconstruction of the image of a moving object from SAR data involves the consideration of the Doppler effect (refer to Glossary of Terms).

Finer details of a target (i.e. greater resolution) can be seen in an image produced with microwaves of shorter wavelengths. For example, sea surface which appears smooth with L-band may not be smooth when sensed with X-band. In common with other EMR, microwaves are polarized into vertical and horizontal components.

At present, imaging radars have few applications in oceanographic studies, although intensive research has been carried out to measure wave length and direction.

ii) non-imaging radars: Unlike imaging radars, the non-imaging radars record a specific physical parameter. Examples of non-imaging radars include the radar scatterometer and the radar altimeter. A radar scatterometer measures the roughness of the sea surface, icebergs, etc., in a broad swath on either side of the spacecraft (refer to Figure 4.9). Measurements yield the amplitude of short surface waves that are approximately in equilibrium with the local wind and from which the surface wind velocity can be estimated. The radar altimeter uses a pencil-beam microwave that measures the vertical distance between the spacecraft and the earth. Measurements yield the topography and roughness of the sea surface from which the ocean grid, surface current and average wave height can be estimated.

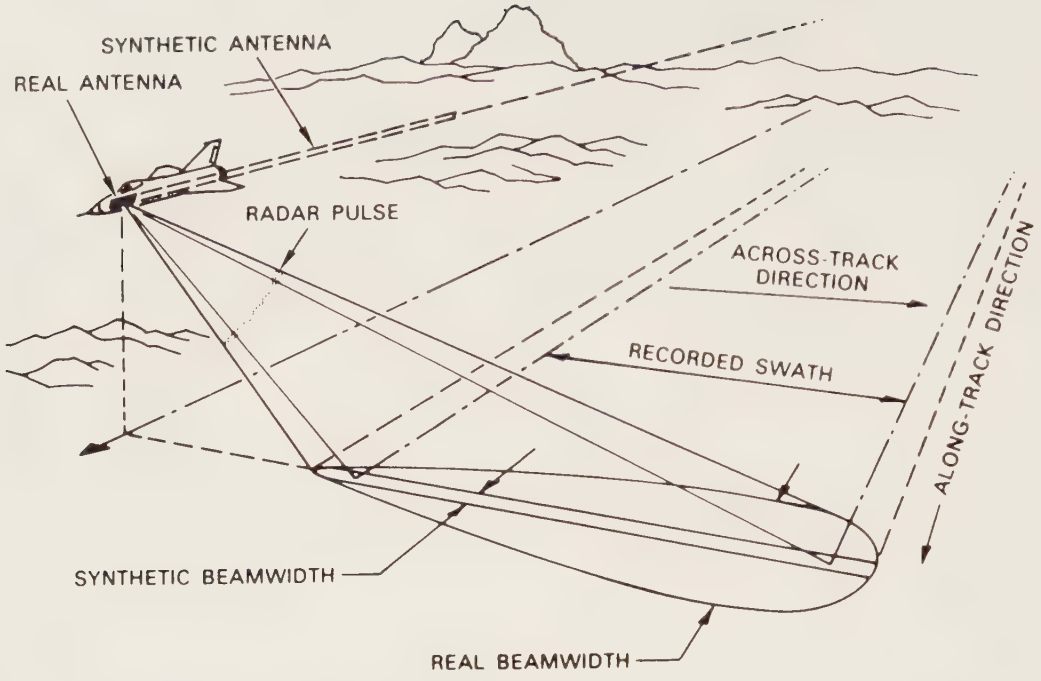

Figure 4.8 A synthetic aperture radar system. (After T.E. Avery and G.L. Berlin, 1985)

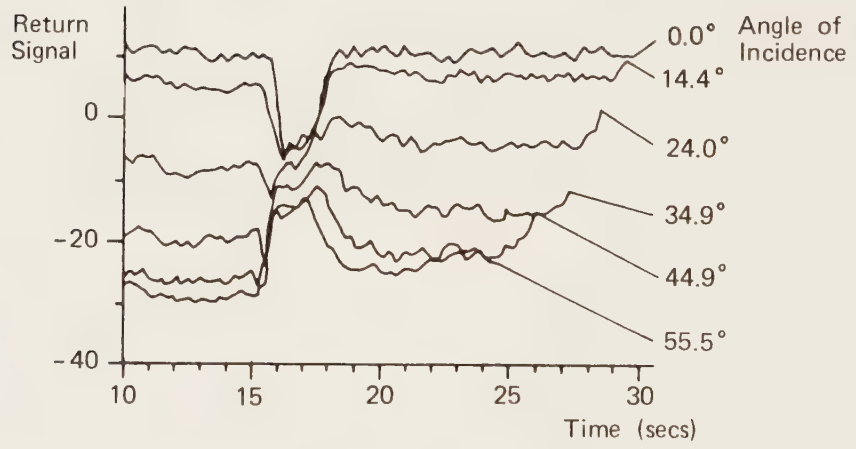

Figure 4.9 Scatterometer output from iceberg as a function of time for different angles of incidence. (After D. Harper, 1983)

4.2.2.3 Lidars (Laser-radars): A lidar is an active sensor emitting and receiving light in the visible and near-infrared wavelengths. Laser (acronym for Light amplification by stimulated emission of radiation) is a device for producing light by emission of energy stored in a molecular or atomic system, when stimulated by an input signal. Lidar uses laser to generate short, high power light pulses. As the pulse passes through the atmosphere, back-scattered light is detected by an optical system and is electronically analyzed to provide a measurement of intensity of light back-scattered by target constituents as a function of the distance from the sensor.

Due to physical limitations it is impossible, to date, to include such sensors in a satellite payload. They are therefore limited to airborne missions. Two kinds of lidars have interesting applications in oceanographic studies: the bathymetric lidar and the fluorescence lidar:

i) bathymetric lidar: This lidar, which is used for bathymetric studies, generates a blue-green signal and a near-infrared signal simultaneously. The near-infrared signal does not penetrate the water and is directly reflected by the sea surface and recorded by the sensor. The blue-green signal, in contrast, penetrates the water, is reflected by the bottom and reaches the sensor at a later time. The difference in time is a direct function of the water depth (refer to Figure 4.10).

ii) fluorescence lidar: This lidar records the emitted fluorescent light induced by the interaction of the lidar transmitted blue-green light with the target. The fluorescence of the target is often unique and therefore provides a means of recognition. This instrument has been used to identify and quantify chlorophyll in water and also to identify and measure the thickness of marine oil slicks (refer to Figure 4.11).

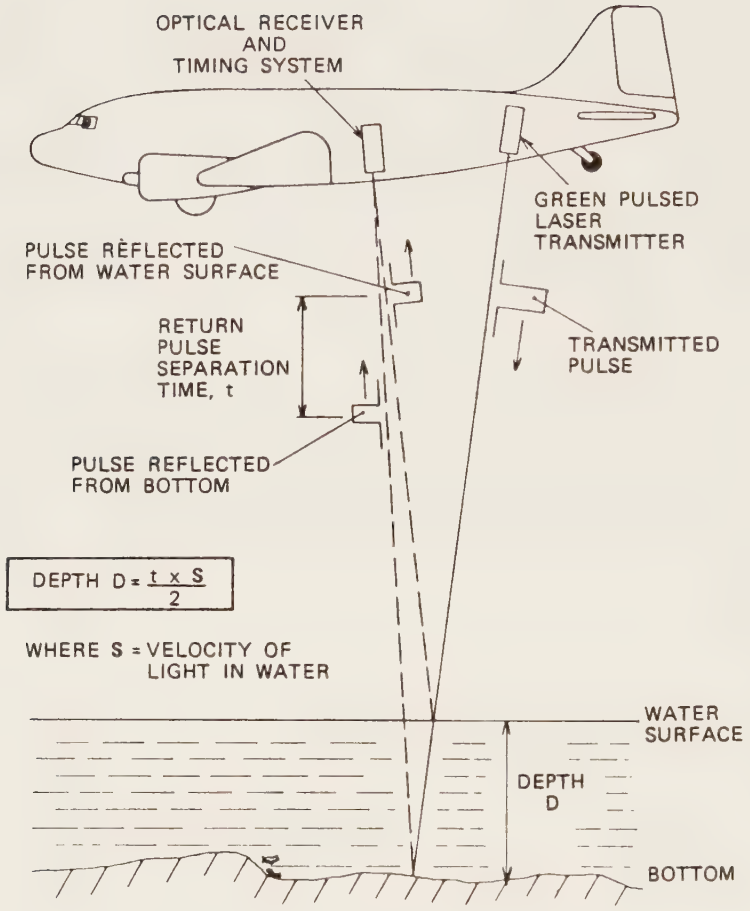

Figure 4.10 Principle of operation of airborne lidar bathymetric system. (After D. Harper, 1983)

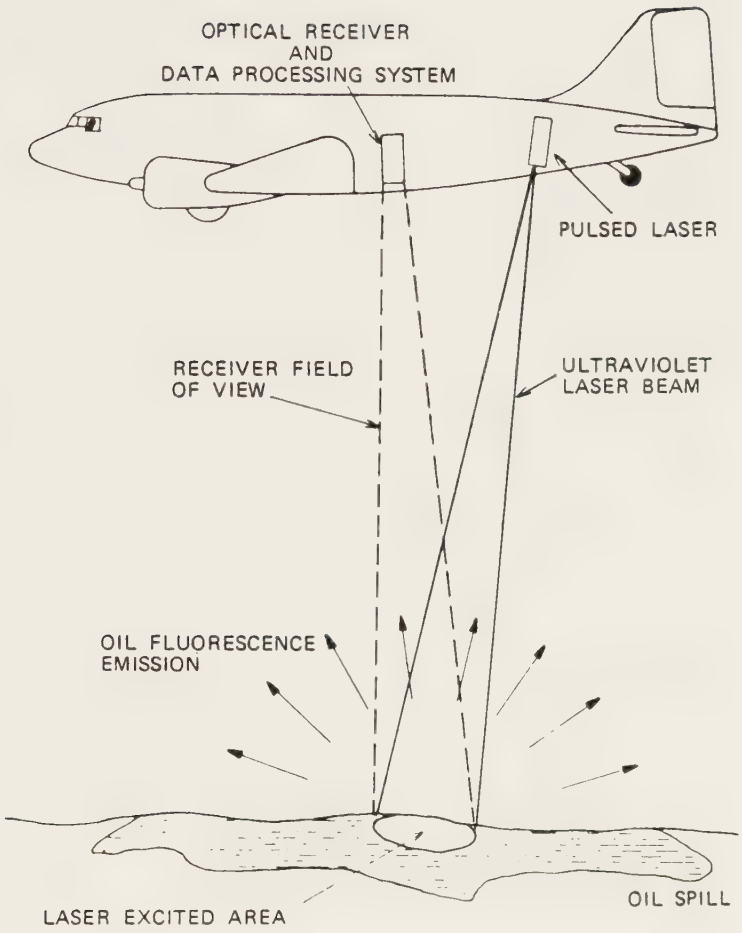

Figure 4.11 Principle of operation of airborne fluorescence lidar. (After D. Harper, 1983)

SECTION 5

5. ENVIRONMENTAL SATELLITES

This section describes the environmental satellites currently aloft, their sensors and their potential use for oceanographic studies. The sensors for some of these satellites are actually out of commission or, in the case of the manned satellites, uninhabitated. Nevertheless, due to the potential interest in the data they have acquired during their activity period, they are included in this section.

The major environmental satellites aloft today are:

1. LANDSAT series - U.S.A.
2. TIROS series - U.S.A.
3. NOAA series - U.S.A.
4. HEAT CAPACITY MAPPING MISSION (HCMM) - U.S.A.
5. NIMBUS series - U.S.A.
6. SEASAT-A - U.S.A. (now defunct)
7. GOES/METEOSAT - U.S.A./E.S.A.
8. SPOT - FRANCE
9. BHASKARA series - INDIA
10. MOS-1 - JAPAN

Environmental remote sensing programs scheduled or proposed include:

1. IRS-1 - INDIA
2. ERS-1 - E.S.A.
3. TOPEX - U.S.A.
4. NROSS - U.S.A.
5. OCI - U.S.A.
6. RADARSAT - CANADA
7. Sea-WIFS - U.S.A.
8. EOS - U.S.A.

5.1 The LANDSAT Series

The LANDSAT series of satellites was formerly known as the Earth Resources Technology Satellites (ERTS). The name LANDSAT is a misnomer since the LANDSAT satellites have significant applicability to ocean and coastal studies. This series can be divided into two generations:

5.1.1 The first generation: LANDSAT-1, 2, 3

LANDSAT-1, 2 and 3 were launched respectively in 1972, 1975 and 1978. LANDSAT-1 was decommissioned in 1978 after a sensor malfunction and LANDSAT-2 and 3 were decommissioned in 1983. These satellites have basically the same orbital parameters and carry the same sensors. Both spacecraft are in near-polar (inclination angle of about 99°) sun-synchronous orbits with a period of 103 minutes. The satellites make 14 revolutions per day with inter-track distances of 2875 km. Each satellite provides coverage of most of the earth every 18 days, i.e. overlays the same track every 18 days (refer to Figure 5.1a, b and c).

LANDSAT-2 and 3 carry two types of imaging sensors:

i) the MultiSpectral Scanner (MSS);
ii) the Return Beam Vidicon (RBV) camera.

The RBV has been used rarely for environmental studies. It is described briefly in Section 4.1.2.

5.1.1.1 MultiSpectral Scanner (MSS): The MSS is an airborne or spaceborne line scanning device which produces a specific number of synchronous images each at a different wave band. The individual scene of

an MSS image covers approximately 185 X 185 km and overlaps its neighbour by about 10% along the spacecraft ground track. At the ground station the images are usually converted from electronic signals to black and white image positives on 7 mm film by an electron beam recorder. The original images have a scale of approximately 1:3,369,000.

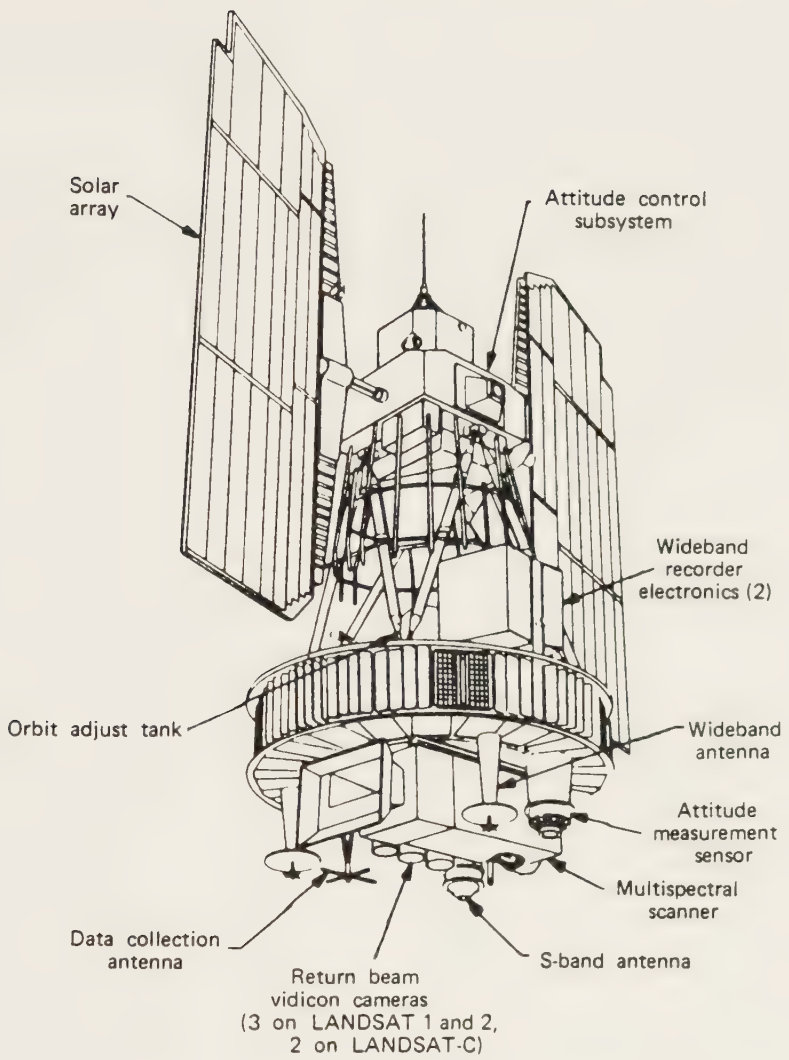

Figure 5.1a LANDSAT configuration.

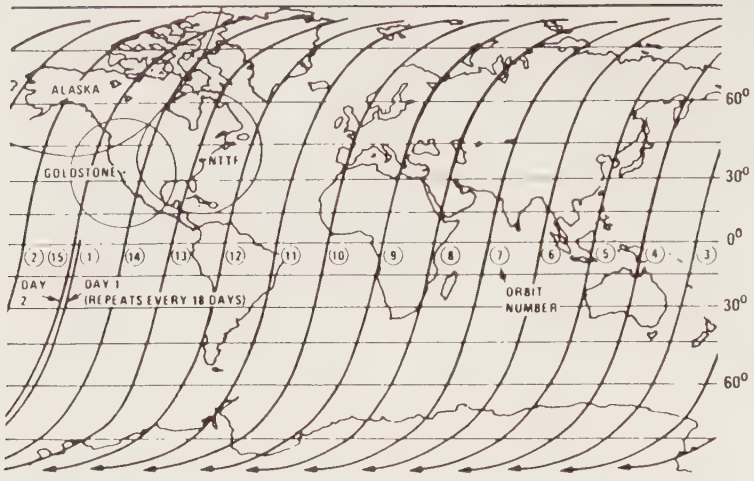

Figure 5.1b Typical daytime LANDSAT orbit paths for a single day. Each day the paths shift westward 160 km at the equator so that every 18 days the paths are repeated. Images are acquired between 9:30 and 10:00 a.m. local sun time, except at high latitudes. Note location and ranges of receiving stations in the United States.

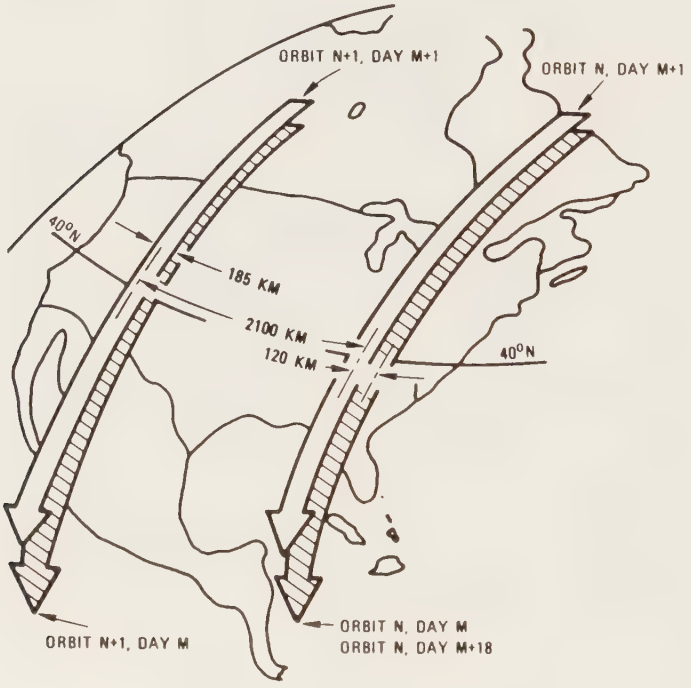

Figure 5.1c LANDSAT orbits over the United States on successive days. Note the 65 km sidelap of successive image swaths at 40°N latitude. The sidelap between adjacent orbits ranges from 14% at the equator to 85% at 80° parallels of latitude.

The LANDSAT-2 MSS operates in four different wave bands. The characteristics of the sensor are given in Table 5.1.

TABLE 5.1

LANDSAT-2 MSS CHARACTERISTICS

Wavelengths:	BAND 4: 0.5 - 0.6 μm (green) BAND 5: 0.6 - 0.7 μm (red) BAND 6: 0.7 - 0.8 μm (near IR) BAND 7: 0.8 - 1.1 μm (near IR)
IFOV:	0.086 mrad
Swath width:	185 km
Ground resolution cell size:	80 m X 80 m

The payload for LANDSAT-3 includes a five band MSS and a two camera RBV. The MSS has four bands identical to those on LANDSAT-2 and a fifth band (thermal IR) which was designed to operate at any time during orbit, including night operations, and at all solar elevation angles but did not become operational. The first four bands are operated only when the solar elevation is greater than 10 degrees.

There are six detectors for each of the four MSS spectral bands and two detectors for the thermal IR band. For this reason, the fifth band has one third the resolution of the other four bands.

5.1.2 The second generation: LANDSAT-4, 5

In the U.S.A., the National Oceanic Atmospheric Administration (NOAA) has been assigned the task of establishing an operational remote sensing system. LANDSAT-4 and 5 are the result of NOAA's mandate. Systems development per se has been the responsibility of NASA.

LANDSAT-4 and 5 were launched respectively in 1982 and 1984. They have an inclination angle of 98.3^{o} and a period of 98.5 minutes. The satellites make 14 to 15 revolutions per day with inter-track distances of 2752 km. They overlay the same track every 16 days.

The major difference between LANDSAT-4 and 5 and the previous LANDSATs is that the RBVs have been removed and have been replaced with a new generation of MSS called the Thematic Mapper (TM). This sensor provides more spectral bands and offers an improved ground resolution.

5.1.2.1 **Thematic Mapper (TM)**: The TM has 3 visible, 1 near and 2 middle IR bands with a 30 m ground resolution cell size and a thermal IR band with a 120 m ground resolution cell size. The characteristics of the sensor are given in Table 5.2.

TABLE 5.2

LANDSAT TM CHARACTERISTICS

Wavelengths:	BAND 1:	0.45	- 0.52 μm	(violet-blue)
	BAND 2:	0.52	- 0.60 μm	(green)
	BAND 3:	0.63	- 0.69 μm	(red)
	BAND 4:	0.76	- 0.90 μm	(near IR)
	BAND 5:	1.55	- 1.75 μm	(middle IR)
	BAND 6:	10.40	- 12.50 μm	(far or thermal IR)
	BAND 7:	2.08	- 2.35 μm	(middle IR)
IFOV:	0.043 mrad (except BAND 6: 0.170 mrad)			
Swath width:	185 km			
Ground resolution cell size:	30 m X 30 m (except BAND 6: 120 m X 120 m)			

The TM has the capacity to monitor a wide range of spectral bands (blue to infrared) and, hence, has a wide range of applications, e.g.:

1. Coastal water mapping (Band 1);
2. Identification of healthy vegetation by green reflectance (Band 2);
3. Plant differentiation by chlorophyll mapping (Band 3);
4. Water body delineation (Band 4);
5. Snow/Cloud measurement (Band 5);
6. Thermal mapping (Band 6);
7. Hydrothermal mapping (Band 7).

The TM provides an overall resolution of 30 m. This high resolution is achieved by sensitive detectors and by an 8 bit quantization in the analog-to-digital conversion process (256 grey levels). In contrast the MSS has only 6 bit quantization (64 grey levels). This means that TM scenes contain larger numbers of pixels with greater radiometric range. This also results in a very high data bit rate of 84.9 megabytes per second.

5.2 The NOAA Series

With the experience gained from the NIMBUS, TIROS and TOS (TIROS Operational Satellite) satellite series, the operational NOAA satellite series was commenced. The U.S. National Oceanic and Atmospheric Administration (NOAA) funded the series, hence the name designation.

The satellites of the NOAA series are dedicated to meteorological observations and sea surface temperature studies. This series can be divided into two generations:

5.2.1 The first generation: NOAA-2 to 5

NOAA-2 to 5 were launched respectively in 1972, 1973, 1974 and 1976. The NOAA satellites were launched into circular, near-polar (inclination angle of 102^{o}) sun-synchronous orbits, arranged to pass over any local receiving station twice a day. These satellites have a period of 115

minutes and they make 12 to 13 revolutions per day with inter-track distances of 3200 km.

They carry the VHRR (Very High Resolution Radiometer), which has been used extensively for oceanographic studies. This sensor will not be detailed in this manual; it became inactive in 1979 and was subsequently replaced in later NOAA satellites by the Advanced Very High Resolution Radiometer (AVHRR), an improved version of the VHRR.

5.2.2 **The second generation: TIROS-N, NOAA-6 to 9**

These satellites were launched respectively in 1978, 1979, 1981, 1983 and 1984. They have an inclination angle of 102° as do the first generation of NOAA satellites. In contrast, they have a period of 99 minutes and they make 14 to 15 revolutions per day with inter-track distances of 2760 km.

TIROS-N (Television and Infrared Observational Satellite) ended its mission in 1981. The main purpose of the TIROS series was weather forecasting and cloud cover observation. TIROS-N was used to test instruments for the NOAA satellite series.

The sensor used on the second generation of NOAA satellites for oceanographic studies, mainly sea surface temperature determination, is the AVHRR (Advanced Very High Resolution Radiometer.

NOAA-8 carries another sensor of interest for fisheries, SARSAT (Search and Rescue Satellite-Aid Tracking), which detects the distress signal emitted by vessels in difficulty.

5.2.2.1 Advanced Very High Resolution Radiometer (AVHRR): The AVHRR is a scanning radiometer of four or five channels (depending on the version) operating in the visible band and the near and thermal infrared bands. The characteristics of the sensor are given in Table 5.3.

TABLE 5.3

NOAA-7 - AVHRR CHARACTERISTICS

Wavelengths:	BAND 1:	0.58	- 0.68 μm	(green-red)
	BAND 2:	0.72	- 1.10 μm	(near IR)
	BAND 3:	3.55	- 3.93 μm	(middle IR)
	BAND 4:	10.50	- 11.50 μm	(far or thermal IR)
	BAND 5:	11.50	- 12.50 μm	(far or thermal IR)
IFOV:	1.3 mrad			
Swath width:	2700 km			
Ground resolution cell size:	1 km X 1 km			

5.3 Heat Capacity Mapping Mission (HCMM)

The Heat Capacity Mapping Mission (HCMM) was launched in 1978. It has an orbit designed to permit the measurement of the earth's temperature at 12-hour time intervals, when the temperature variation is at a maximum. This day/night temperature difference can be used to determine thermal inertia. The circular and sun-synchronous orbit has an inclination angle of 98°. The satellite makes 14 to 15 revolutions per day with an inter-track distance of 2712 km. It overlays the same track every 16 days at an altitude of 620 km.

The sensor onboard HCMM is the HCMR (Heat Capacity Mapping Radiometer) which was functional from 1978 to 1980.

5.3.1 Heat Capacity Mapping Radiometer (HCMR)

The HCMR is a two channel scanning radiometer and its characteristics are described in Table 5.4.

TABLE 5.4

HCMM - HCMR CHARACTERISTICS

Wavelengths:	BAND 1: 0.5 - 1.1 μm (blue - near IR) BAND 2: 10.5 - 12.5 μm (far or thermal IR)
IFOV:	0.83 mrad
Swath width:	716 km
Ground resolution cell size:	500 m X 500 m (BAND 1) 600 m X 600 m (BAND 2)

The two channels provide measurements of reflected solar and emitted thermal energy respectively. In addition to terrestrial studies, the HCMR was designed for research in the following areas:

i) Coastal zone thermal gradient determination. This includes mapping of thermal gradients in coastal zones and diurnal heat exchanges of the oceanic surface layer;

ii) Monitoring of large-scale marine pollution effects, mainly oil;

iii) Study of the life span, formation, transportation rate, decay and aggregation of mesoscale ocean eddies.

Due to calibration problems and the short life of the sensor, its oceanographic applications were not fully explored.

5.4 NIMBUS Series

The NIMBUS satellite program was initiated by NASA in 1960 to study the atmosphere and the earth's surface. The latest in this series of satellites, NIMBUS-7, was launched in November 1978. This satellite is

one of the few dedicated to oceanographic studies. The sun-synchronous near-polar orbit of NIMBUS-7 has an inclination angle of 99°. The satellite has a period of 104 minutes and makes 13 to 14 revolutions per day with an inter-track distance of 2904 km. It overlays the same track every 6 days and carries nine sensors, two of which are important to oceanography: the Coastal Zone Colour Scanner (CZCS) and the Scanning Multichannel Microwave Radiometer (SMMR).

5.4.1 Coastal Zone Colour Scanner (CZCS)

CZCS is a 6 channel radiometer designed specifically for ocean colour mapping. The characteristics of the NIMBUS-7 CZCS are included in Table 5.5.

TABLE 5.5

NIMBUS-7 CZCS CHARACTERISTICS

Wavelengths:	BAND 1:	0.43 - 0.45 μm (violet - blue)
	BAND 2:	0.51 - 0.53 μm (blue - green)
	BAND 3:	0.54 - 0.56 μm (green)
	BAND 4:	0.66 - 0.68 μm (red)
	BAND 5:	0.70 - 0.80 μm (near - IR)
	BAND 6:	10.50 - 12.50 μm (far or thermal IR)
IFOV:	0.865 mrad	
Swath width:	1566 km	
Ground resolution cell size:	825 m X 825 m	

Five of these bands can sense solar energy and, therefore, water colour as affected by absorption and scattering due to chlorophyll, sediment and gelbstoffe. Chlorophyll strongly absorbs energy in the wavelength bands centred at 0.44 and 0.52 micrometres (Bands 1 and 2) respectively. The wavelength of 0.50 micrometres (Band 3) is the hinge point, the wavelength of minimum absorption. The ratios of measured energies in these bands have been shown to closely parallel the surface chlorophyll concentrations. The data from the CZCS is processed to produce maps of the above measured materials. The measurement of pigment concentration is made possible by unique characteristics of the CZCS, i.e. the fine spectral resolution centered on specific wavelengths in the blue and green spectral regions and the extreme sensitivity suitable to discriminate the subtle variations of the oceanic signal caused by various water constituents. These characteristics are not shared by other sensors observing visible light, such as the MSS, TM or HRV. The temperature of coastal waters and the open ocean is measured in a spectral band centred at 11.5 micrometres (Band 6).

5.5 SEASAT-A

This is the first of a series of satellites specifically designed for oceanographic research (refer to Figure 5.2). SEASAT-A was launched by NASA in 1978 into a near-polar orbit with an inclination angle of 108°, a period of 100.7 minutes and an altitude of an 800 km. It ceased to function after a few months, apparently because of a power failure.

SEASAT-A carries five high resolution sensors: Scanning Multichannel Microwave Radiometer (SMMR); Radar Altimeter (Alt); Radar Scatterometer (SASS - SEASAT-A Satellite Scatterometer); Synthetic Aperture Radar (SAR); and Visible and Infrared Radiometer (VIRR).

5.5.1 Scanning Multichannel Microwave Radiometer (SMMR)

This type of microwave radiometer also was installed onboard NIMBUS-7. It provides information on numerous parameters, particularly sea surface temperature and sea ice cover. The characteristics of the NIMBUS-7 and SEASAT-A SMMR are included in Table 5.6

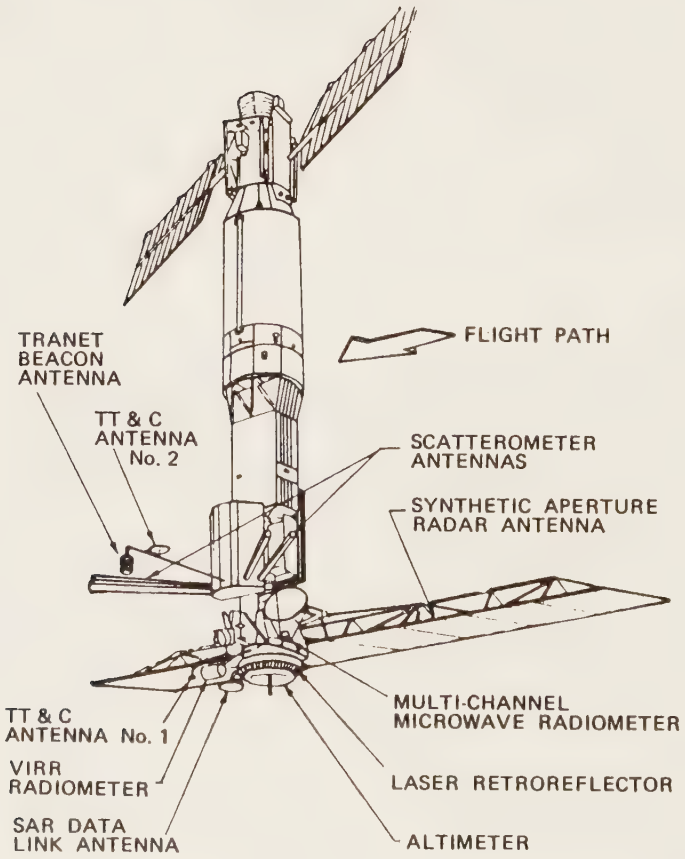

Figure 5.2 SEASAT-A configuration.

TABLE 5.6

NIMBUS-7/SEASAT - SMMR CHARACTERISTICS

Frequencies:	BAND 1: 6.6 GHz BAND 2: 10.7 GHz BAND 3: 18.0 GHz BAND 4: 21.0 GHz BAND 5: 37.0 GHz
Swath width:	900 km
Ground resolution cell size:	50 km X 50 km

5.5.2 Radar Altimeter (Alt)

The Radar Altimeter illuminates a target from 1.6 to 12 km in diameter at the nadir. The main purpose of this sensor is to measure the sea level (ocean geoid) with an accuracy of 0.1 metre and to determine the average wave height with an accuracy of 0.5 m.

The characteristics of the Radar Altimeter are included in Table 5.7.

TABLE 5.7

SEASAT - RADAR ALTIMETER CHARACTERISTICS

Frequency:	13.5 GHz (Ku-Band)
Footprint:	1.6 to 12 km

5.5.3 SEASAT-A Satellite Scatterometer (SASS)

The main purpose of this radar sensor is to measure near surface wind speed over the oceans in all weather conditions. The SASS was designed to record wind speed and wind direction with errors not exceeding 10%.

The characteristics of the Radar Scatterometer are included in Table 5.8.

Table 5.8

SEASAT - RADAR SCATTEROMETER CHARACTERISTICS

Frequency:	14.6 GHz (Ku-Band)
Swath width:	1000 km
Ground resolution cell size:	50 km X 50 km

5.5.4 Synthetic Aperture Radar (SAR)

The Synthetic Aperture Radar of SEASAT-A was the first imaging SAR system used as a scientific sensor from earth orbit. This sensor is used for wave characterization (wave height, wave length, etc.). It provided a resolution of 25 m and covered a 100 km swath on the north side of the satellite ground track. The SAR was operated on a real time basis only, when near a receiving station and at the latters command. This was mainly due to the very high rate (110 megabytes per second) at which the data was recorded and to the problems associated with the storage of such a large volume of data onboard the satellite.

The characteristics of SAR are included in Table 5.9.

TABLE 5.9

SEASAT - SAR CHARACTERISTICS

Wavelength:	23.5 cm (L-Band)
Swath width:	100 km
Ground resolution cell size:	25 m X 25 m

5.5.5 Visible and Infrared Radiometer (VIRR)

The purpose of this sensor is to provide IR and visible low resolution images of the ocean surface, cloud positions and clear air sea temperature.

5.6 GOES/METEOSAT Series

These high altitude (36,000 km) geostationary satellites are used for global meteorological observations and communications (refer to Figures 5.3 and 5.4 respectively). The aspects of meteorology that are the focus of these satellites include cloud mapping and infrared and visible imaging of the earth's surface to detect large-scale changes in ocean parameters.

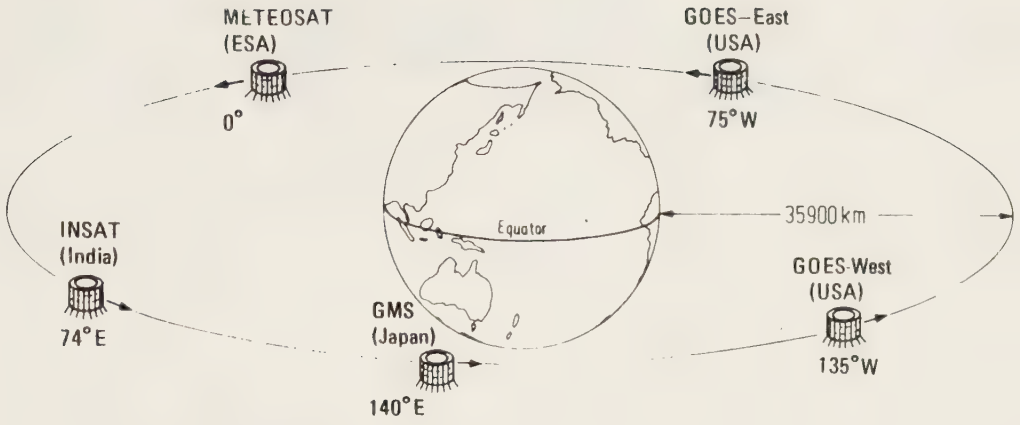

Figure 5.3 Positions of the five geo-synchronous meteorological satellites that provide global weather watch capabilities. (After J.A. Richards, 1986)

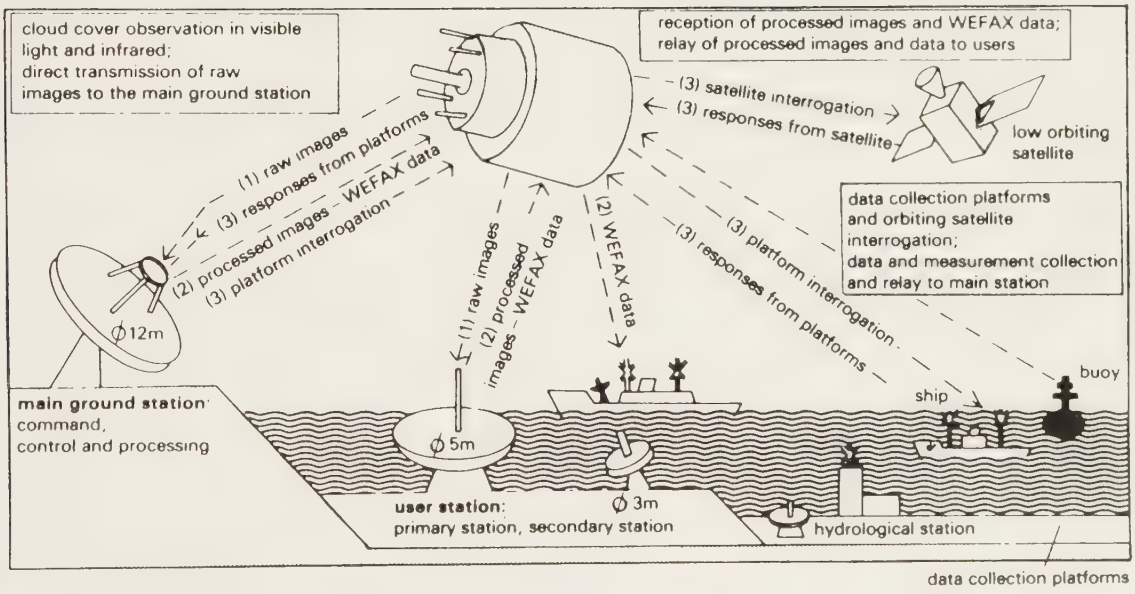
cloud cover observation in visible light and infrared; direct transmission of raw images to the main ground station
reception of processed images and WEFAX data; relay of processed images and data to users
(3) satellite interrogation
(3) responses from satellite
low orbiting satellite
(1) raw images
(3) responses from platforms
(2) processed images - WEFAX data
(3) platform interrogation
data collection platforms and orbiting satellite interrogation; data and measurement collection and relay to main station
(1) raw images
(2) processed images - WEFAX data
(2) WEFAX data
(3) platform interrogation
(3) responses from platforms
buoy
ship
ϕ12m
main ground station: command, control and processing
ϕ5m
ϕ3m
user station: primary station, secondary station
hydrological station
data collection platforms

Figure 5.4 METEOSAT data collecting system.

The countries and agencies which are participating in the WMO (World Meteorological Organization) program are the European Space Agency (ESA), the U.S.A., Japan and the U.S.S.R. Five satellites, GOES West (U.S.A.), GOES-East (U.S.A.), METEOSAT (ESA), INSAT (India) and GMS (Japan), collectively allow the earth to be fully imaged each 30 minutes.

The first satellite of the GOES (Geostationary Operational Environmental Satellite) series was launched in 1974. The latest in the series, GOES-4 (West) and 5 (East), were launched in 1980 and 1981 respectively. GOES-4 and 5 carry a special scanner, a spin scan radiometer, which has six infrared detectors.

The characteristics of the scanning radiometer onboard METEOSAT are described in Table 5.10. Note that the given ground resolution cell size corresponds to the nadir view of the sensor.

TABLE 5.10

METEOSAT - SCANNING RADIOMETER CHARACTERISTICS

Wavelengths:	BAND 1: 0.4 - 1.1 μm (blue-near IR)	
	BAND 2: 5.7 - 7.1 μm (middle IR)	
	BAND 3: 10.5 - 12.5 μm (far or thermal IR)	
Swath width:	12,500 km	
Ground resolution cell size:	BAND 1 :	2.5 km X 2.5 km
	BAND 2,3:	5.0 km X 5.0 km

5.7 SPOT

This satellite was launched in 1986 and is dedicated to land observation, although it has oceanographic applications as does LANDSAT.

It has a sun-synchronous near-polar orbit with an inclination angle of 99° and a period of 101 minutes. It makes 14 to 15 revolutions per day and overlays the same track every 26 days with an inter-track distance of 2818 km. The altitude of this satellite is 820 to 840 km. The sensor onboard is the push-broom radiometer, HRV (Haute Résolution Visible).

5.7.1 Haute Résolution Visible (HRV) radiometer

The special feature of this scanner is that it has a multispectral (3 bands) ground resolution of 20 metres. The scanners are also pointable by ground control to allow imaging of the same scene from different orbital tracks with an incidence angle from 0° (nadir) to a maximum of 27°. The images are obtained using two identical "push-broom" HRV scanning radiometers which permit stereoscopic imaging (refer to Figure 5.5). The characteristics of the HRV are described in Table 5.11.

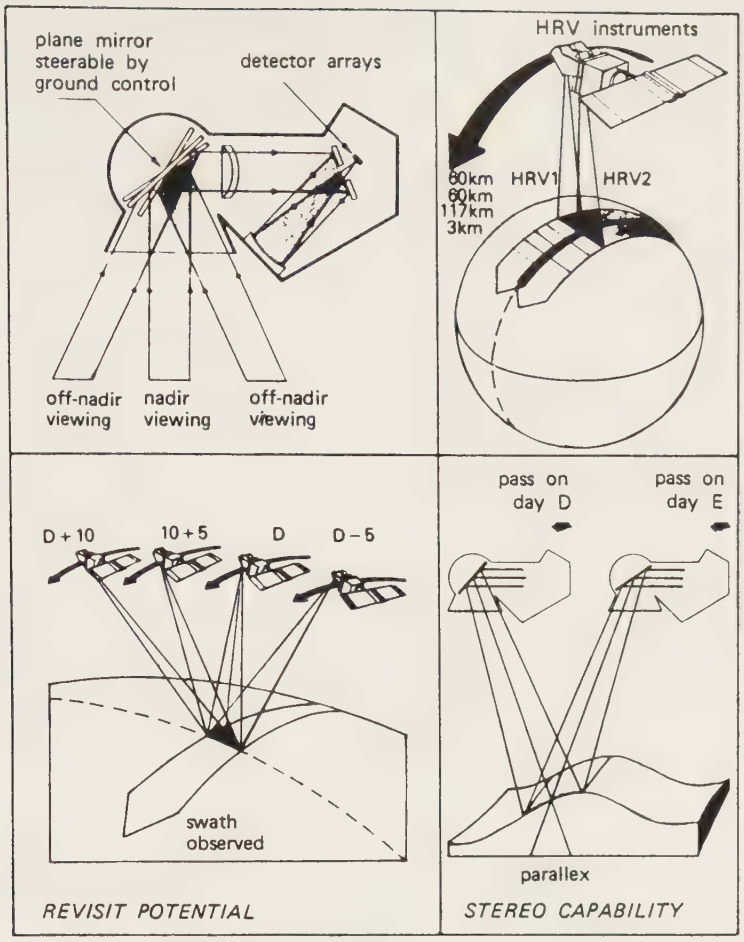

Figure 5.5 Attributes of the SPOT system. (After D.J. Carter, 1986)

TABLE 5.11

SPOT - HRV CHARACTERISTICS

	Panchromatic mode	Multi-channel mode
Wavelengths:	0.57 - 0.73 μm (green-red)	0.50 - 0.59 μm (green) 0.61 - 0.68 μm (red) 0.79 - 0.89 μm (near IR)
Swath width(per HRV):	60 km	60 km
Total swath width:	117 km (3 km overlap)	117 km (3 km overlap)
Ground resolution cell size:	10 m X 10m	20 m X 20 m

5.8 Space Shuttle and Space Stations

The space shuttle is not the first manned satellite to be used as a remote sensing platform. The U.S.A. launched an orbital station, SKYLAB, in 1973 which received astronauts in 1973 and 1974. The remote sensors onboard included two photographic cameras, which acquired 35,000 photographs, and a multispectral (13-channel) radiometer, which recorded 800 km of magnetic tape. Three years later the U.S.S.R. launched the SOYUZ station which carried a photographic camera similar to the main SKYLAB equipment. Numerous sensors have been used in the space shuttle of which three have oceanographic applications:

i) SIR-A (Shuttle Imaging Radar), an improved version of the SEASAT SAR;

ii) SMIRR (Shuttle Multispectral Infrared Radiometer), a 10-channel infrared radiometer with a spectral range of 5 to 25 micrometres;

iii) OCE (Ocean Colour Experiment), an 8-channel scanning radiometer with a spectral range of 0.49 to 0.79 micrometres.

5.9 Bhaskara Series

The Bhaskara-1 and 2 satellites were launched by India in 1979 and 1981 respectively with the assistance of the U.S.S.R. A radiometer operating at frequencies of 19 and 22 GHz is carried onboard both satellites for ocean survey purposes. The Bhaskara satellites are no longer operational.

5.10 MOS-1

MOS-1 is the first Japanese earth observation satellite and was launched successfully in February 1987. Data collected by this satellite will be available in early 1988. This is an experimental satellite designed to collect information on sea colour and sea surface temperature in addition to terrestrial parameters.

The instruments onboard this satellite are: Multispectral Electronic Self Scanning Radiometer (MESSR); Visible and Thermal IR Radiometer (VTIR), to measure sea surface temperature (SST); and Microwave Scanning Radiometer (MSR), to measure atmospheric water vapour. The Japanese also plan to launch MOS-2 and 3 which will carry active microwave sensors.

5.11 Satellites of the Future

Numerous satellites are planned for launching in the late 1980's and in the 1990's. The following will be dedicated to oceanographic studies:

5.11.1 IRS-1

IRS-1 (Indian Remote Sensing Satellite 1) of India is scheduled for launching in the late 1980's from the U.S.S.R. It will carry two push-broom sensors, LISS 1 and 2 (Linear Imaging Sensor System), whose bands and resolution (both radiometric and spatial) are comparable to MSS.

5.11.2 ERS-1

ERS-1 (ESA Remote Sensing Satellite) will be the first ESA (European Space Agency) satellite and is proposed for launching in 1989. The objectives of this satellite may be compared to those of the defunct SEASAT satellite. Its primary task will be the measurement of wind and waves over the ocean but other objectives include coastal ocean monitoring, ice movement studies and global weather studies.

The sensors that it will carry include: Synthetic Aperture Radar (SAR) with 30 metre resolution; Imaging Microwave Radiometer (IMR); a scatterometer for wind direction and velocity; and a radar altimeter for sea state determination (refer to Figure 5.6).

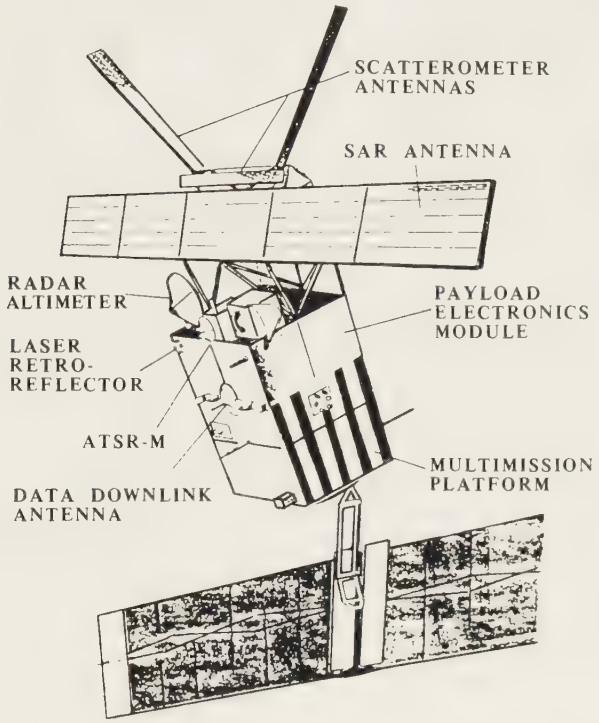

Figure 5.6 ERS-1 configuration.

5.11.3 TOPEX

TOPEX (Topographic Experiment) is a satellite designed exclusively for ocean scientific research. This satellite, designed by the Jet Propulsion Laboratory, Pasadena, U.S.A., the organization which designed and managed SEASAT-A, is proposed for launching in the late 1980's. The main objective of TOPEX is microwave sounding of the atmosphere to establish water vapour corrections.

5.11.4 NROSS

The U.S. Navy Remote Ocean Sensing System (NROSS) is scheduled for a three year mission beginning in 1989. The major sensor onboard will be the NASA scatterometer (NSCAT) designed to measure wind vectors in a 600 km swath on either side of the spacecraft.

5.11.5 OCI

The primary goal of the Ocean Colour Imager (OCI) mission, proposed for launching in 1990 by the U.S.A., is to measure visible and near-infrared ocean radiance to derive chlorophyll concentration as an estimate of ocean productivity and to provide flow visualization for ocean currents. The OCI is a development of the present Coastal Zone Colour Scanner (CZCS) carried onboard NIMBUS-7.

5.11.6 **RADARSAT**

RADARSAT, a Canadian satellite, is proposed for launching in the early 1990's. Its major sensor will be an advanced Synthetic Aperture Radar (SAR) for the monitoring of ice, the measurement of ocean waves and winds, and the detection of ships, oil slicks, etc.

5.11.7 **The Sea Wide Field Sensor (Sea-WIFS) Program (NASA/EOSAT)**

The Sea-WIFS program, which has been planned jointly by the National Aeronautics and Space Administration (NASA) and the Earth Observation Satellite Company (EOSAT), is designed to meet the needs of ocean science and industry communities for space-acquired ocean colour and sea surface temperature information in the 1990's. The Sea-WIFS sensor will be flown on the LANDSAT-6 satellite scheduled for launching in early 1991. The Sea-WIFS will build on the experience gained from the Coastal Zone Colour Scanner (CZCS) mission, flown by NASA on the NIMBUS-7 satellite from 1978-1986.

5.11.8 **Earth Observing System (EOS)/NASA**

Important global-scale research in oceanography, geology, limnology, hydrology, glaciology and terrestrial ecology is just beginning to be addressed with the most advanced kinds of sensors now available on satellites. A new generation of optical sensors, imaging spectrometers, is currently flying on aircraft and is scheduled to fly aboard the polar-orbiting space platform in the mid-1990's as part of the Earth Observing System (EOS). These new generation sensors include:

- Airborne Visible and Infrared Imaging Spectrometer (AVIRIS)
- High-Resolution Imaging Spectrometer (HIRIS)
- Moderate-Resolution Imaging Spectrometer (MODIS)

The EOS concept envisions the synergistic use of a number of remote sensing instruments together with an advanced data management system to provide global data sets to further our understanding of geological and glaciological processes, the hydrologic cycle, oceans and inland waters, and biogeochemical cycles. Only with such an integrated program can a rational sampling strategy be planned to obtain measurements needed to produce and verify models of Earth-System processes.

SECTION 6

6. DIGITAL IMAGE PROCESSING

6.1 Digital Images

In the previous chapters it was shown that sequential acquisition systems acquire information pixel by pixel, i.e. the smallest area discriminated by the sensor. For example, the Thematic Mapper of LANDSAT discriminates areas as small as 30 m X 30 m. The recorded scene is restored in the form of a grid of pixels. The radiance from each of the pixels is recorded by the detector(s) and then digitized to allow computer manipulation. The radiances that are measured in remote sensing can take any value between 0 and a maximum of R_{max}. The value is dependent on the wavelengths being sensed and the characteristics of the sensor.

The digitization process transforms continuous analog data into discrete digital data, i.e. a finite number of integer values is used to represent all the values of the original continuous data. The larger the number of integer values (N) used for digitization, the better the digital data conforms to the original analog data. Due to the configuration of computers, the number N is always a power of 2: ($N = 2^n$). The value of n ranges from 6 to 32 (depending on the sensor) and is defined as the "bit". For example, if the digitization process is carried out with 256 values (or levels), the data is encoded in 8 bits ($256 = 2^8$).

Before the digitization process can proceed, the operator must decide, on the basis of sensor hardware and programming software available, how to assign the infinite number of radiances to the finite number of digital levels available. For example, the zero radiance, R_0, may be given the digital value 0, and the maximum radiance, R_{max}, the digital value $2^n = N$. Any radiance value x will therefore correspond to a digital value Y:

$$y = \text{INT}\left[\frac{2^n}{R_{max} - R_0}\, x\right]$$ (where INT (A) is the integer value of A).

Example: n = 8 bits, therefore $2^n = 256$

$R_{max} = 20\text{mW} \cdot \text{cm}^{-2} \cdot \text{sr}^{-1} \cdot \text{m}^{-1}$ $R_0=0$

mW = milliwatts

sr = steradian, the unit of measurement for solid angles

$x = 20$ $y = \text{INT}\left[\frac{256}{20} \text{ X } 20\right] = \text{INT}(256)=256$

$x = 19.99$ $y = \text{INT}\left[\frac{256}{20} \text{ X } 19.99\right] = \text{INT}(255.87)=255$

$x = 19.98$ $y = \text{INT}\left[\frac{256}{20} \text{ X } 19.98\right] = \text{INT}(255.74)=255$

$x = 0.05$ $y = \text{INT}\left[\frac{256}{20} \text{ X } 0.05\right] = \text{INT}(0.64)=0$

$x = 1$ $y = \text{INT}\left[\frac{256}{20} \text{ X } 1\right] = \text{INT}(12.8)=12$

$x = 0$ $y = \text{INT}\left[\frac{256}{20} \text{ X } 0\right] = 0$

The larger the value of $R_{max} - R_0$, the greater the range of x values corresponding to the scene y values, resulting in less detailed digitization. The range $R_{max} - R_0$ can be reduced to a range $R_{sup} - R_{inf}$ of "interesting" values by using a sensor dedicated to a particular mission or target. In the visible part of the spectrum, the water-leaving radiance is very low compared with the land-leaving radiance. A sensor dedicated to water studies typically reduces the digitization range between 0 and R_{sup}, which is less than R_{max}. Any value greater than R_{sup} is assigned to the value 2^n, thus R_{sup} is the "saturation value" of the sensor. By this method, the radiances of real interest are imaged with more detail, i.e. more digital values are available to represent them. For example, the values of R_{sup} for LANDSAT MSS and NIMBUS-7 CZCS are given below:

i) Maximum radiance at saturation of MSS (gain=1):

BAND 4: $R_{sup} = 24.8$ mW · cm^{-2} · sr^{-1} · μm^{-1}; λ =550 nm

BAND 5: $R_{sup} = 20.0$ mW · cm^{-2} · sr^{-1} · μm^{-1}; λ =650 nm

BAND 6: $R_{sup} = 17.6$ mW · cm^{-2} · sr^{-1} · μm^{-1}; λ =750 nm

BAND 7: $R_{sup} = 46.0$ mW · cm^{-2} · sr^{-1} · μm^{-1}; λ =950 nm

ii) Maximum radiance at saturation of CZCS (gain=1):

BAND 1: $R_{sup} = 11.46$ mW · cm^{-2} · sr^{-1} · μm^{-1}; λ =443 nm

BAND 2: $R_{sup} = 7.64$ mW · cm^{-2} · sr^{-1} · μm^{-1}; λ =520 nm

BAND 3: $R_{sup} = 6.21$ mW · cm^{-2} · sr^{-1} · μm^{-1}; λ =550 nm

BAND 4: $R_{sup} = 2.88$ mW · cm^{-2} · sr^{-1} · μm^{-1}; λ =670 nm

BAND 5: $R_{sup} = 23.90$ mW · cm^{-2} · sr^{-1} · μm^{-1}; λ =750 nm

iii) Maximum radiance at saturation of CZCS (gain=4):

BAND 1: $R_{sup} = 5.41$ mW · cm^{-2} · sr^{-1} · μm^{-1}; λ =443 nm

BAND 2: $R_{sup} = 3.50$ mW · cm^{-2} · sr^{-1} · μm^{-1}; λ =520 nm

BAND 3: $R_{sup} = 2.86$ mW · cm^{-2} · sr^{-1} · μm^{-1}; λ =550 nm

BAND 4: $R_{sup} = 1.34$ mW · cm^{-2} · sr^{-1} · μm^{-1}; λ =670 nm

BAND 5: $R_{sup} = 23.90$ mW · cm^{-2} · sr^{-1} · μm^{-1}; λ =750 nm

Since it is known that CZCS is 8 bit-digitized (onboard) compared to 6 bits for MSS, the digitization of the green band of each sensor for low (water-leaving) radiances may be compared as follows:

MSS (gain=1)		CZCS (gain=4)	
$y=INT \frac{64}{24.8} x$		$y=INT \frac{256}{3.50} x$	
x=0.01	y=0	x=0.01	y=0
x=0.05	y=0	x=0.05	y=3
x=0.1	y=0	x=0.1	y=7
x=0.2	y=0	x=0.2	y=14
x=0.3	y=0	x=0.3	y=21
x=0.4	y=1	x=0.4	y=23

It is apparent, therefore, that more brightness differentiation is allowed by the CZCS (24 digital levels for a radiance range of 0.4) than by the MSS (2 digital levels for the same range of radiance). On the other hand, CZCS (band 2, gain 4) will not discriminate pixels having a radiance in excess of 3.50 whereas MSS (band 4, gain 1) allows the discrimination of radiances up to 24.8.

6.1.1 **Image display**

At this stage the data has been recorded, digitized and stored on magnetic tape in the form of a grid of pixels, each pixel being assigned an integer value from 0 to 2^n. If the data has been acquired with an imaging system it may be restored as an image on a monitor.

The magnetic tape is read by a computer which can, for display purposes, assign to each integer value (or range of values as discussed in Section 6.2.3.5 - Density slicing) a particular character or a particular colour, so each value may be visually distinguished. Encoding by characters was common in the past but is now obsolete. Different methods may be used to encode the data:

i) rainbow encoding:
each digital value is assigned to a different colour arbitrarily chosen,

e.g., 0=red, 1=blue ... 255=yellow;

ii) grey scale encoding:
each value is assigned to a grey level, generally in an ascending order,

e.g., 0=black, 1=dark grey ... 254=light grey,
255=white;

iii) colour scale encoding:
each value is assigned to a single colour level, generally in an ascending order,

e.g., 0=dark red ... 255=light red.

Colour scale encoding is used when it is necessary to display more than one image at the same time. In this case each image is encoded in a particular colour (e.g., red, green, blue) and the final image is a colour composite of the original images. The original images may be the same scene acquired at different wavelengths (multispectral analysis) or at different periods in time (multi-temporal analysis).

6.2 Image Processing

After digitization the data is appropriately formatted for computer manipulation and analysis. The data may now be transformed by any chosen mathematical function. Each image processing system has its own particular software, i.e. its own package of programs, each performing a different task. The sequence of tasks applied to an image is referred to as "image processing", which may be varied depending on the goals being sought. The following sequence gives a step-by-step example of currently used image processing techniques.

6.2.1 Radiometric corrections

Target radiance is altered (attenuated) by the atmosphere through which the radiance passes on its way to the sensor. The sensor itself further distorts this radiance that has reached it.

Correction for atmospheric attenuation is especially important for dark targets such as water bodies. With relatively clear, deep and, therefore, dark water targets, together with somewhat hazy atmospheric conditions, the total radiance reaching the sensor may be composed of only 20% water-leaving radiance and 80% atmospheric path radiance. Although this is an extreme case, useful signals over water targets tend to be overwhelmed by atmosphere-generated noise.

A subjective evaluation of a single image does not require atmospheric correction. When, however, the objective is to extract quantitative information (e.g., chlorophyll concentration, bathymetric depth, etc.) or to compare two images in tonal values, atmospheric effects must be removed.

There are a variety of techniques used for atmospheric correction: the simplest techniques include "dark pixel subtraction" and "histogram matching" which are more prone to error. The more complex involve the mathematical modelling of the atmospheric condition at the time and place of the image, which often requires information taken at the site of the image and at the time of imaging.

Correction of sensor noise is of two types: relative and absolute. Once again, absolute calibration is needed only if quantitative or multi-image analysis is to be performed. Ancillary information sent down by the satellite is used to perform absolute calibration. This is often carried out at the stage of processing when the computer compatible tape (CCT) is created.

Relative correction for sensor "banding" is generally performed when the CCT is produced for the user. The "banding" phenomenon occurs because a single channel in a sensor actually contains a number of detectors. In a mirror-scanning system such as the LANDSAT MSS, there are six detectors per channel while in a push-broom system such as the SPOT HRV, there are thousands. During sensor construction, the detectors are matched in terms of sensitivity as much as possible. Detector sensitivity will slowly change with time, making one detector more (or less) sensitive to radiance than its neighbour. The apparent result is that the same target will be depicted as different brightnesses by detectors with different

sensitivities. Again, ancillary sensor data is used in the pre-processing (on ground) stage to correct this image defect.

6.2.2 Geometric corrections

Geometric distortion is produced by the curvature of the earth, the non-uniformity of scanner motion, the non-linearity of the scanner mirror and the rotational movement of the satellite.

The correction of these geometric distortions can be accomplished in two ways:

i) the actual positions of the picture elements are changed but the elements retain their intensity values. Because of its limited accuracy, this method is used only for simple geometric corrections such as skew;

ii) the image is resampled, i.e. a digital image, geometrically distorted, is transformed to a picture on a non-distorted equally spaced grid. The intensity values of the pixels on the derived grid must be determined by interpolation, using neighbouring pixels from the distorted image.

6.2.3 Image enhancement

Enhancement methods are usually applied to an image in which image degradation (radiometric and geometric) has been corrected. Enhancements are designed to aid the human analyst in the extraction and interpretation of pictorial information. This is achieved by emphasizing the features or patterns of interest, e.g., the human visual system can discriminate many more colours than shades of grey, hence a colour display can represent more detailed information, i.e. rainbow encoding rather than grey scale encoding.

6.2.3.1 Contrast enhancement: Contrast enhancement is a process of accentuating the relative intensity of image elements. It is accomplished in a variety of ways, depending upon the needs of the particular task, e.g.:

i) linear modification	$y=ax+b$
ii) logarithmic modification	$y=b \times \log(ax)+c$
iii) exponential modification	$y=b \times \exp(ax)+c$
iv) external non-linear modification	$y=f(x)$

Where x represents the value of an element in the raw image, y is the modified value and a, b and c are constants. The result of contrast enhancement is an image wherein subtle distinctions between shades of grey have become emphasized and therefore easier to distinguish by eye.

6.2.3.2 Edge enhancement: This is another method of changing the intensity values in a digital image to improve the detectability of edge-like features in the scene. It is particularly useful for the detection of linear elements, either oceanographic (warm or cold water fronts) or man-made (canals, waterways). It is carried out with mathematical (high-pass) filters which emphasize the details of an image.

6.2.3.3 Colour enhancement: The human visual system can discriminate only 20-30 shades of grey under a given adaptation level. Under the same conditions, it discriminates a much larger number of colours; thus the use of colour provides a dramatic increase in the amount of information that can be perceived.

6.2.3.4 **Multi-image enhancement**: Multi-images (multispectral, multi-temporal) convey more information than single images. Multi-image enhancement techniques involve independent contrast enhancement of the component images. The enhanced components are then displayed as a false-colour composite. This allows the use of colour as a tool for detecting differences between bands or image dates (i.e. images of the same target recorded at different times).

6.2.3.5 **Density slicing**: It is possible to simplify the information content of an image presented in digital form by the reduction of the number of available digital levels. High contrast images with only two levels can be produced by the assignment of a dark colour to one level and no colour to the other. The division of grey scale levels into different classes can be made arbitrarily or according to some specification of the user.

This method is often used for the separation of land and water. In this case a specific wavelength band (generally near infrared) for which land and water radiances are different is chosen. Thus, a histogram of the data would show two very distinct shapes which allow the user to define a threshold to separate them. The pixels having a radiance level below this limit are assigned to a particular colour while those having a radiance level above the limit are assigned to another colour.

6.2.4 Image interpretation

After enhancement the image has to be interpreted, in order to extract the real meaning of the digital data, i.e. the environmental significance of the radiances recorded by the sensor.

6.2.4.1 **Image classification**: An image can be divided into distinct classes so that pixels which have similar spectral properties are grouped into the same class. Separating these classes is usually done with statistical or geometric methods. The separation of classes or "classification" is more successful if the targets are spectrally very different. Accuracy of classification suffers when the targets to be separated have near-similar spectral characteristics. An excellent knowledge of surface conditions at representative sites in the area to be mapped is a prerequisite for a successful application of image classification techniques.

6.2.4.2 **Pattern recognition**: Pattern can be defined as an image having spatial or geometrical character in two or three dimensions. For example, the wake of a boat moving on the surface of the sea makes a pattern by which it can be identified in an aerial photograph. Similarly, man-made structures or natural features can be identified by their geometrical shapes. When the identification of pattern or structure is carried out by computer, it is referred to as pattern recognition.

SECTION 7

7. APPLICATION OF REMOTE SENSING TO FISHERIES

The sea covers two thirds of the earth's surface. To a large extent, man is dependent on it for food species which include fish, shellfish, marine mammals, turtles, aquatic plants and algae. To exploit these resources more effectively, fishermen must catch the most fish possible (within biological constraints) while, at the same time, minimizing costs and optimizing the scheduling of their operations. Reliable environmental information is required from the scientific community for these purposes. Remote observations of the sea surface can provide a significant part of the information needed to assess and improve the potential yield of the fishing grounds. In the past, remote sensing was used predominantly to assist in the efficient harvesting of natural resources. Today it is being used for resource management, conservation and exploitation.

Variations in environmental conditions affect the recruitment, distribution, abundance and availability of fishery resources. It is not possible to measure remotely the entire range of information needed to assess changes in the marine environment. Knowledge of particular conditions and processes affecting fish populations, however, may often be deduced using measurements made by remote sensors, e.g., concentration of dissolved and suspended matter, variations in primary production levels, distribution of surface isotherms, location of frontal boundaries, regions of upwelling, currents and water circulation patterns. The parameters providing information on these environmental factors may allow a forecast of fish distribution or more generally the definition of marine fish habitats. These are often easier to sense remotely than the presence of fish.

Remote sensing techniques can be utilized directly, indirectly or as general aids in the detection and assessment of fishery resources.

7.1 Direct Methods of Fish Detection

The most direct and simple method of remote sensing in fisheries is visual fish spotting. Fishing fleets which exploit major fisheries such as tuna and menhaden are dependant on visual fish spotting from aircraft to direct their fleets.

Aerial photography per se is of little importance to the majority of commercial fisheries. The location of mobile fish schools, for example, cannot be provided fast enough to the fishermen. Aerial photography, however, can be of assistance to a fisheries scientist as it provides information about the distribution and relative abundance of pelagic fish, particularly the schooling species. The pattern of distribution and the location may identify the species observed, and the surface area of a school, measured from an aerial photograph, has been shown to be correlated with the biomass of some species.

Echo-sounders and sonars have been in use as remote sensors for at least 50 years and are now widely used by the fishing fleets of the world. Sonars are useful for the detection of fish and biomass estimation.

In recent years, high powered laser systems operating in the blue-green portion of the visible spectrum (lidar) have shown promise for the evaluation of fishery resources. A lidar carried on aircraft flying at an approximate altitude of 1700 m can detect fish at depths to 16 m.

7.2 Indirect Methods of Fishery Assessment

Estimation of a fishery resource can be assisted by the measurement of parameters which affect its distribution and abundance. Much of the research dealing with environmental effects related to fisheries are concerned with the correlation of a single parameter with the spatial and temporal distribution of fish. It is most likely, however, that fish respond to the sum total of environmental factors. Thus, it becomes necessary to correlate a large number of parameters, obtained by remote sensing techniques, with fish distribution.

The environmental parameters most commonly measured from airborne and spaceborne sensors are as follows: surface optical or bio-optical properties (diffuse attenuation coefficient, total suspended matter, yellow substance, chlorophyll pigments and macrophytes, commonly grouped under the general term of ocean colour); surface temperature; vertical and horizontal circulation features; salinity; oil pollution; and sea state.

7.2.1 Surface optical properties

The optical properties in the marine surface layer are determined by the presence of dissolved and suspended matter. Under normal conditions, visible light penetrates marine waters to a depth of tens of metres. As the concentration of the water constituents increases, i.e. the water becomes more turbid, the penetration of sunlight is reduced as a result of absorption and scattering processes. Depending on the specific characteristics of the materials present in the water, i.e. on their spectral signature, the absorption and scattering processes will vary with the wavelength of the incident radiation. Multispectral observations, therefore, can be employed to estimate the nature and concentration of the water constituents. Passive sensors working in the visible wavelengths (mainly CZCS but also MSS, TM, HRV) are commonly used to image water colour. Active sensors providing their own source of illumination, e.g., lidar, can also be used but only from aircraft and for sampling, rather than for imaging purposes. The main parameters which can be derived remotely from water emergent radiation, through the use of empirically constructed algorithms, are listed below.

7.2.1.1 **Diffuse attenuation coefficient**: The diffuse attenuation coefficient at a specific wavelength is an apparent optical property. Its magnitude depends on the light distribution as a result of spreading, scattering and absorption that exists at the in situ point of measurement. This parameter, when correlated with Secchi disk depth and Munsell colour hues, provides the means of physically categorizing water according to colour. Its value can be interpreted as a measure of water turbidity and it constitutes a valuable tool in fisheries studies. It has been shown, for example, that turbidity and menhaden sighting in the Mississippi Sound are highly correlated.

7.2.1.2 **Total suspended matter (seston)**: In addition to optical parameters, the total concentration of the absorbing and scattering agents can be used to classify surface waters by means of their colour. The utilization of this parameter may be most appropriate when classifying waters where inorganic and/or organic sediments make an important contribution to the optical properties of the surface layer. It may also be appropriate if sediment concentration has to be used as a natural tracer for the identification of water movement and frontal boundaries (refer to Figure 7.1).

7.2.1.3 **Yellow substance**: The term yellow substance may be defined as the material derived from the degradation of land and marine organic matter. It is an important parameter to monitor in the context of polluted coastal waters, since it may be used to identify marine areas where the

exploitation of filter feeders, e.g., shellfish, could be hazardous. In certain regions of the world, for example the North Sea, this parameter exhibits some correlation with the salinity of surface waters.

7.2.1.4 Chlorophyll pigments: The concentration of chlorophyll pigments (the photosynthetic pigments of phytoplankton) is often considered as an index of biological productivity and, in an oceanic environment, it can be related to fish production. Chlorophyll concentrations above 0.2 mg/cu.m indicate the presence of sufficient planktonic life to sustain a viable commercial fishery (Gower, 1972). Chlorophyll pigments have a specific and distinctive spectral signature since they absorb blue (and red) light and reflect strongly the green, thus affecting ocean colour. Multispectral observations from airborne or spaceborne sensors, therefore, allow the deduction of phytoplankton concentration (refer to Figure 7.2).

7.2.1.5 Macrophytes: In coastal areas it is common to find macrophytic vegetation (seaweed). Some species are of economic importance but all species play an important role in supporting marine life. Different kinds of seaweed have different light reflection properties, for example, reflect more green or red radiation. This distinction which allows the differentiation of some seaweed species can be detected from airborne or spaceborne passive visible sensors. Due to the low intensity of the light as it leaves the water, however, it is usually more effective to employ airborne sensors such as aerial cameras or radiometers (refer to Figure 7.3).

7.2.2 Surface temperature

Since 1973, the US National Oceanic and Atmospheric Administration (NOAA) has been engaged in sea surface temperature (SST) determination from satellite derived data. The process of extracting SST information from IR radiometer data is well established (refer to Figure 7.4). Global sea surface temperature charts are produced on an operational basis. They are in the form of computer printouts or contour maps with spatially smooth and radiometrically corrected measurements. It has been possible with data derived from TIROS, NOAA and the METEOSAT satellites to produce SST charts with an accuracy of 0.5^{o} - $2^{o}C$ and in near real time.

The heliosynchronous satellites of the NOAA series provide high resolution (1 km) pictures twice daily while the geostationary satellites (GOES, METEOSAT) provide pictures every 1/2 hour but with a resolution of only 5 km. The geostationary satellites are principally used for the near-equatorial area where the sensor's resolution is at its best. For latitudes higher than 40^{o} the image distortion is generally too extreme for operational use.

The occurrence of cloud or haze contaminates data to a certain extent but a knowledge of day-to-day variations or trends enables corrections to be made by interpolation. The sea truth information provided by ships is of further assistance in deducing the precise temperature fields.

To date, SST maps are mainly used by the salmon and tuna fishing fleets. It is well known that some tuna species feed on the warm seaward side of thermal fronts while salmon feed on the cold landward side. The occurrence of some other species can also be correlated with SST. In addition, physical features such as gyres, eddies, inversions and upwelling which are of importance to fisheries can be detected using SST maps.

Figure 7.1 Suspended sediment concentrations in the Bay of Fundy, Canada, as derived from LANDSAT MSS data.

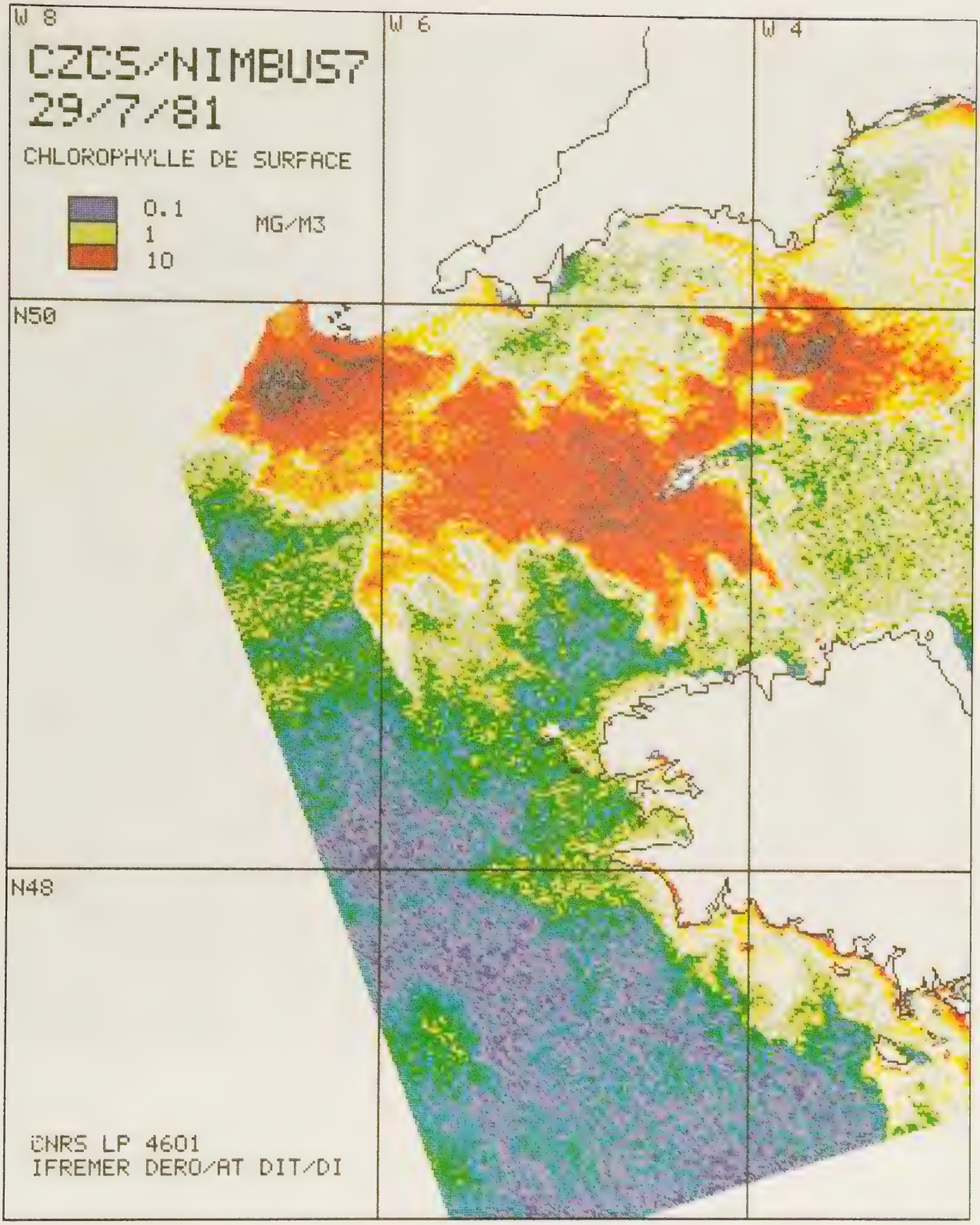

Figure 7.2 Chlorophyll concentration off the West coast of France, derived from a CZCS image (July 1981). A dinoflagellate bloom is shown as a red region.

Figure 7.3 Colour infrared aerial photograph (1:10,000) of the Chausey Islands, France, taken on April 24, 1982, at low tide. Five species of seaweed can be distinguished.

Figure 7.4 Sea surface temperature image of the Northwest Atlantic Ocean recorded by IR radiometer aboard NOAA-9.

7.2.3 Circulation features

Several remote sensing techniques can provide information regarding surface circulation features of importance in defining marine fish habitats. These include the location and evolution of frontal boundaries, upwelling areas, currents and circulation patterns in general. Optical and thermal characteristics of surface waters can be used as natural tracers of dynamic patterns. Hence, the previous discussion of sea surface colour and temperature should be considered again in light of this application. Microwave techniques, particularly the use of active sensors (radar altimeter), also have applications regarding large-scale circulation features. For example, remote measurements of water surface vertical displacements can provide information on the dynamic characteristics of a basin.

7.2.4 Salinity

The measurement of salinity from remotely sensed data is not operational at the present time. Research, however, indicates the possibility of determining salinity with the use of microwave sensors to an accuracy of one part per thousand. The microwave properties of the sea surface are a function of its physical and chemical state. The emissivity of sea water is related to salinity. Changes in salinity cause significant changes in the emissive brightness temperature of water for frequencies less than 5 GHz. Hence the salinity of sea water can be determined remotely by measuring accurately the emissive brightness temperature. The precision afforded by this technique may be adequate for mapping the spread of fresh water at a river mouth or for studying estuaries and near shore waters.

7.2.5 Oil pollution

The numerous methods used for oil detection at the sea surface include visual detection by eye, aerial camera, MSS and CZCS; microwave detection by SMMR and SAR; fluorescence detection by lidar; and thermal detection by IR scanner.

The visual method images the change in colour and brightness due to the presence of oil. Other visible-light phenomena used to detect oil slicks include EMR interference effects (colour banding) and the suppression of solar speckle by slicks. The microwave method, when passive techniques are used, is based on the difference of emissivity between the sea surface and the oil slick. Active radar sensors depend on small capillary wave backscatter to be dampened by the oil slick as a means of oil detection. Fluorescent properties of hydrocarbons may be detected and discriminated by appropriate lidars. These laser fluorosensors can also identify the basic types of oil (heavy, light, etc.) and provide a measurement of oil slick thickness. Thermal sensors identify oil by means of the difference in solar absorption and thermal emissivity between oil and water and they also provide a basic measurement of oil thickness.

7.2.6 Sea state

It has been known for some time that rough sea conditions created by wind have an effect on the distribution of fish. SAR equipped aircraft or satellites can survey the sea state of fishing grounds in near-real time. This information can be relayed to fishermen via a ground control station.

The microwave sensors on board SEASAT were capable of measuring the following with a high degree of accuracy:

i) radar altimeter: wave height and the microtopography of the ocean surface;

ii) synthetic aperture radar SAR: wave length and direction (refer to Figure 7.5);

iii) radar scatterometer SASS: near surface wind speed over the oceans in all weather conditions.

The ERS-1 satellite, scheduled to be launched in 1989, will carry a payload of sensors similar to that of SEASAT. These should be available for the same applications as noted above.

Although the effect of waves on the distribution of fish have been studied by several researchers, no attempt has been made so far to relate quantitatively the abundance of fish to any parameter of sea state.

7.3 General Aids to Fishing Operations

Satellites can assist the fishing industry in many ways other than the locating of fish per se. Most of these aids are also of assistance to mariners other than fishermen. The types of assistance that satellites can offer include the following:

i) search and rescue operations: The satellite NOAA-8 carries a special sensor, SARSAT (Search and Rescue Satellite Tracking), which detects the distress signals emitted by vessels in difficulty. The recorded signal is used to locate the position of the vessel. Sensors carried on board the Russian satellite series COSPAS-1, 2 and 3, launched respectively in 1982, 1983 and 1984, fulfill a similar function to SARSAT;

ii) weather reports: Environmental satellites such as NOAA, GOES or METEOSAT can provide weather information over a wide area at a given time (refer to Figure 7.6). This may assist fishermen to plan their fishing operations. In higher latitudes, ice and icebergs are major hazards; environmental satellites can assist in identifying ice and spotting icebergs;

iii) bathymetry: Remote sensing using passive or active visible sensors may be used for bathymetric measurements. With the exception of acoustic methods (sonar), airborne sensors provide the most accurate bathymetric measurements. In addition, active sensors such as bathymetric lidar are more reliable than the passive devices.

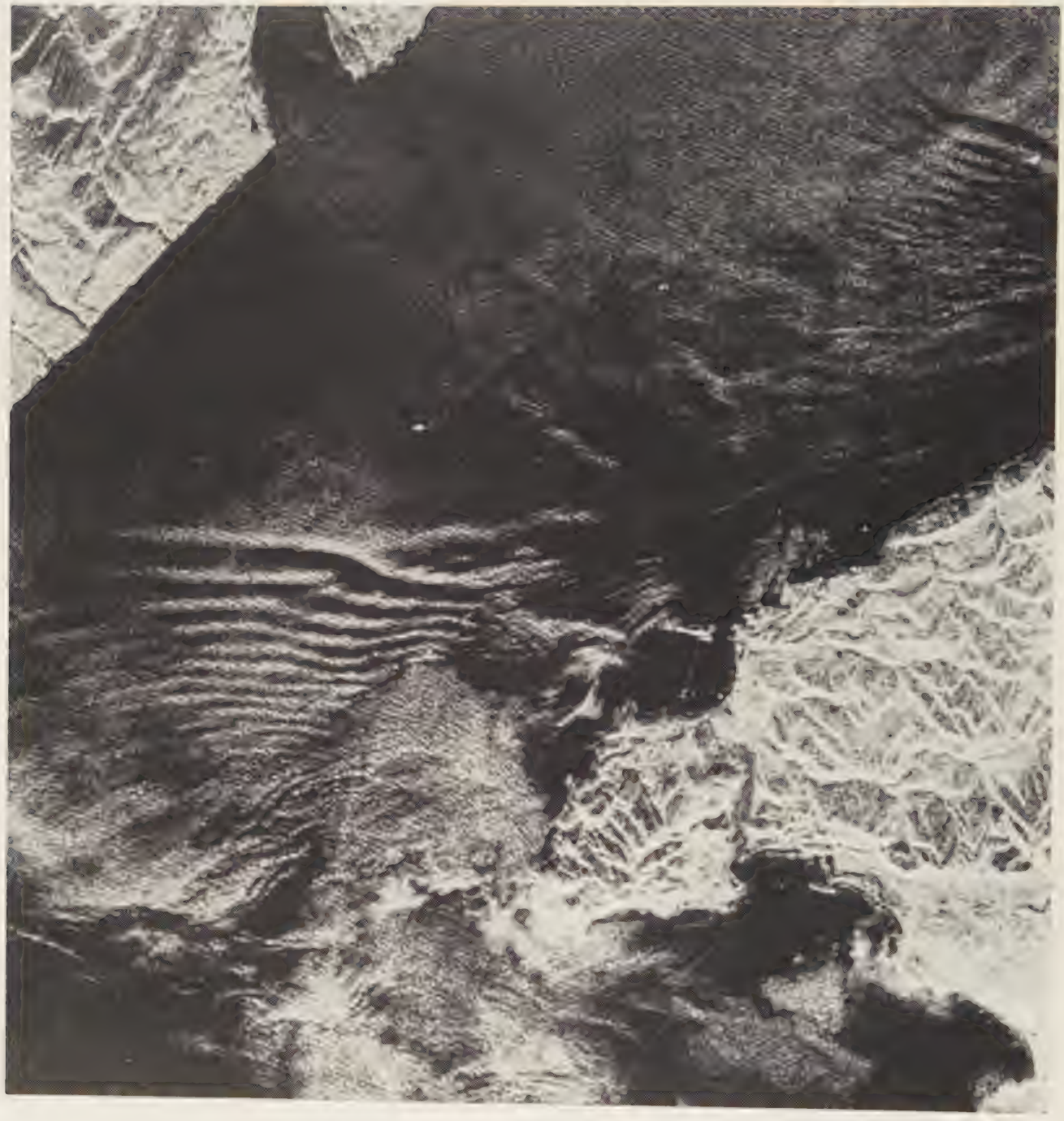

Figure 7.5 SEASAT image of the Strait of Juan de Fuca taken on August 13, 1978, at an altitude of 805 km. The image from L-band SAR has a resolution of 25 m. Gravity waves, internal waves and patches of smooth water may be observed.

Figure 7.6 Visible band image from GOES West taken at 18:00 on November 15, 1984.

SECTION 8

8. REMOTE SENSING CASE STUDIES

The following case studies are intended to expose the reader to a range of remote sensing techniques and applications. The case studies have been arranged in an order which reflects the primary objective of the experiment:

Fish Detection

Direct Technique:
- School dimension (Case Study No. 1)

Indirect Techniques:
- Fishing boat count (Case Study No. 2)
- Echo sounding (Case Study No. 3)
- Bioluminescence (Case Study No. 4)
- Chlorophyll (Case Studies No. 5 and 6)
- Water turbidity and ocean colour (Case Study No. 7)
- Sea surface temperature (Case Studies No. 8 and 9)
- Phytoplankton and sea surface temperature (Case Study No. 10)
- Ocean colour and sea surface temperature (Case Study No. 11)
- Ocean colour, chlorophyll and phytoplankton (Case Studies No. 12 and 13)

Invertebrate Detection

Indirect Techniques:
- Buoy count (Case Study No. 14)
- Bottom habitat (Case Study No. 15)

Marine Plant Detection

Direct Technique:
- Spectral signature (Case Studies No. 16 and 17)

Bottom Habitat Identification

Direct Technique:
- Spectral signature (Case Study No. 18)

Physical Oceanographic Parameter Measurement

- Bathymetry (Case Study No. 19)
- Sea surface temperature (Case Study No. 20)
- Currents (Case Study No. 21)
- Surface water velocity (Case Study No. 22)

8.1 Case Study No. 1

Reference:

Hara, I., 1985,
Moving direction of Japanese sardine school on the basis of aerial surveys. Bull.Japan.Soc.Sci.Fish., 51(12):1939-45

Remote Sensing Technique:

Airborne Remote Sensing:
Platform - Cessna U-206G;
Sensor - Visual Observation and Aerial Camera.

Objective:

To detect, identify and monitor the shape and movement of schools of sardines, Sardinops melanosticta, off the southeast coast of Hokkaido, Japan.

Experimental Rationale:

Aerial surveys are more appropriate for the observation of sardine schools than sonar measurements or underwater observations because they are more synoptic, cover a wider geographic area and facilitate mapping.

Method:

The shape, colour and movement of schools of sardines were determined by viewing a 1 km swath from a small aircraft at an altitude of 500 m (refer to Figures 8.1 and 8.2). The schools were subsequently measured from aerial photographs (refer to Figure 8.3). Movement of the fish schools was determined by reference to three yellow dye dispensers which were attached to floating devices (refer to Figure 8.4).

Results and Conclusions:

The dark blue colour of the front of the schools and the "watery blue" colour of the rear allow the determination of school movement with a single observation.

The relative dimensions of sardine schools in the surveyed area were 33 - 50:5:1 indicating the ratio of breadth:length:vertical extent, respectively. The greatest dimension, breadth, is usually the leading edge of a school.

This experiment indicated that aerial survey methods are effective for the study of fish school behaviour. It would be desirable, however, to establish a coordinated and synchronized system of air and ship-borne observations.

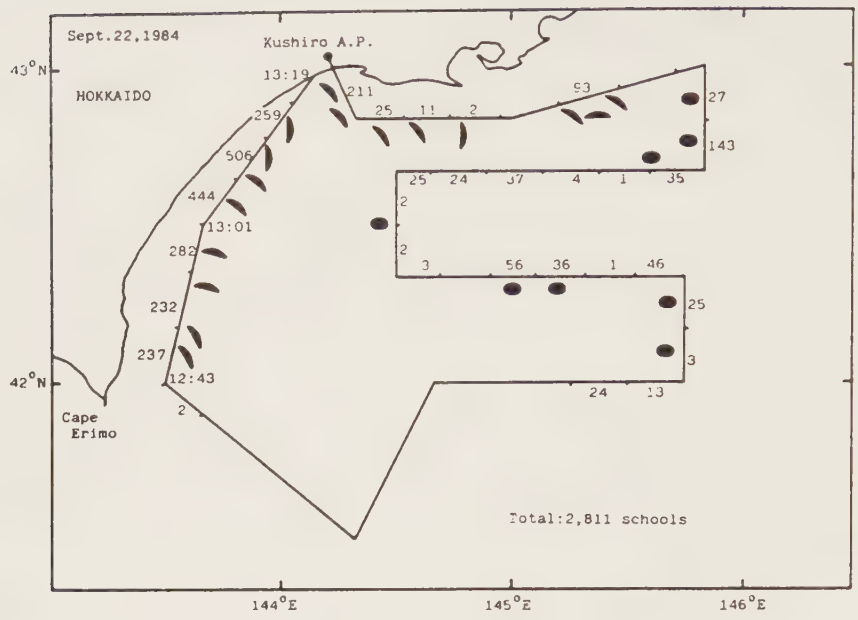

Figure 8.1 Flight line for visual observation on September 22, 1984. The number of sardine schools sighted is indicated.

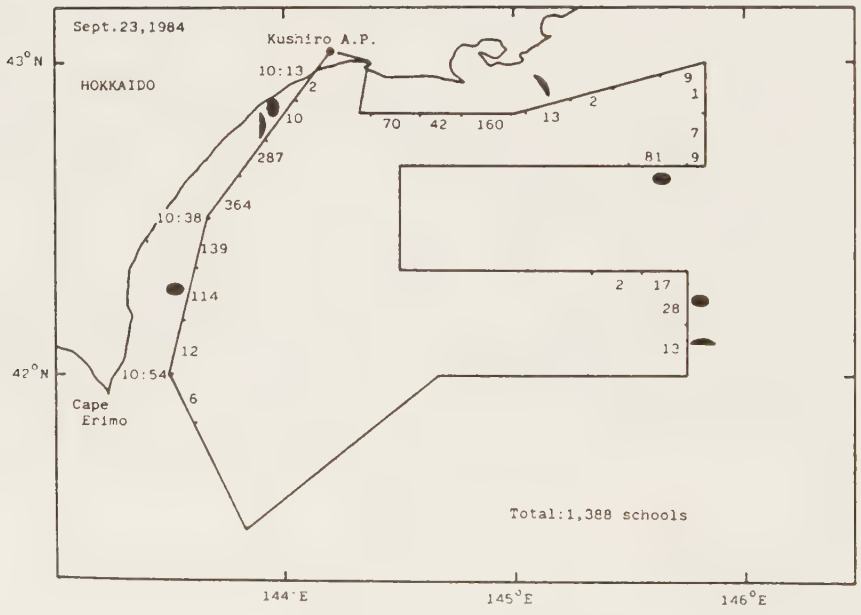

Figure 8.2 Flight line for visual observation on September 23, 1984. The number of sardine schools sighted is indicated.

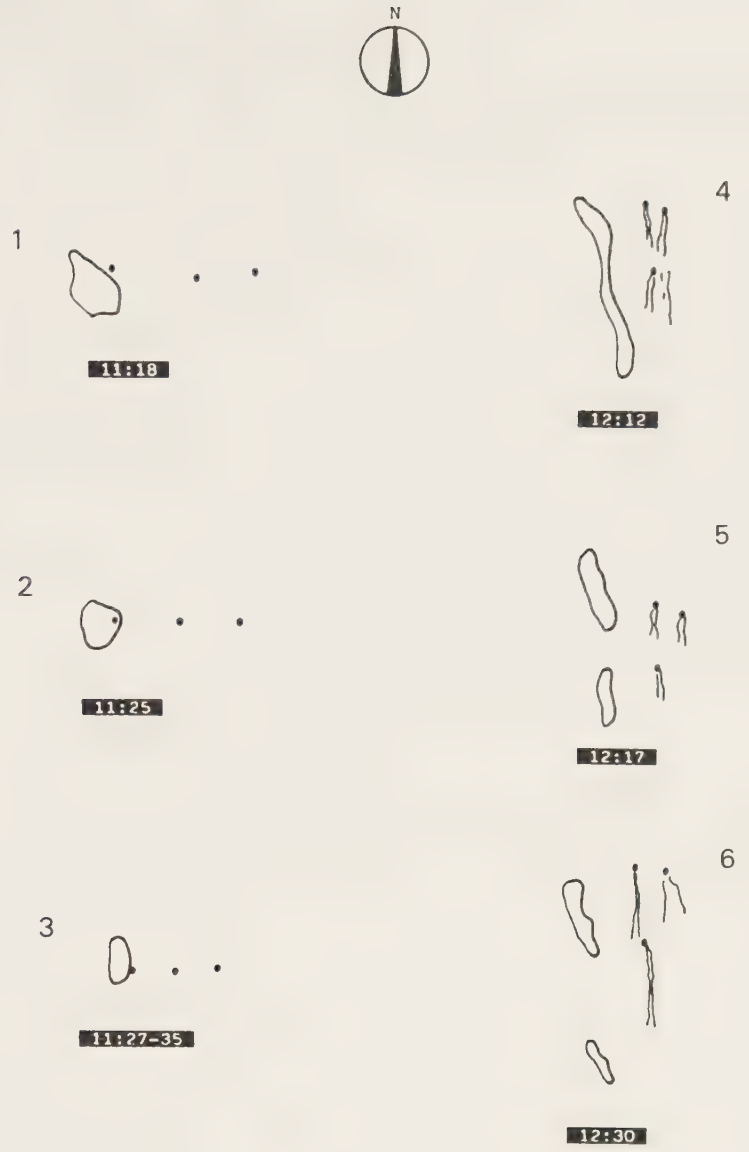

Figure 8.3 Changes in oval-shape school sketched from vertical or oblique photography. The time of observation is indicated. The three dots represent the airdropped floats and the two thin lines depict a yellow plume from the attached seamarker.

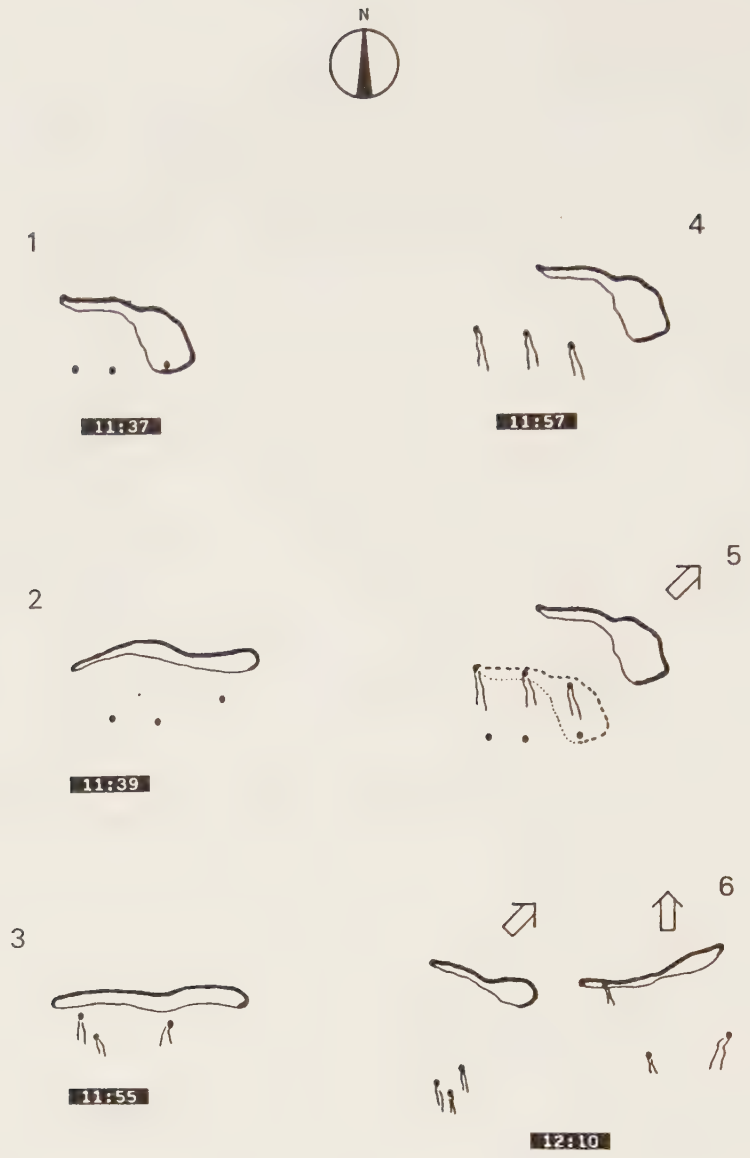

Figure 8.4 The changes of the elongate and the intermediate-shape schools expressed in the same manner as Figure 8.3. The arrow indicates the direction of school movement.

8.2 Case Study No. 2

Reference:

Bazigos, G.P. et al., 1979,
Aerial frame survey along the southwest coast of India. Rome, FAO, UNDP/FAO Pelagic fishery investigation project on the southwest coast of India. FIRM-IND/75/038:104 p.

Remote Sensing Technique:

Airborne Remote Sensing:
Platforms - Twin Beech and E18-S-Type Aircraft;
Sensor - Human Eye (Aerial Spotting).

Objective:

1. To assess the area of distribution and level of localization of the inshore sector of the fishing industry;

2. To provide current estimates of the number of operational fishing craft seen by type and by major fishery, i.e. non-mechanized fishery and mechanized fishery;

3. To provide information on the level of fishing activity of the operational fishing boats at the beginning of the fishing season.

Experimental Rationale:

This survey was based on the ability of well trained fishery biologists to differentiate types of fishing craft and gear from an aircraft flying at a height of 500 feet and moving at a speed of 120 nautical miles per hour.

Method:

Two groups of experienced researchers (3 in each group) were briefed before the flight. The responsibility of group I was to obtain measurements of the fishing boats seen on the coastline/landing places. The duty of group II was to obtain measurements of the fishing boats seen on the water. Separate records were kept during the survey flight for the non-mechanized and mechanized boats.

The Aerial Frame Survey (AFS) included only operational fishing boats in its list. The survey area covered the entire eastern coast and southern tip of India. This long coastline was divided into time/space units in order to increase the accuracy of eye estimation.

An error that occurs in a survey of this nature is the omission of the mechanized boats operating beyond the areas covered by the AFS. In order to unbias the calculated estimates of the total number of mechanized boats seen on the water, a small-scale coverage check survey (CCS) of the AFS was carried out.

The coverage check survey was comprised of a sample sonar-exploratory fishing cruise conducted for the project soon after the completion of the AFS. The findings of the survey (refer to Figure 8.5) were divided into two categories:

1) mechanized boats and non-mechanized boats seen on the water operating within the area covered by the AFS;

2) mechanized boats and non-mechanized boats seen on the water operating beyond the area covered by the AFS.

The analysis of data was carried out by the following methods:

1) determination of the co-efficient of fishing activity, i.e. the percentage of fishing boats in the water;

2) determination of the concentration of fishing boats, i.e. the number of standard craft per unit area or unit length. A medium size canoe was taken as the standard;

3) determination of the geographic relation between non-mechanized and mechanized boats;

4) determination of the spatial distribution pattern of all types of fishing boats.

Results and Conclusion:

When compared with government statistics, the results showed a substantial discrepancy in the number of craft for certain areas. This was mainly due to government data not being up-to-date. In a situation when the existing statistics are not reliable, there is no method to test the validity of an AFS.

Because fisheries in the project area were more dynamic in character than anticipated, two aerial frame surveys were recommended during the fishing season.

In the statistical analysis, an attempt was made to assess the operational distribution and level of localization of the surveyed fisheries. A mathematical model was developed to express the spatial distribution.

Figure 8.5 Pictorial chart of the distribution of the marine fishing boats covered by the AFS in the project area by one degree of latitude.

8.3 Case Study No. 3

Reference: Blindheim, J., G.H.P. de Bruin and G. Saetersdal, 1979, A survey of the coastal fish resources of Sri Lanka. Report No. 2, April - June 1979. Reports on surveys with R/V DR. FRIDTJOF NANSEN. Bergen, Institute of Marine Research, 63 p.

Remote Sensing Technique: Echo-Sounding:
Platform - Research Vessel (DR. FRIDTJOF NANSEN);
Sensors - Echo-Sounder, Sonar.

Objective: To describe and assess the demersal, semi-demersal and pelagic resources available in the coastal region of Sri Lanka.

Experimental Rationale: Echo-sounding can be used as a sampling technique for fish populations. Assuming that the distribution of fish in a particular area is uniform and that the speed of the ship is constant, the area of a fish trace made on the echo-sounder recording can be considered to be proportional to the size of the fish school. The conversion factor for this proportionality was deduced by test experiments. The character of the sea bottom can also be determined by an echo-sounder recording.

Method: Fishing and echo-sounding surveys of the waters around Sri Lanka were carried out with the fishery research vessel DR. FRIDTJOF NANSEN for three seasons, August-September 1978, April-June 1979 and January-December 1980. Fishing experiments were made on a total of 133 fishing stations with different types of fishing gear including bottom trawl, pelagic trawl, bottom long line and oyster dredge (refer to Figure 8.6).

The remote sensing equipment used in this study was two echo-sounders (38 KH_Z and 120 KH_Z) and a searchlight sonar (18 KH_Z).

The echo-integrator attached to this acoustic equipment recorded the analog data at a rate of 1 mm per nautical mile.

The bottom condition of the shelf floor was classified into 4 groups: "even flat", "uneven", "very rough" and "steep slope". By analyzing the echo recording of the bottom, the general characteristics of the continental shelf of Sri Lanka were found to be "even flat" with an "uneven" and "very rough" outer edge. Mapping of the sea bottom with echo-sounders, coupled with experimental fishing, identified the favourable fishing grounds.

For the sake of navigation and safety, charting of the sea was confined to regions deeper than 10 metres. Species could be differentiated by the pattern of the recordings. Small sized pelagic fish, e.g., clupeoids and scads, were found in well defined schools. Semi-demersal fish, e.g., snappers, breams, jack mackerel,

etc., were found in looser aggregations. Refer to Figures 8.7, 8.8 and 8.9 for examples. The discrimination of the fish into different species with echo-recording was confirmed by the fish catch.

Although no detailed quantitative analysis of the echo-recording was made, it was possible to differentiate echo-traces to three arbitrary types regarding fish biomass: very scattered (1-10 mm per nautical mile), scattered (11-20 mm per nautical mile) and dense (greater than 20 mm per nautical mile). The echo-integrator readings in mm per nautical mile are relative measures proportional to fish density, i.e. one unit of 1 mm per nautical mile represents a certain number of individual fish of a particular species per square nautical mile. A conversion factor is needed to determine absolute fish biomass from the relative echo-integrator values.

This survey also included the determination, by conventional methods, of temperature, salinity and dissolved oxygen in nine sections across the shelf.

Results and Conclusions:

Observations on the bottom condition revealed that good trawling grounds were limited to the shallow inshore parts of the shelf and to the shallow northern area.

Hydrographic observation permitted a description of the water masses on the continental shelf. The dissolved oxygen content in waters of the Northwest, Northeast and East coasts was found to be insufficient to support commercial fish species. The survey described the distribution of fish of commercial importance along the coast from Negombo to Pedro Bank; the total standing crop was assessed at approximately 500,000 tonnes. On the basis of some simple assumptions concerning mean density of biomass in the northern shallow waters not covered by this survey, the total biomass of Sri Lanka's coastal shelf and immediately adjacent waters was estimated to be 750,000 tonnes. The sustained annual potential yield from these resources was calculated to be about 250,000 tonnes, of which 80,000 tonnes represent large demersal or semi-demersal species. This estimate may well prove to be conservative, but it does indicate that the present level of catch of 100,000 tonnes at least can be doubled.

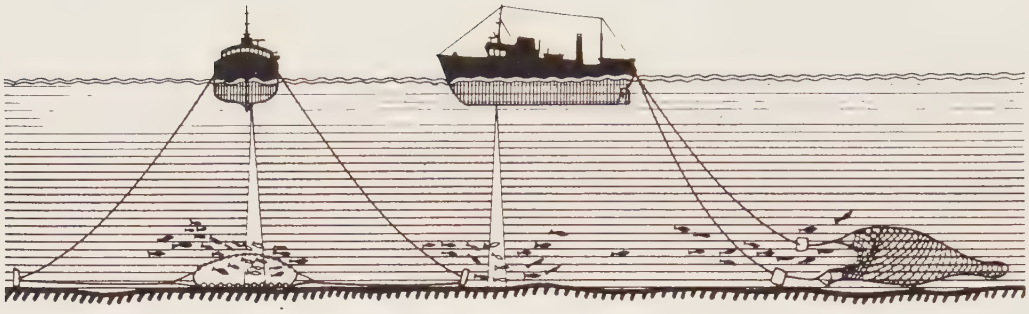

Figure 8.6 Dimensions of the sound beam from the echo sounder at 20 m echo depth in relation to the distance between trawl doors and wind ends of the trawl net.

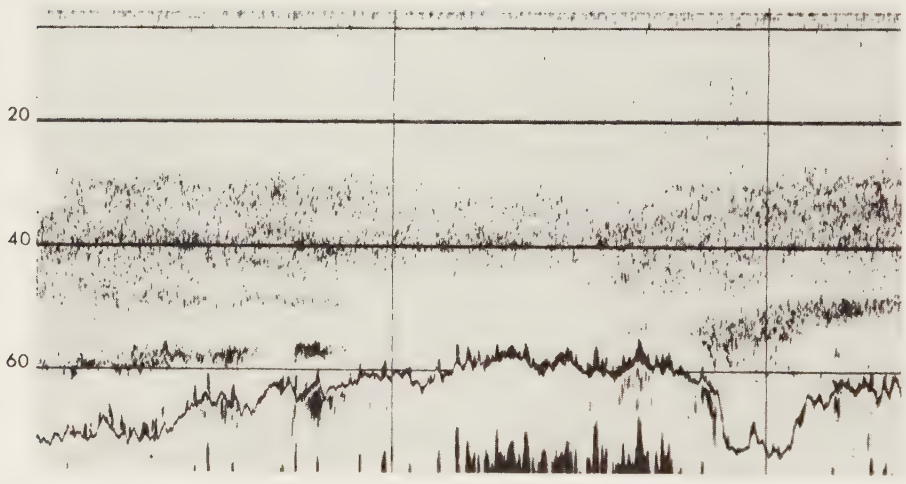

Figure 8.7 Example of "Type A" echo recordings of demersal and semi-demersal fish.

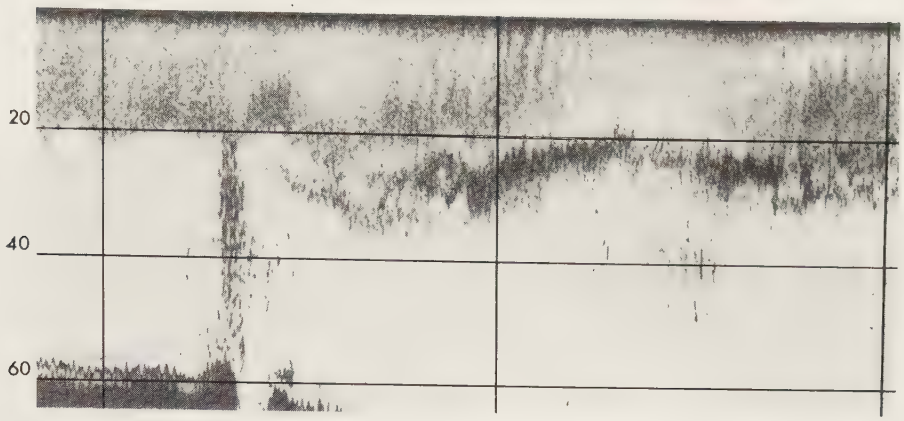

Figure 8.8 Example of "Type B" echo recordings of dispersed pelagic fish.

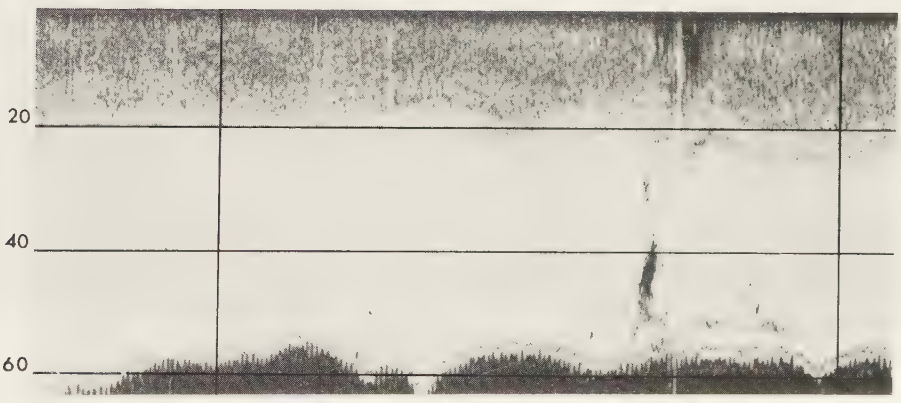

Figure 8.9 Example of "Type C" echo recordings of schooling small pelagic fish among recordings of dispersed larger pelagic fish (Type B).

8.4 Case Study No. 4

Reference:

Roithmayr, C.M., 1970,
Airborne low-light sensor detects luminescing fish schools at night. Commer.Fish.Rev., 32(12):42-51

Remote Sensing Technique:

Airborne Remote Sensing:
Platform - Aircraft;
Sensors - Aerial Camera, Spectrometers.

Objective:

To assess fish stocks at night using low-light sensors.

Experimental Rationale:

Bioluminescence is light produced by living animals and plants including plankton. The responsible light-emitting substance, luciferin, when disturbed absorbs energy and emits light. When fish schools disturb the water, many of these organisms emit light by which the presence of fish can be detected.

Method:

During 1968, tests were conducted in waters off Florida aboard a commercial seiner. A starlight scope was used to detect bioluminescence associated with Spanish mackerel schools. With the use of a scope coupled to a closed circuit television camera, the image of luminescing schools was recorded on video tape.

During dark nights luminescing fish schools were recorded on video tape with a SANOS (Stabilization Airborne Night Observation System) scope and closed-circuit television. Luminescing schools at the surface could be detected by a low-light detector at an altitude of 1,600 m (5,000 feet).

Results and Conclusion:

Low-light detectors proved to be efficient in detecting fish schools on moonless nights (refer to Figure 8.10). This can be of great assistance to fishermen in reducing their search time. It also will give scientists an opportunity to study the behaviour of fish schools at night.

The airborne sensor could greatly assist in resource assessment by providing "real time" observations on the number and size of fish schools.

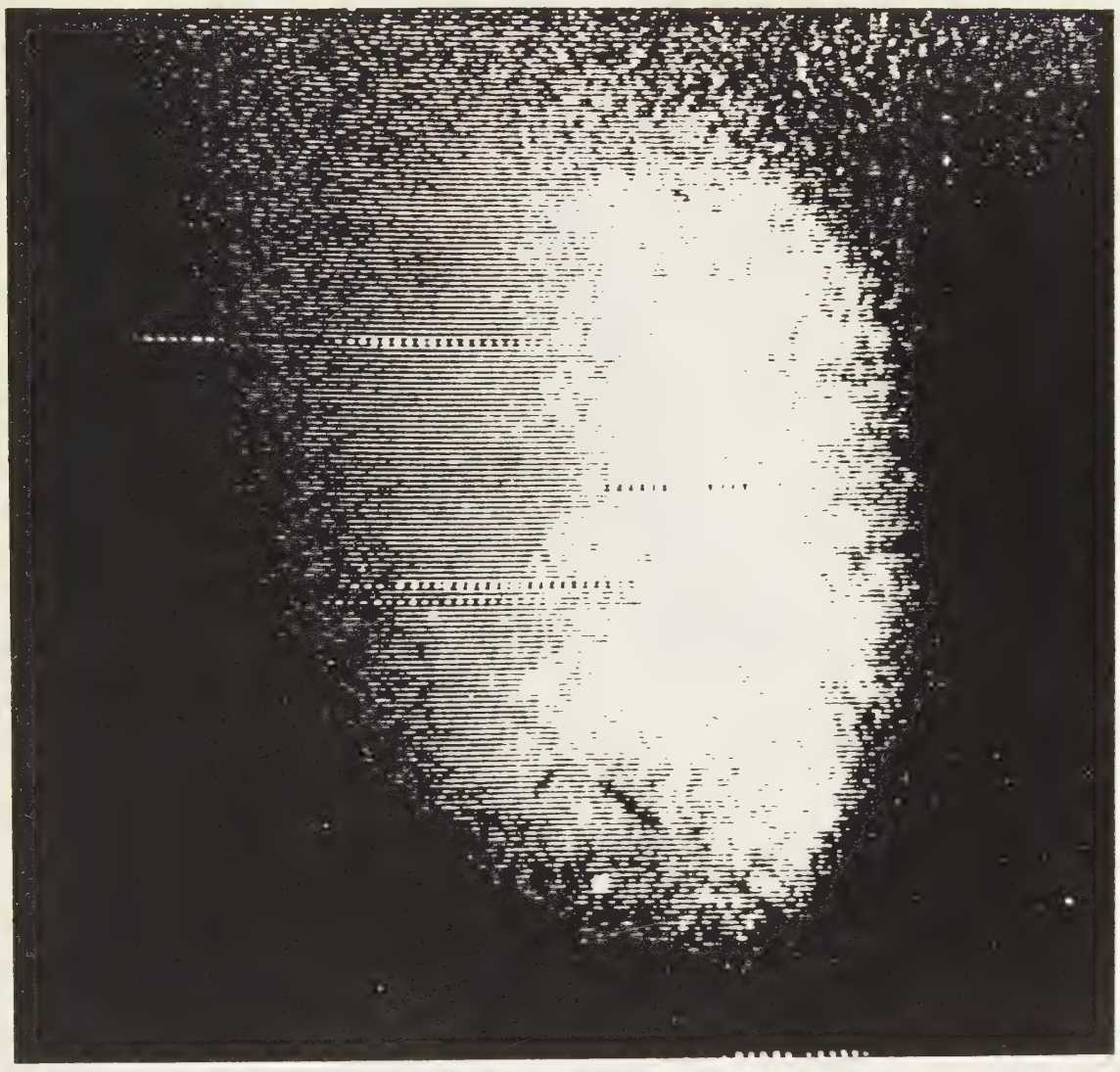

Figure 8.10 A large luminescing school of thread herring, 160 m (500 ft.) in diameter, amplified by airborne low-light sensor.

8.5 Case Study No. 5

Reference:

Cram, D.L., 1979,
A role for the NIMBUS-9 coastal zone colour scanner in the management of a pelagic fishery. Fish.Bull./Visserij-Bull.,Cape Town, (11):1-9

Remote Sensing Technique:

Satellite Remote Sensing:
Platforms - NIMBUS-G, LANDSAT-1;
Sensors - CZCS, MSS.

Objective:

To detect and measure chlorophyll concentrations with the aid of CZCS imagery to determine pilchard distribution off the coast of South West Africa.

Experimental Rationale:

Pilchard schools tend to avoid areas of dense phytoplankton and zooplankton abundance. Because of the difference in spectral signatures between brown-green phytoplankton (Fragilaria karstenii), which was the most dominant species in South West African waters, and sea water, the former could be discriminated in CZCS imagery. This provided an important method of delineating pilchard distribution.

Method:

CZCS imagery was analysed in order to delineate areas of phytoplankton occurrences. Variations in ocean turbidity, deduced from LANDSAT-1 data, were compared with pre-existing fisheries, and oceanographic and remotely sensed data in an attempt to identify biological features off the south-west coast of Africa.

An attempt was also made to discriminate areas of zooplankton abundance, mainly euphausiids, from LANDSAT images.

Results and Conclusions:

The CZCS of NIMBUS-G imagery was found to be efficient in detecting and measuring the chlorophyll-a content of water. LANDSAT MSS imagery was used to delineate areas of zooplankton (refer to Figure 8.11). With the knowledge of the areas of occurrences of phytoplankton and zooplankton, it was possible to infer the occurrence of pilchard, mainly because pilchard tend to occupy zones where the phytoplankton and zooplankton are present in intermediate densities.

This information could be used to minimize the search component of fishing effort and to refine assessments of pilchard stock by means of catch-per-unit-effort calculations.

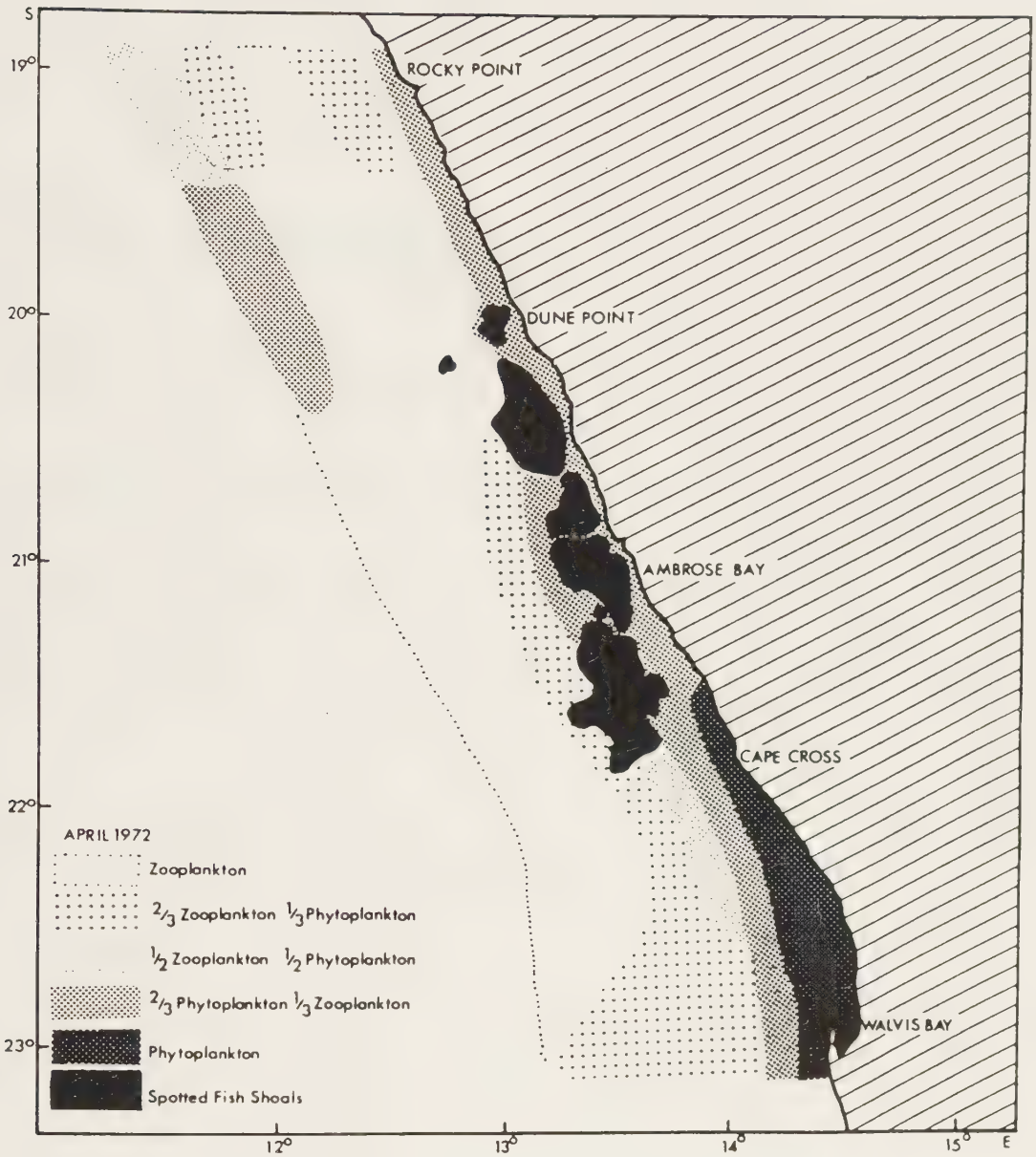

Figure 8.11 Plankton distribution and observed positions of pilchard shoal (school) groups - cumulative over 10 days.

8.6 Case Study No. 6

Reference:

Caraux, D. and R.W. Austin, 1983, Delineation of seasonal changes of chlorophyll frontal boundaries in Mediterranean coastal waters with NIMBUS-7 coastal zone colour scanner data. Remote Sensing Environ., 13(3):239-49

Remote Sensing Technique:

Satellite Remote Sensing;
Platform - NIMBUS-7;
Sensor - CZCS.

Objective:

To determine the seasonal changes of major chlorophyll boundaries in the northwestern Mediterranean (Golfe du Lion) using CZCS imagery.

Experimental Rationale:

The Coastal Zone Colour Scanner (CZCS) of NIMBUS-7 was primarily designed to detect chlorophyll content of the coastal waters.

Delineation of chlorophyll frontal boundaries using CZCS imagery has been carried out for several years.

The concentration of chlorophyll was considered to be a function of the difference of reflectance values in two channels. Varied combinations of bands and values for constants in the mathematical model were used for different types of water, i.e. reflectance values changed according to the concentration and composition of suspended particles, etc.

Method:

Cloud free images of the Golfe du Lion were obtained for the year 1979. The images were corrected for atmospheric attenuation. Using specific algorithms, maps were produced depicting the distribution of chlorophyll for the area under investigation (refer to Figure 8.12).

Conclusion:

The chlorophyll-like pigment boundaries determined in this study showed a resemblance to those previously identified by other workers using thermal infrared radiometry.

The results demonstrate that phytoplankton distribution is a good indicator of seasonal variations of oceanic fronts, with which many fish species are associated. Features such as coastal upwellings, cyclonic eddies or plumes could be monitored.

Figure 8.12 Monitoring of chlorophyll frontal boundaries in the Golfe de Lion throughout 1979. Boundaries were delineated after attributing different colours to chlorophyll concentration ranges obtained on CZCS images. The different tilt and scan angles of the CZCS radiometer account for variations in the area covered.

8.7 Case Study No. 7

Reference:

Kemmerer, A.J., 1980,
Environmental preferences and behaviour patterns of Gulf menhaden (Brevoortia patronus) inferred from fishing and remotely sensed data. ICLARM Conf.Proc., (5):345-70

Remote Sensing Technique:

Satellite and Airborne Remote Sensing;
Platforms - LANDSAT-1 and 2, Aircraft;
Sensors - MSS, Aerial Camera, T.V.

Objective:

To evaluate and subsequently to demonstrate the feasibility of using remotely acquired data to enhance the management and utilization of coastal pelagic fishery resources, especially menhaden.

Experimental Rationale:

The distribution of menhaden was found to be correlated with water turbidity and colour. The distributional pattern of these fish can therefore be predicted in relation to these parameters.

Method:

Most of the data considered in this paper were collected from three areas in the Northern Gulf of Mexico in 1972, 1975 and 1976. These areas were selected because of the LANDSAT coverage, logistics and location of the fishing fleet. In 1972 aerial photography and a low-light level imaging television system were used extensively to collect data on menhaden distribution and abundance.

In addition to the commercial fish catches, oceanographic data were also collected, including: sea surface temperature, salinity, light penetration, colour, surface chlorophyll-a and water depth.

Results:

The only oceanic parameters that had any correlation with the distribution of menhaden were light penetration and ocean colour. Although the distribution of this fish could not be inferred from LANDSAT images, the radiance values of each spectral band were found to be significantly correlated. On the basis of turbidity and colour the LANDSAT images were classified to give the highly probable areas of menhaden occurrences (refer to Figure 8.13). In 1976 a satellite-aided fishery harvest and assessment system was demonstrated and was subsequently established. It is now possible to produce in near real-time probability charts of menhaden occurrences using LANDSAT MSS imagery.

Conclusion: The ability to infer fish distribution patterns synoptically from environmental data collected by spacecraft will have profound management implications. It will enable resource investigators to improve sampling design and subsequent analyses for more efficient and accurate stock assessments. Long term monitoring of these patterns will enable resource managers to detect and subsequently to predict natural and man-induced resource perturbations.

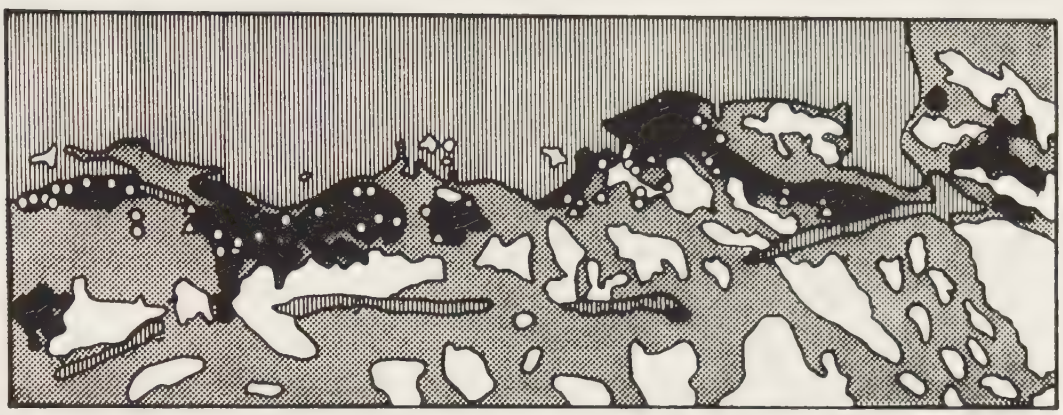
LAND
CLOUDS
LOW PROBABILITY FISHING AREA
HIGH PROBABILITY FISHING AREA
O POSITIVELY IDENTIFIED FISH SCHOOLS USED TO GENERATE COMPUTER CLASSIFICATION
Δ POSITIVELY IDENTIFIED FISH SCHOOLS FROM REMAINDER OF DAY

Figure 8.13 Classification of LANDSAT MSS data from May 20, 1975, into high and low probability menhaden fishing areas for the eastern half of the Mississippi Sound.

8.8 Case Study No. 8

Reference:

Lasker, R. et al., 1981,
The use of satellite infrared imagery for describing ocean processes in relation to spawning of the northern anchovy (Engraulis mordax). Remote Sensing Environ., 11:439-53

Remote Sensing Technique:

Airborne Remote Sensing:
Platform - NOAA-6;
Sensor - AVHRR.

Objective:

To relate variations in mesoscale (approximately 200 km) sea surface temperature distributions with anchovy spawning and to identify and delineate important ocean processes that might influence the survival of fish eggs and larvae.

Experimental Rationale:

This project attempted to evaluate the influence that surface water temperature has on the movement and reproduction of the Northern Anchovy, by means of satellite imaging of sea surface temperature patterns. This relationship could lead to predictive methods for the identification of optimal fishing sites.

Methods:

The AVHRR data were converted to sea surface temperatures. Temperature calibration was done by relating pixel grey scale values to same-day sea surface temperature observations from ships at several locations.

Oceanographic and biological parameters were acquired by the NOAA research vessel David Starr Jordan using a thermosalinograph, plankton net and midwater trawl.

Results and Conclusions:

The distribution of first-day anchovy eggs clearly showed that nearly all spawning was confined to the Southern California Bight. The seaward extent of spawning was apparently confined by the southward intrusion of recently upwelled water indicated by the 14°C isotherm (refer to Figure 8.14).

In March-April 1980 anchovy did not enter water colder than 12.5°C nor warmer than 17°C. In earlier years appreciable spawning took place at temperatures above 16.5°C and in water colder than 14°C. The modal temperature for anchovy spawning was 14° - 15°C from 1969 to 1979 but was 15° to 17°C in 1980. For this reason the authors were led to the conclusion that temperature was not the sole environmental variable responsible for anchovy distribution in 1980. Temperature, however, can be used as an indicator of water mass distribution.

Wind, chlorophyll and sea state sensors used in conjunction with the AVHRR should provide more reliable information on fish egg and larval distribution.

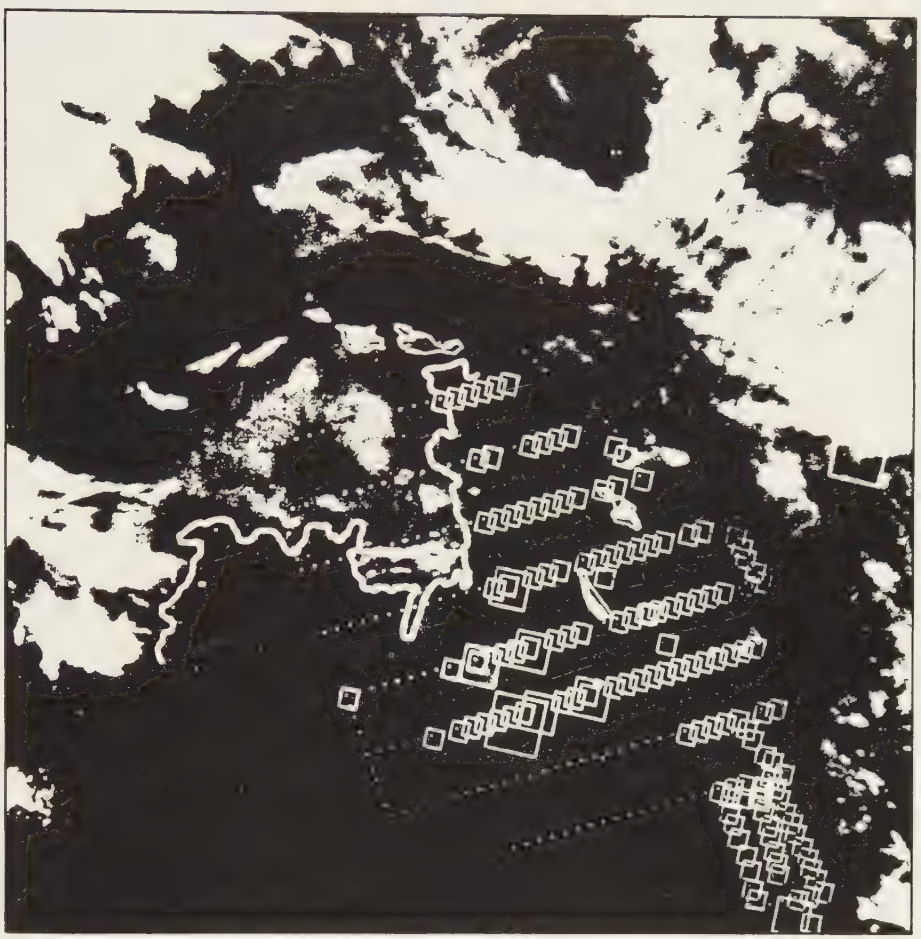

Figure 8.14 Distribution of anchovy eggs superimposed on the thermal image of the Southern California Bight. The 14°C isotherm plotted from satellite grey-scale calibration has been drawn on the image. Squares indicate number of anchovy eggs under one square metre of sea surface.

8.9 Case Study No. 9

Reference:

Cornillon, P. et al., 1986, Sea surface temperature charts for the southern New England fishing community. Marine Technology Society Journal, 20(2):57-65

Remote Sensing Technique:

Satellite Remote Sensing:
Platform - NOAA-7;
Sensor - AVHRR.

Objective:

To evaluate the potential assistance of satellite-derived SST charts to fishing activities on the continental shelf.

Experimental Rationale:

A number of fish species have a preference for seawater which has a specific and limited temperature range. Fishermen, therefore, can take advantage of sea surface temperature (SST) charts to assist in the locating of optimal fishing areas.

Method:

During 1983 and 1984, the Sea Grant Marine Advisory Service and the Graduate School of Oceanography at the University of Rhode Island (URI) prepared 37 SST maps from AVHRR data and mailed them to Southern New England fishermen. Throughout the program, user response was sought and, in order to meet user requirements, three different products were delivered: a temperature map covering the full study region (refer to Figure 8.15); a temperature map featuring an enlargement of a subregion of particular interest (refer to Figure 8.16); and a temperature gradient map showing areas of high horizontal SST gradients (refer to Figure 8.17).

The AVHRR data were received at the University of Rhode Island 24 to 36 hours after their acquisition. They were then processed and the results were immediately mailed to fishermen who received them the next day.

Results and Conclusions:

The interaction between URI and the users during the experiment allowed the development of products that fishermen recognized as being useful. Many fishermen, however, wanted greater spatial resolution and several considered the charts to be outdated by the time they were received. Although fishermen considered that they saved money due to decreased search time, few were willing to spend more than $50 per year to receive the charts. Two problems were identified: infrared sensors such as the AVHRR do not see through clouds, resulting in periods where no SST data can be acquired. Microwave sensors, however, can produce SST data through clouds but these sensors are not currently available on civilian satellites. Secondly, the delay between the satellite pass and the delivery of the SST chart to the fishermen was excessive. This delay could be greatly reduced by the use of electronic data transfer methods.

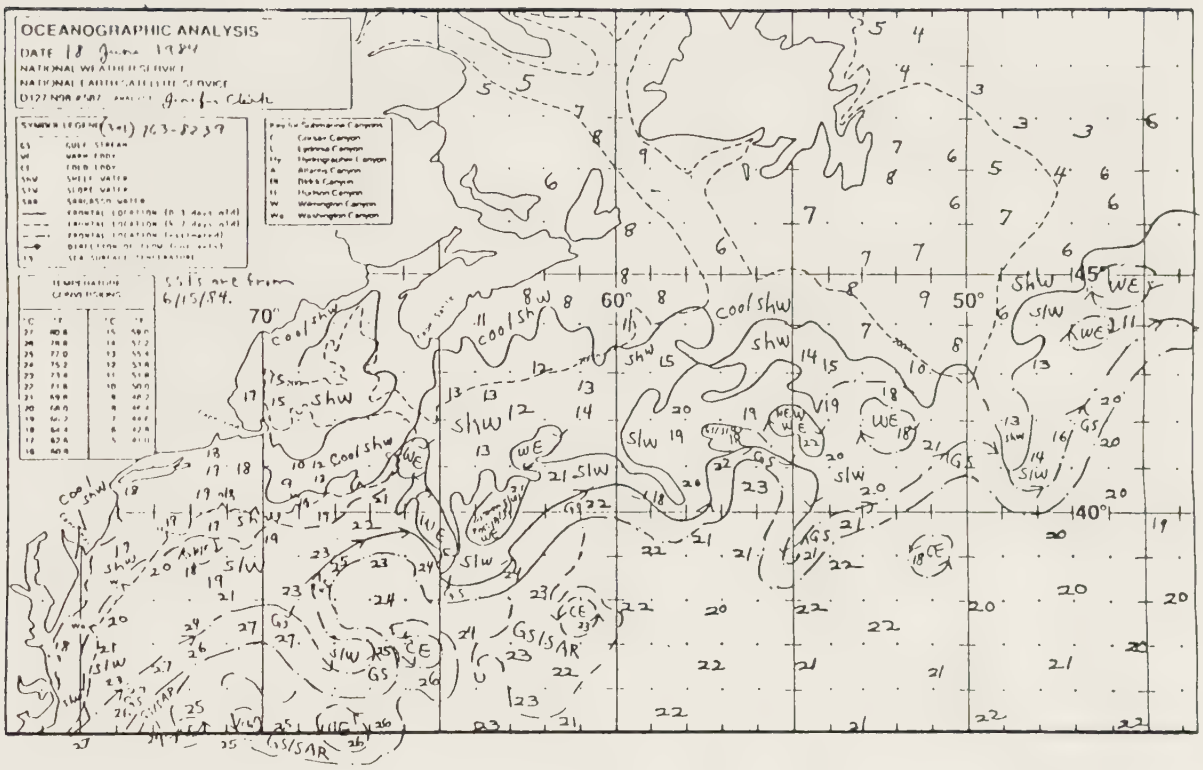

Figure 8.15 NOAA/NESDIS (National Environmental Satellite Data and Information Service) oceanographic analysis chart for June 18, 1984.

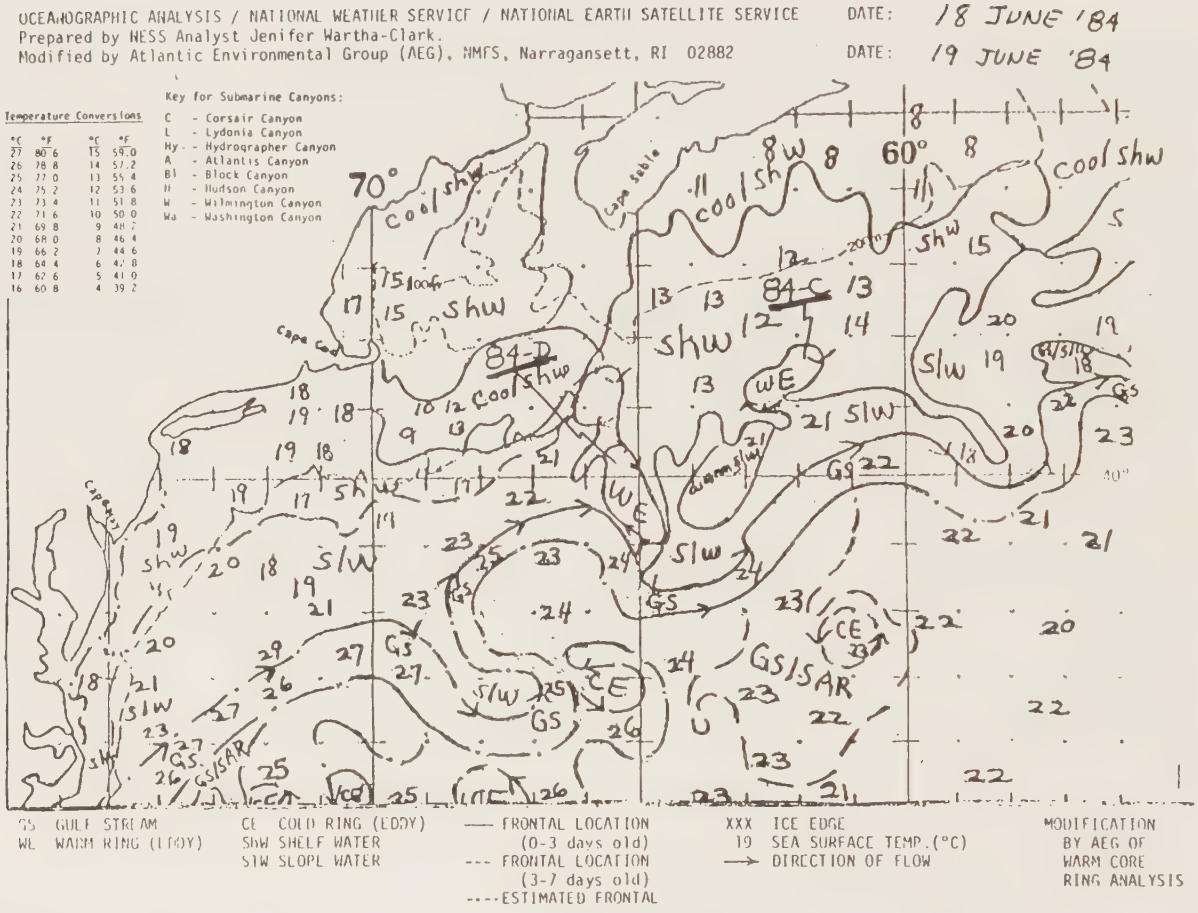
OCEANOGRAPHIC ANALYSIS / NATIONAL WEATHER SERVICE / NATIONAL EARTH SATELLITE SERVICE
DATE: 18 JUNE '84
Prepared by NESS Analyst Jenifer Wartha-Clark.
Modified by Atlantic Environmental Group (AEG), NMFS, Narragansett, RI 02882
DATE: 19 JUNE '84
Temperature Conversions
Key for Submarine Canyons:
C - Corsair Canyon
L - Lydonia Canyon
Hy - Hydrographer Canyon
A - Atlantis Canyon
Bl - Block Canyon
H - Hudson Canyon
W - Wilmington Canyon
Wa - Washington Canyon
70°
60°
40°
Cape Cod
Cape Sable
GS GULF STREAM
WE WARM RING (EDDY)
CE COLD RING (EDDY)
SHW SHELF WATER
SLW SLOPE WATER
FRONTAL LOCATION (0-3 days old)
FRONTAL LOCATION (3-7 days old)
ESTIMATED FRONTAL
XXX ICE EDGE
19 SEA SURFACE TEMP.(°C)
DIRECTION OF FLOW
MODIFICATION BY AEG OF WARM CORE RING ANALYSIS

Figure 8.16 Subsection of the NOAA/NESDIS chart shown in Figure 8.15, modified by NMFS (National Marine Fisheries Service).

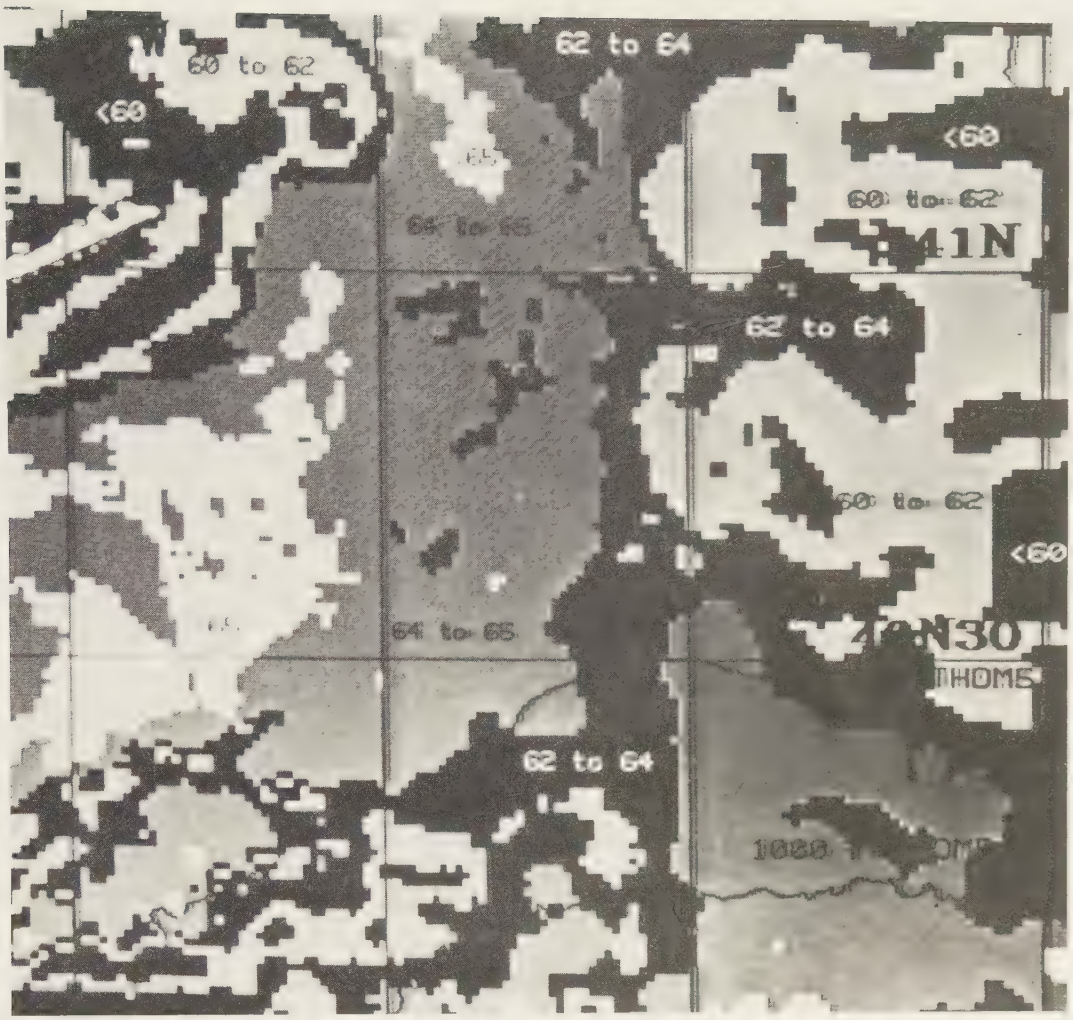

Figure 8.17 Enlargement of the region east of Long Island, mailed to fishermen.

8.10 Case Study No. 10

Reference:

Laurs, R.M. *et al.*, 1984, Albacore tuna catch distributions relative to environmental features observed from satellites. *Deep-Sea Res.*, 31(9):1085-99

Remote Sensing Technique:

Satellite Remote Sensing:
Platforms - NOAA-7, NIMBUS-7;
Sensors - AVHRR, CZCS.

Objective:

To determine the relationship between hydrographic patterns, as imaged by satellite sensors, and albacore distribution.

Experimental Rationale:

It is well known that the occurrence of albacore is closely related to oceanographic conditions in the North Pacific. The AVHRR allows the recognition of thermal fronts while the CZCS provides an accurate measurement of chlorophyll content, hence, phytoplankton distribution. Used together, they should provide valuable information on albacore distribution and should guide fishermen to optimal fishing regions.

Method:

The satellite data collection and processing network utilized for this experiment is indicated in Figure 8.18. The CZCS radiances were converted to phytoplankton pigment concentration using a pigment algorithm (band ratio), while the AVHRR radiances were converted to temperature and corrected for atmospheric effects.

Finally, the sea surface temperature images were registered to control points taken from the CZCS image so that the two images could be co-registered (superimposed).

Albacore catch data were obtained from daily logs submitted by fishermen. The catch data for periods from two days before to two days after each pair of satellite passes were plotted on the temperature and phytoplankton pigment images.

Results and Conclusion:

The results clearly showed the existence of a relationship between oceanic fronts and albacore distribution. Shoreward intrusions of oceanic water were particularly favourable sites for albacore aggregation. The results also showed that, in offshore water, commercial concentrations of albacore were associated with oceanic boundaries marked by colour fronts resulting from phytoplankton distribution and concentration, but without sea surface temperature gradients. Thus phytoplankton concentration seemed to be at least as important as temperature in explaining and predicting the occurrence of albacore (refer to Figures 8.19 and 8.20).

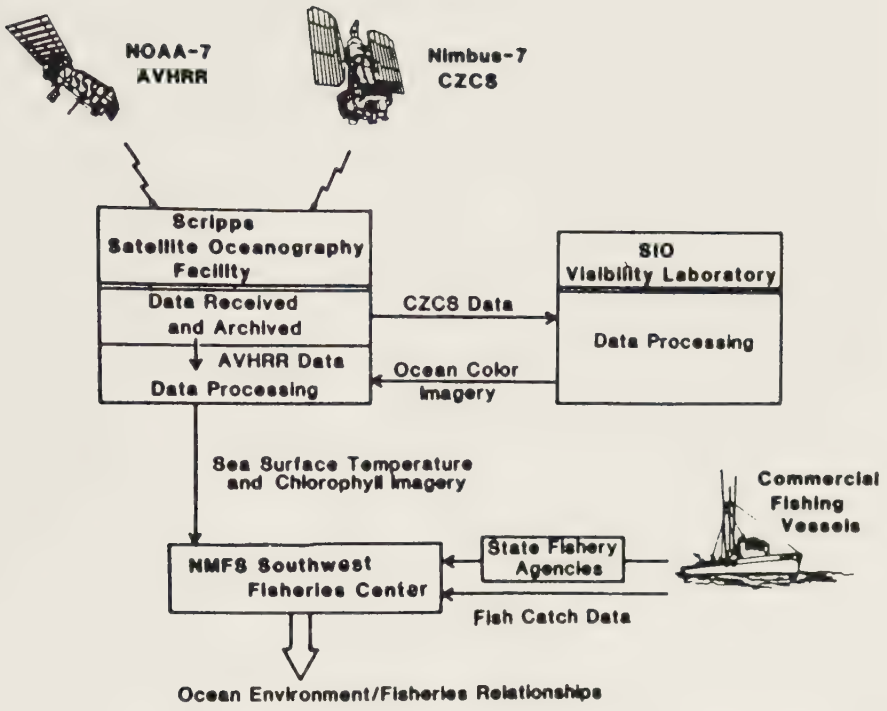

Figure 8.18 Satellite data collection and processing network utilized by US National Marine Fisheries Service (Southwest Fisheries Centre).

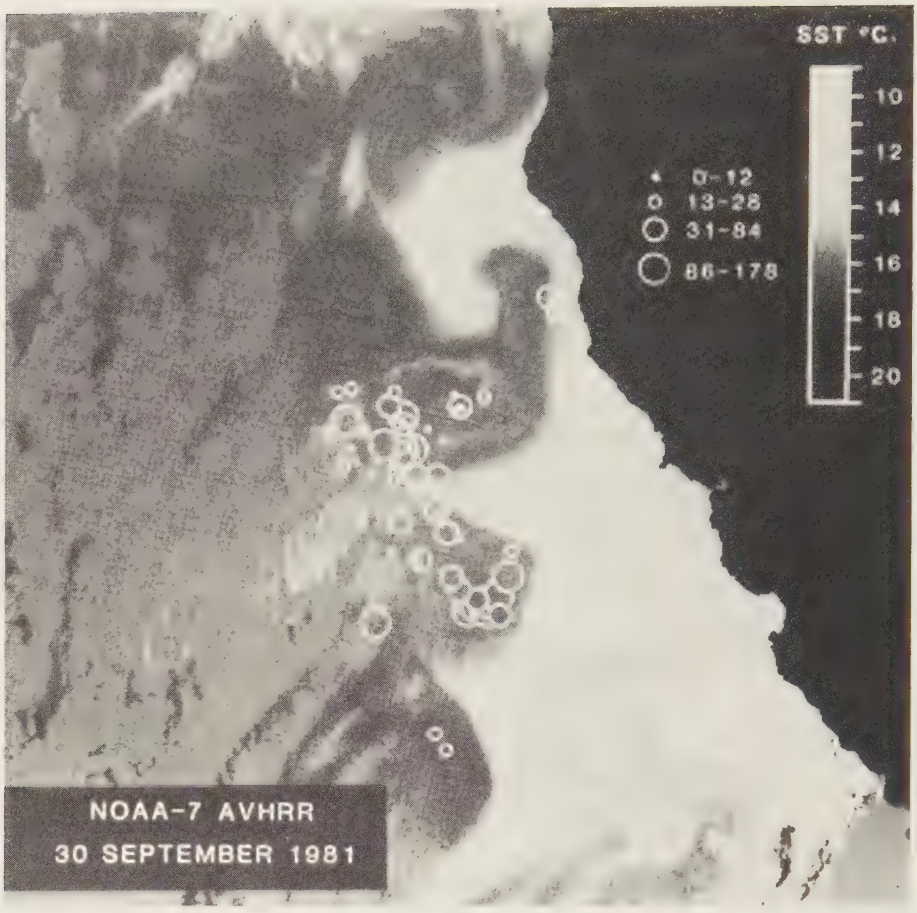

Figure 8.19 Central California daily albacore catches, 27 September to 2 October, 1981, superimposed on the NOAA-7 AVHRR sea surface temperature, 30 September, 1981, 14:02 PST.

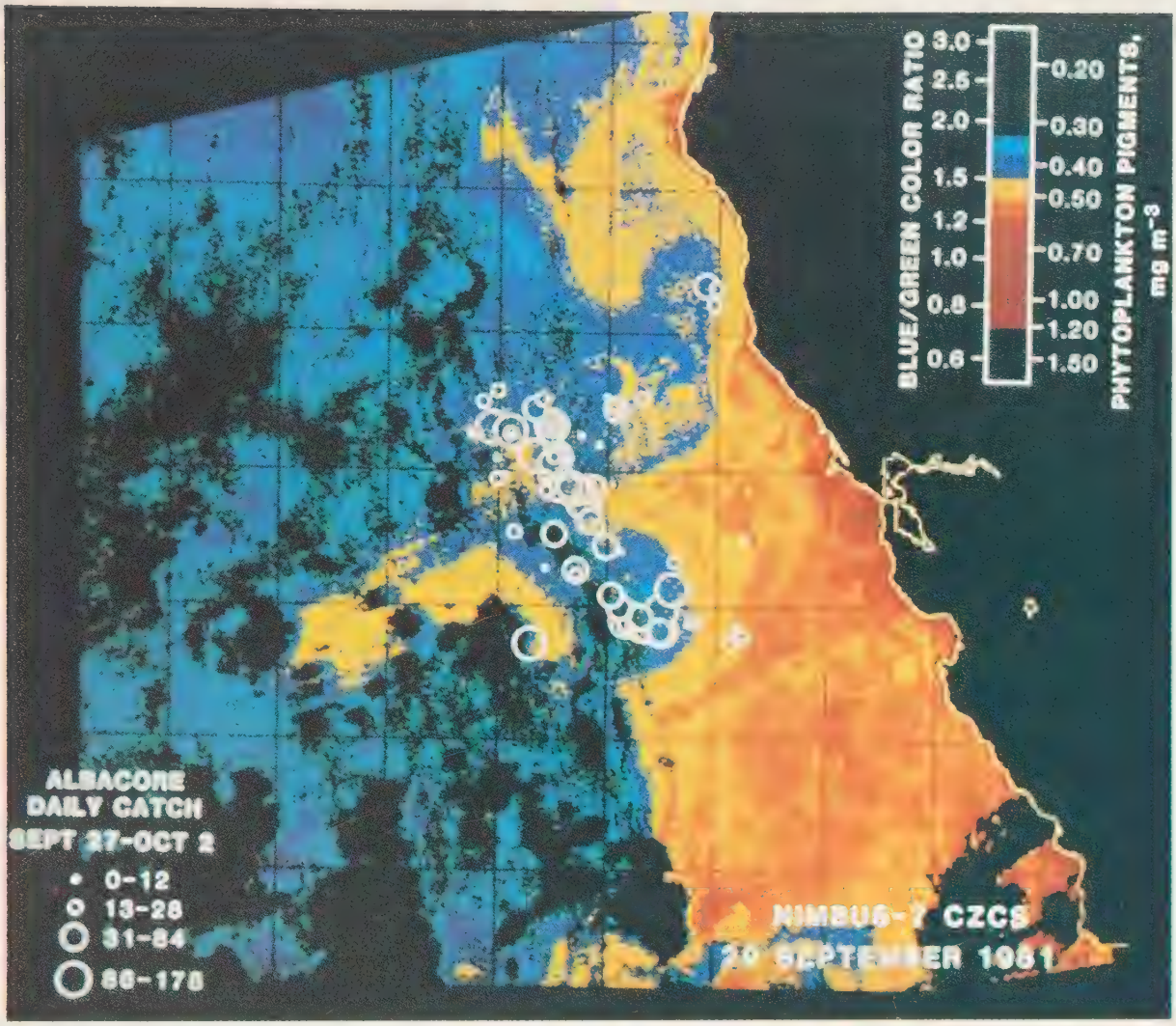

Figure 8.20 Central California daily albacore catches, 27 September to 2 October, 1981, superimposed on the NIMBUS-7 CZCS blue-green colour ratio and phytoplankton pigment concentration, 29 September, 1981, 11:30 PST.

8.11 Case Study No. 11

Reference: Montgomery, D.R. et al., 1986, The applications of satellite-derived ocean color products to commercial fishing operations. Marine Technology Society Journal, 20(2):72-86

Remote Sensing Technique: Satellite Remote Sensing:
Platform - NIMBUS-7;
Sensor - CZCS.

Objective: To assess the utility and benefit of specially prepared environmental charts designed for commercial fishing operations.

Experimental Rationale: It appears that ocean colour and sea surface temperature data are complementary in defining the environmental limits of the distribution of albacore tuna, Thunnus alalunga. Satellite-derived data can provide a wide geographic and synoptic coverage in comparison to that obtained by ship or aircraft.

Method: The CZCS data from the NIMBUS-7 satellite were received and processed by the Scripps Satellite Facility in California. The image pre-processing steps included atmospheric correction, blue/green ratio image creation and resampling to Mercator projection. Data analysis involved the identification of water masses, the creation of a false-colour composite and, finally, the production of boundary charts from the interpreted image.

Since the transmission of colour facsimile is a complex and expensive process, the data were converted to a black and white chart, and annotated with water type codes (refer to Figure 8.21). Water colour information, so obtained, was integrated with other fisheries-aid charts which were prepared by meteorologists/oceanographers working from a variety of sources (refer to Figure 8.22). Fishermen were able to obtain these data by mail or by radio transmission (facsimile and voice).

Results and Conclusion: The program demonstrated that conventional and satellite-derived data on the marine environment, when properly combined and correlated, can offer to the commercial fisherman tactical tools which can result in the selection of fishing strategies for more efficient and economical operations. This program found limitations in operation due to inconsistent CZCS coverage caused by satellite programming and cloud cover. Other problems were related to the high cost of preparation of the ocean colour charts (approximately $1000 each) and to the difficulty of transmitting the charts by high frequency radio to the near shore regions.

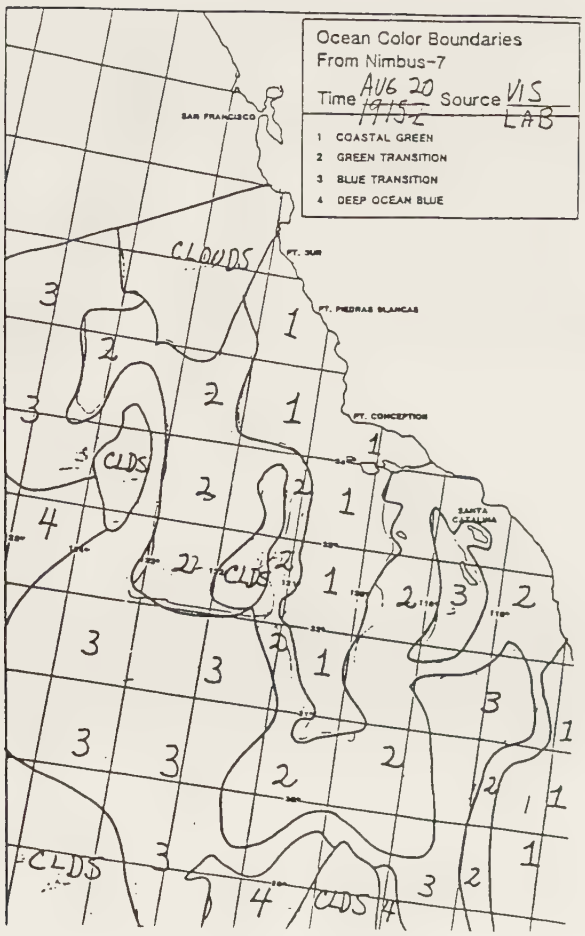

Figure 8.21 Chart forwarded by telecopier to radio facsimile broadcast stations for subsequent transmission to participating fishing vessels.

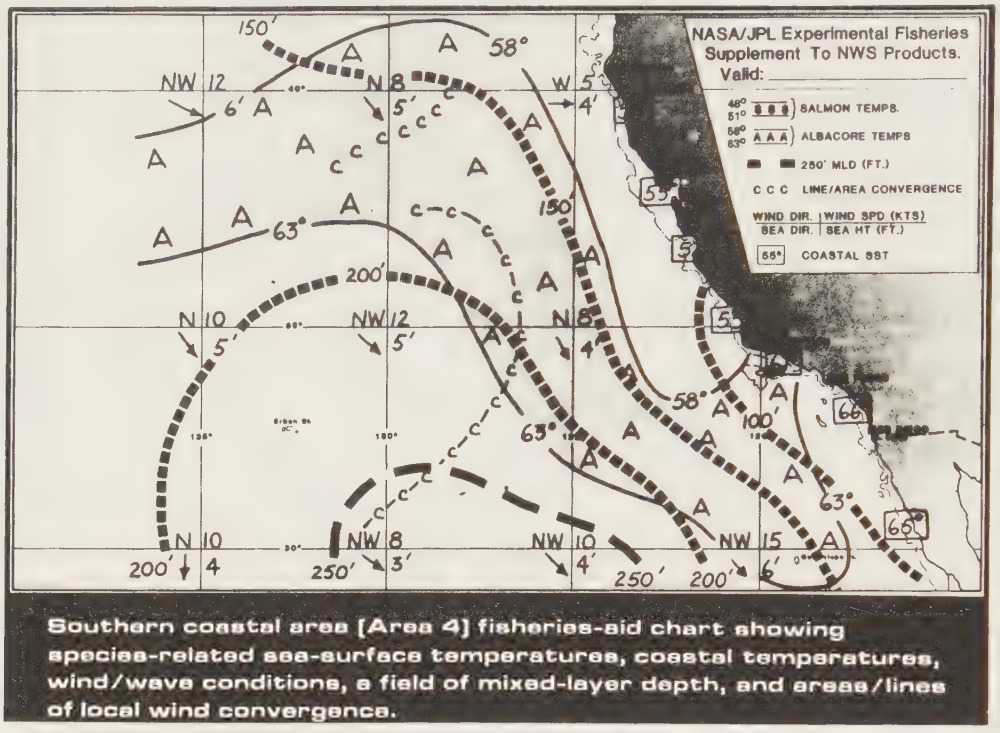

Figure 8.22 Representative chart generated as part of fisheries demonstration effort.

8.12 Case Study No. 12

Reference:

Feldman, G.C., 1986,
Variability of the productive habitat in the Eastern Equatorial Pacific. EOS Transactions, American Geophysical Union, 67(9):106-8

Remote Sensing Technique:

Satellite Remote Sensing:
Platform - NIMBUS-7;
Sensor - CZCS.

Objective:

To show that satellite ocean colour data can be used to define the spatial extent of the region of enhanced biological production (productive habitat) in the eastern equatorial Pacific (refer to Figure 8.23). To determine the degree of interannual variability in the areal extent of the productive habitat and in the estimated primary production of the region.

Experimental Rationale:

The changes in ocean colour detected by the CZCS provide a quantitative measure of phytoplankton pigment concentrations in the surface layer of the ocean. These concentrations are an index of phytoplankton biomass and may be empirically related to primary production. Examination of a series of large-scale images, covering the entire eastern equatorial Pacific, allows the determination of the temporal and spatial scales of oceanic processes and of the resulting variability in the distribution and abundance of phytoplankton. Phytoplankton represent the first link in the food chain and their patterns of distribution in time and space may indicate how oceanographic processes regulate primary production.

Method:

A sequence of CZCS scenes was processed to derive images of chlorophyll-like pigment concentration coregistered to a uniform spatial grid covering the eastern equatorial Pacific region. Subsequently, these images were composited to produce seasonal mean pigment maps for the 1978-79, 1979-80 and 1982-83 winter periods. Finally a comparison of the results obtained for each of these three periods was made with reference to previous descriptive and modelling studies of the eastern equatorial Pacific environment.

Results:

Significant coherence in the distribution and abundance of phytoplankton was found, in both time and space, within each of the three periods considered. The primary production estimates from the CZCS data show a close agreement with those from ship sampling obtained in the same periods. The time/space composite images retain the major features observed during each period and appear to be the best means for quantifying the high degree of interannual variability evident from the imagery. This interannual signal was found to be greater than that observed over the shorter time scales involved in constructing the seasonal composites. Surprisingly, the largest variability occurred between

the 79-80 period and the other two periods, i.e. 78-79 and 82-83, which actually have similar characteristics in spite of the El Nino event of the 82-83 period (refer to Figure 8.24). In the 79-80 winter, the area classified as productive habitat (pigment concentrations greater than 1 mg/cu.m) was about one order of magnitude larger than in the other two winters, reaching almost 30% of the study area versus 3-10% in 78-79 and 82-83 respectively. Therefore, the major question raised by this study does not revolve around El Nino, but rather in trying to understand the reasons for the variability between 78-79 and 79-80, since in these periods the conditions throughout the region have been characterized as being close to normal (refer to Figure 8.25).

Conclusion:

This work demonstrates the potential of remotely sensed pigment measurements for the assessment of primary production and productive habitat extent on a regional or even global scale. For the eastern equatorial Pacific, there is evidence that there may be significant large-scale oceanic and atmospheric differences even when El Nino type phenomena are not active. Variations in the strength, location and timing of intensified undercurrent flows (e.g, the Equatorial and Peru Undercurrents) could alter the large-scale patterns of vertical mixing and nutrient input, i.e. upwelling along the Peru coast, thereby influencing phytoplankton production and the fish population sustained by this production. Perhaps the system is periodically purged. Low primary production during certain periods of time results in a significant reduction in the abundance of herbivores such as copepods and anchovies. The associated reduction in grazing pressure would then allow a large increase in planktonic abundance if accompanied by sufficient nutrient levels. A "boom and bust" type of cycle could then be established in the ecosystem of the region. The quantitative information derived from the satellite images allows the primary production to be estimated for the entire study area, as well as the production arising from specific regions. The repetitive character of the information makes it possible to follow the evolution of this production. Marine resource exploitation strategies may be identified by such analyses.

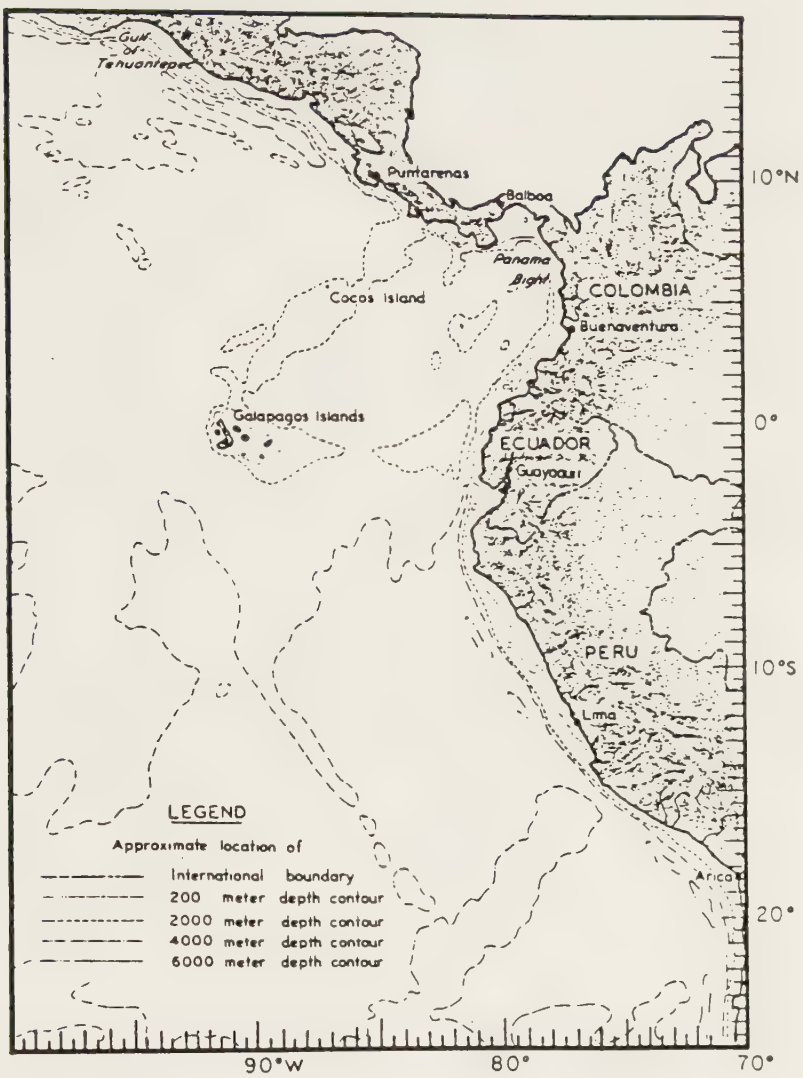

Figure 8.23 Map of the eastern equatorial Pacific Ocean, showing the major features of the submarine bathymetry.

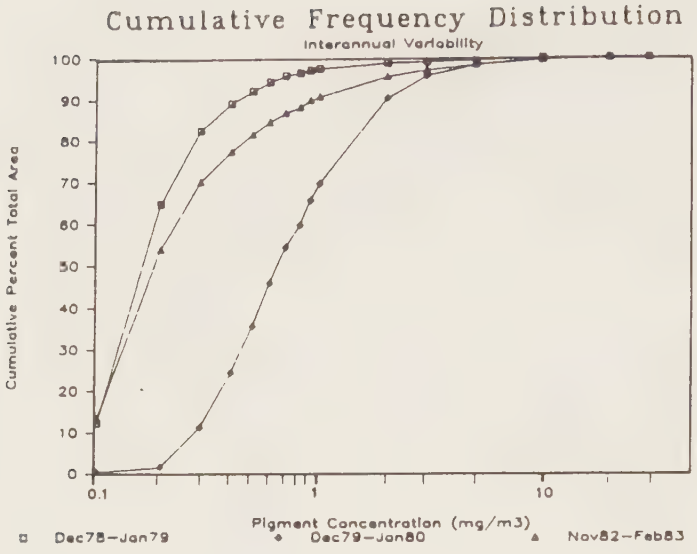

Figure 8.24 Cumulative frequency distributions of satellite-derived phytoplankton pigment concentrations (in milligrams per cubic metre) versus the percentage of total cloud-free surface area covered by each concentration range for the eastern equatorial Pacific, as observed by the CZCS.

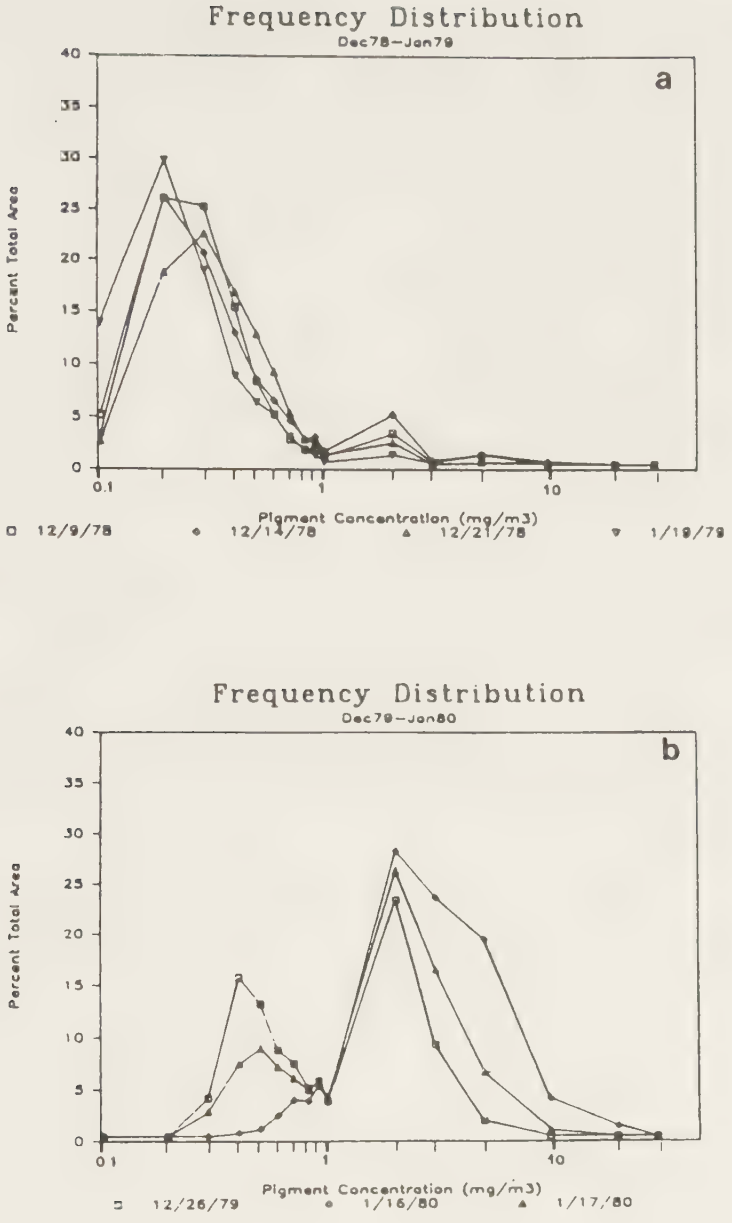

Figure 8.25 Frequency distributions of satellite-derived phytoplankton pigment concentrations (in milligrams per cubic metre) versus the percentage of total cloud-free surface area covered by each concentration range for the region 0^{o}-10^{o}S, 87^{o}-78^{o}W, as observed by the CZCS.

8.13 Case Study No. 13

Reference: Barale, V. et al., 1986, Space and time variability of the surface color field in the Northern Adriatic Sea. J.Geophys.Res., 91(C11):12957-74

Remote Sensing Technique: Satellite Remote Sensing:
Platform - NIMBUS-7;
Sensor - CZCS.

Objective: To investigate the variability of the surface bio-optical field in terms of phytoplankton pigment concentration derived from CZCS data and its correlation with possible steering factors, over the entire northern Adriatic basin at interannual, seasonal and monthly scales.

Experimental Rationale: A time series of corrected, coregistered CZCS images can be used to provide some simple statistics of the surface colour field, describing the heterogeneity of phytoplankton distribution. The patterns of primary productivity have spatial and temporal characteristics associated with the main oceanographic properties of a basin such as the Northern Adriatic Sea. By comparing these patterns with a suite of environmental factors, it is possible to investigate their relationship and the conditions and processes which regulate food chain dynamics.

Method: The available CZCS data for 1979 and 1980 were used to construct a two year time series of Northern Adriatic Sea visible imagery. The original images were corrected for atmospheric contamination, processed into maps of chlorophyll-like pigment concentration and remapped to a standard geographical grid with a pixel resolution of about 1 km X 1 km. This allowed the derivation of yearly and monthly mean and standard deviation images and of two image sequences suitable for empirical orthogonal function analysis. These statistics were compared with analogous statistics of air temperature, wind velocity and coastal runoff. In particular, quantitative estimates of the spatial scale of high pigment concentration patterns, derived from the monthly averaged images, were correlated with the corresponding averages of outflow from the major river (the Po) entering the Northern Adriatic Sea. The results were interpreted in terms of the established oceanographic knowledge of the basin and of numerical modelling and laboratory experiments.

Results: The phytoplankton pigment concentrations derived from CZCS data exhibited a high correlation with sea truth measurements performed during seven surveys in the summer of both years. A comparison of the mean pigment fields from 1979 to 1980 indicates an increase in the concentration values and the spatial extent of coastal features (refer to Figure 8.26). This variability may

be linked to the different patterns of nutrient influx due to coastal runoff. The distribution of surface features is consistent with a general cyclonic circulation pattern, even though surface colour can not be considered a passive tracer of the flow in every instance. The pigment heterogeneity appears to be governed by fluctuations of freshwater discharge. The dominant wind fields do not appear to have important direct effects. The Po River discharge results in a plume which spreads over most of the northern basin with scales positively correlated with its outflow. The spatial scales of the western coastal layer in which the southward component of the cyclonic circulation is confined are instead negatively correlated with the Po River outflow and the plume scales (refer to Figure 8.27). Both results are consistent with theoretical and experimental results which indicate a dynamic balance between nonlinear advection and bottom friction, with the predominance of one of the two effects on an alternating basis.

Conclusion:

The analysis of time series of visible imagery can be a powerful tool for the assessment of ecological conditions and relationships in the marine environment. For the test site and for the two years considered in this study, the freshwater input from coastal runoff had a profound influence on the pigment field in addition to the thermohaline condition of the basin. The planktonic environment is significantly affected by both long and short term variations in runoff, possibly as a result of the associated variations of nutrient influx.

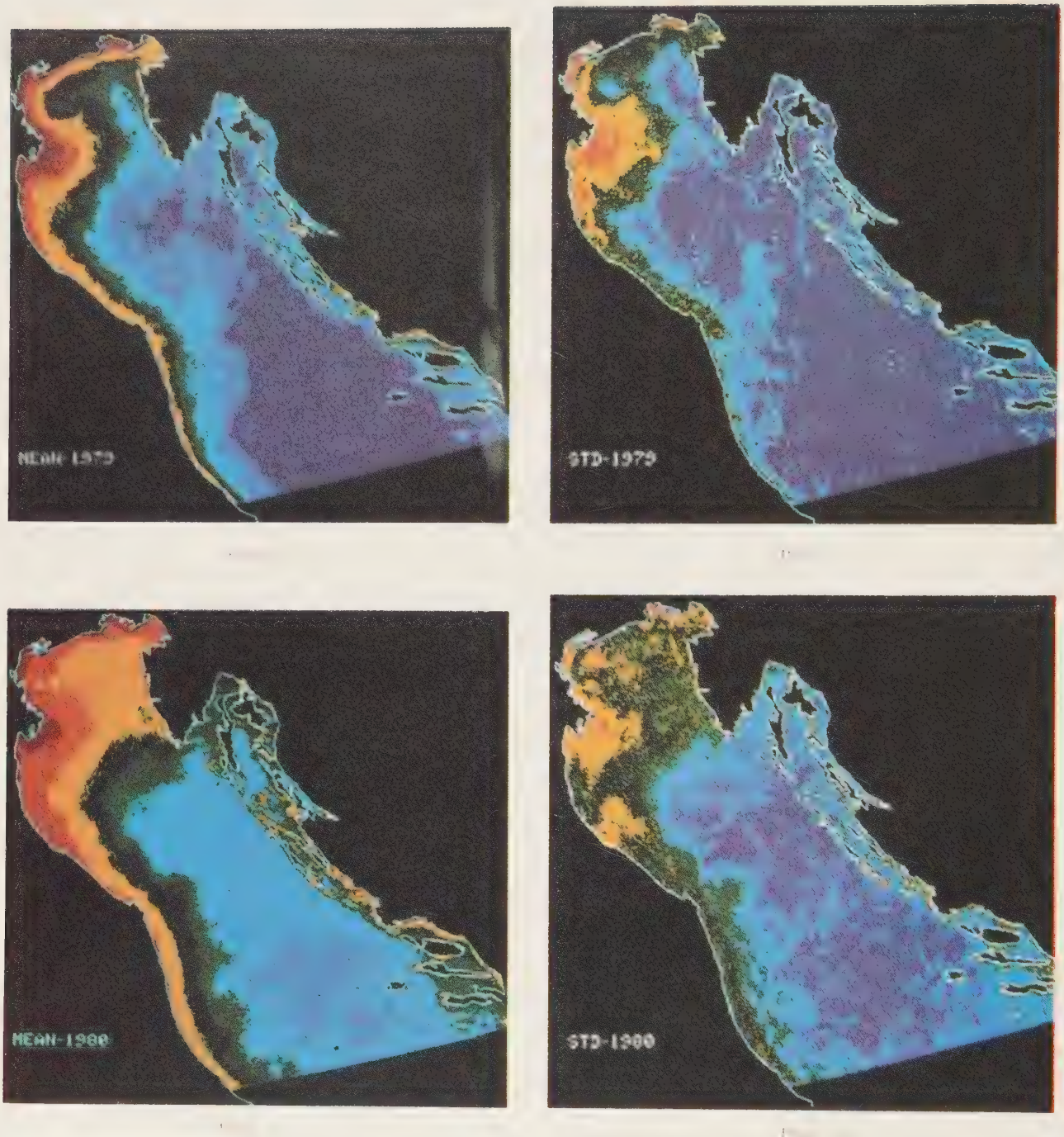

Figure 8.26 Average conditions of the surface colour field in the Northern Adriatic Sea: 1979 yearly (a) mean and (b) standard deviation of phytoplankton pigment concentration; 1980 yearly (c) mean and (d) standard deviation of phytoplankton pigment concentration. In all images, obtained from 35 individual CZCS scenes per year, high pigment concentrations (above 2 mg/cu.m) are shown in red; intermediate concentrations (between 1 and 2 mg/cu.m) in yellow and green; lower concentrations (below 1 mg/cu.m) in shades of blue.

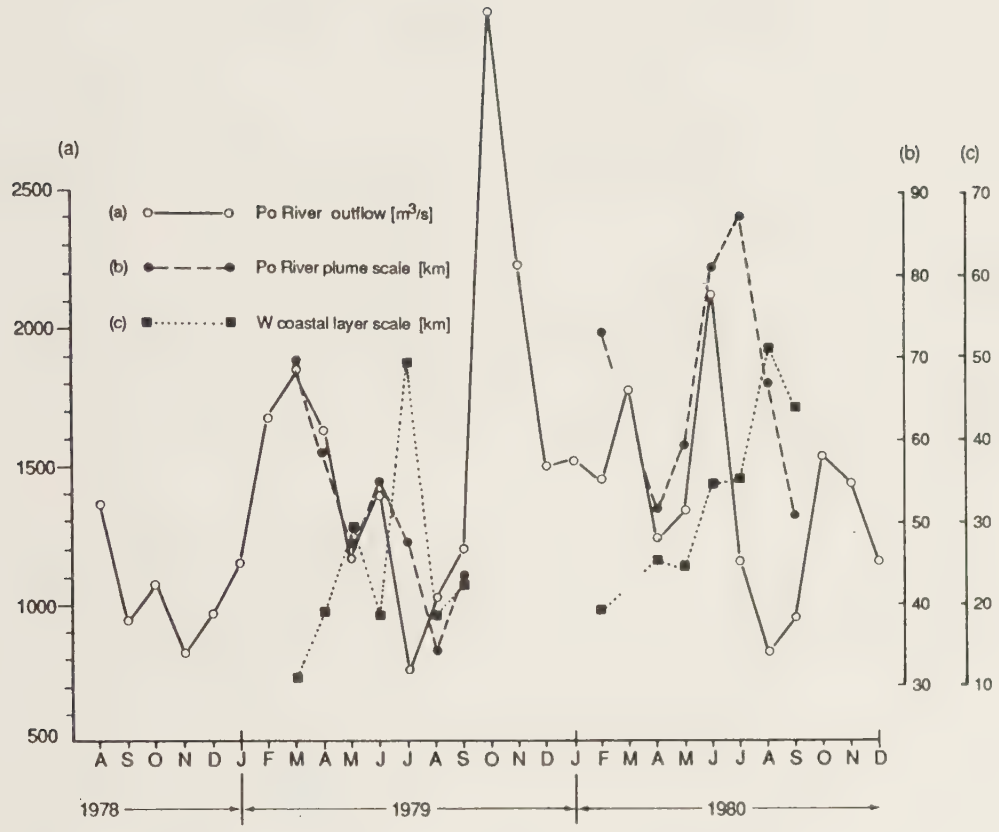

Figure 8.27 Comparison of monthly averaged Po river outflow (in cubic metres per second) with Po river plume scale and western coastal layer scale (in kilometres) for the period from August 1978 to December 1980. The scales of surface colour features are indicative of regions with very high phytoplankton pigment concentrations (above 1 mg/cu.m).

8.14 Case Study No. 14

Reference: Pringle, J.D. and R.E. Duggan, 1983, A remote sensing technique for quantifying lobster fishing effort. Can.Tech.Rep.Fish.Aquat.Sci., 1217:16 p.

Remote Sensing Technique: Airborne Remote Sensing:
Platform - Aircraft (Aztec Pa-23);
Sensor - Aerial Camera.

Objective: To determine the lobster fishing effort in the Scotia-Fundy region of Atlantic Canada with the aid of colour aerial photography.

Experimental Rationale: The lobster fishing effort was considered to be proportional to the number of traps in use for a given time period and area. The number of traps had a direct relationship to the number of buoys to which they were attached (1:1 in the present study). The brightly coloured buoys could be identified in colour aerial photographs.

Method: Based on the results of a series of trials, it was decided to utilize colour positive film at an altitude of 915 metres (3000 ft), giving the photographs a scale of 1:6,000 and a coverage of 1,840.2 square metres. A 2 km stretch of coastline along St. Margaret's Bay, Nova Scotia, was photographed using a Fairchild K-17 aerial camera with a 15.24 cm lens and a Kodak HF-3 filter. A surface survey of buoys was also conducted for ground verification. Using a back-lit digitizing table, buoys identified on the photographs were digitized and mapped with a Geographic Information System (refer to Figure 8.28).

Results: There was a difference of 28.5% between ground truth and aerial photograph counts; this was attributed to poor weather conditions. In areas where weather was favourable the error was reduced to 11.3%.

Conclusion: Aerial photography using a Fairchild K-17 or Wild RC-8 camera with a 15.24 cm lens, Kodak no. 2448 colour positive film and a Kodak HF-3 filter gave sufficient resolution to detect buoys when the maximum altitude flown was 915 metres and the sun angle was less than 25°.

Recommendations:

1. Flights should be made during calm weather conditions to minimize error.

2. An evaluation of the test area to identify other fisheries using the same type of buoys should be made.

3. This technique is appropriate for spot-checking critical geographic areas because of its accuracy, rapidity and aerial coverage. The cost, however, is relatively high.

Figure 8.28 Map of buoy locations - actual fishery.

8.15 Case Study No. 15

Reference:

Bour, W., L. Loubersac and P. Rual, 1986, Thematic mapping of reefs by processing of simulated SPOT satellite data: application to the Trochus niloticus biotope on Tetembia Reef (New Caledonia). Mar.Ecol.Prog.Ser., 34:243-9

Remote Sensing Technique:

Airborne Remote Sensing:
Platform - Aircraft (Simulated SPOT);
Sensor - Deadalus radiometer (Simulated HRV).

Objective:

To determine the potential stock size of Trochus (Trochus niloticus) by means of an assessment of the areal extent of its coral habitat.

Experimental Rationale:

Exploitation of Trochus (Trochus niloticus) is important to Pacific Islanders. The shell yields valuable mother-of-pearl of which 2000 tons were exported from New Caledonia in 1978. Knowledge of the exploitable stock requires a good estimate of the surface area occupied by this gastropod. Trochus live in shallow water on reef flats consisting of dead coral slabs with many crevices and scattered coral rubble. This bottom type can be found on most of the reef formations in the lagoon (fringing reef, inner lagoon reef and barrier reef). The environment inhabitated by trochus stocks represents a large portion of the 20,000 km^2 of the New Caledonia lagoon. It is, however, difficult to access and synoptic methods of estimation are required such as SPOT.

Method:

In December 1983 the Groupement pour le Développement de la Télédetection Aérospatiale (GDTA) coordinated a SPOT Simulation Program focussed on New Caledonia. In addition to observation of reef environments, the program included bathymetric studies, identification of aquaculture sites and geological studies.

SPOT, launched into sun-synchronous orbit in February 1986, passes vertically over New Caledonia every 26 days at 10:15 local solar time. Because of off-nadir viewing the same area (60 X 60 km^2) of the equator can be targeted 7 times during the 26 day cycle. Simulated SPOT imagery, recorded before the launching of the satellite, was achieved by radiometric methods using an airborne Deadalus radiometer. These data were restructured to give a radiometry equivalent to that of the HRV channels.

The different spectral responses of the four channels are used to discriminate the different reef types:

Channel 1	0.50 - 0.59 green	20 m resolution
Channel 2	0.61 - 0.69 red	20 m resolution
Channel 3	0.79 - 0.89 (near IR)	20 m resolution
Channel 4	0.51 - 0.73 panchromatic	10 m resolution

The green and red channels penetrate water to various depths; they are used together to differentiate underwater features at depths of 0 to 5 metres. At greater depths only Channel 1 (green) allows bottom types to be discriminated. The high resolution panchromatic channel provides morphological details.

A first classification defined 5 classes of pixels. Ground verification and reference to black and white aerial photographs supported these 5 general themes and areas (refer to Figure 8.29).

The pixels of the class identified as reef flat or hard bottom covers were then isolated, analyzed by principal components and classified. Five bionomic themes were identified and corroborated by ground verification (refer to Figure 8.30).

Conclusion:

The processing of simulated SPOT image data successfully located the trochus biotope and permitted the calculation of the surface areas with reasonable precision. The repetitiveness of current SPOT coverage will permit the monitoring of habitat changes with time.

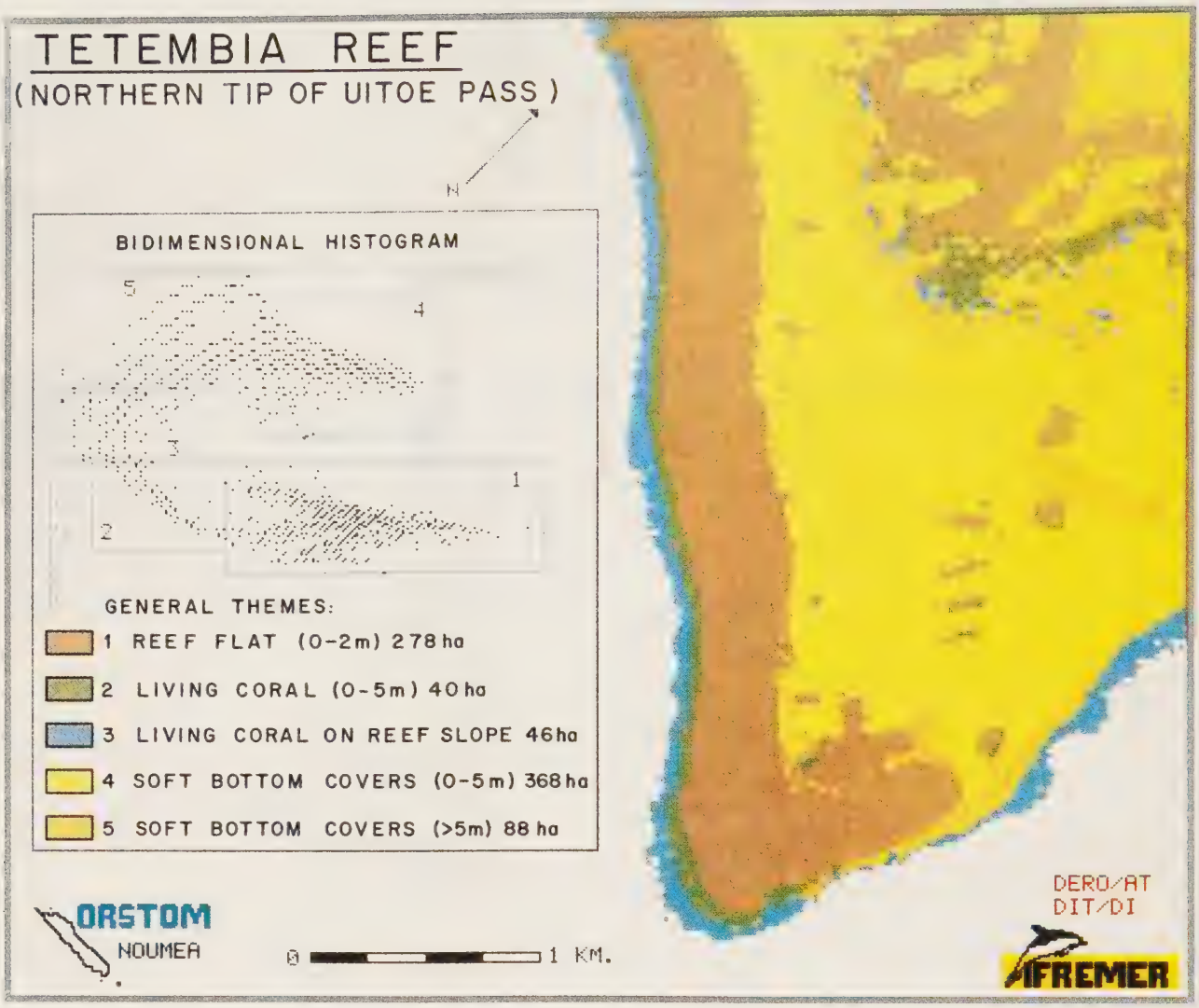

Figure 8.29 Tetembia reef: general themes.

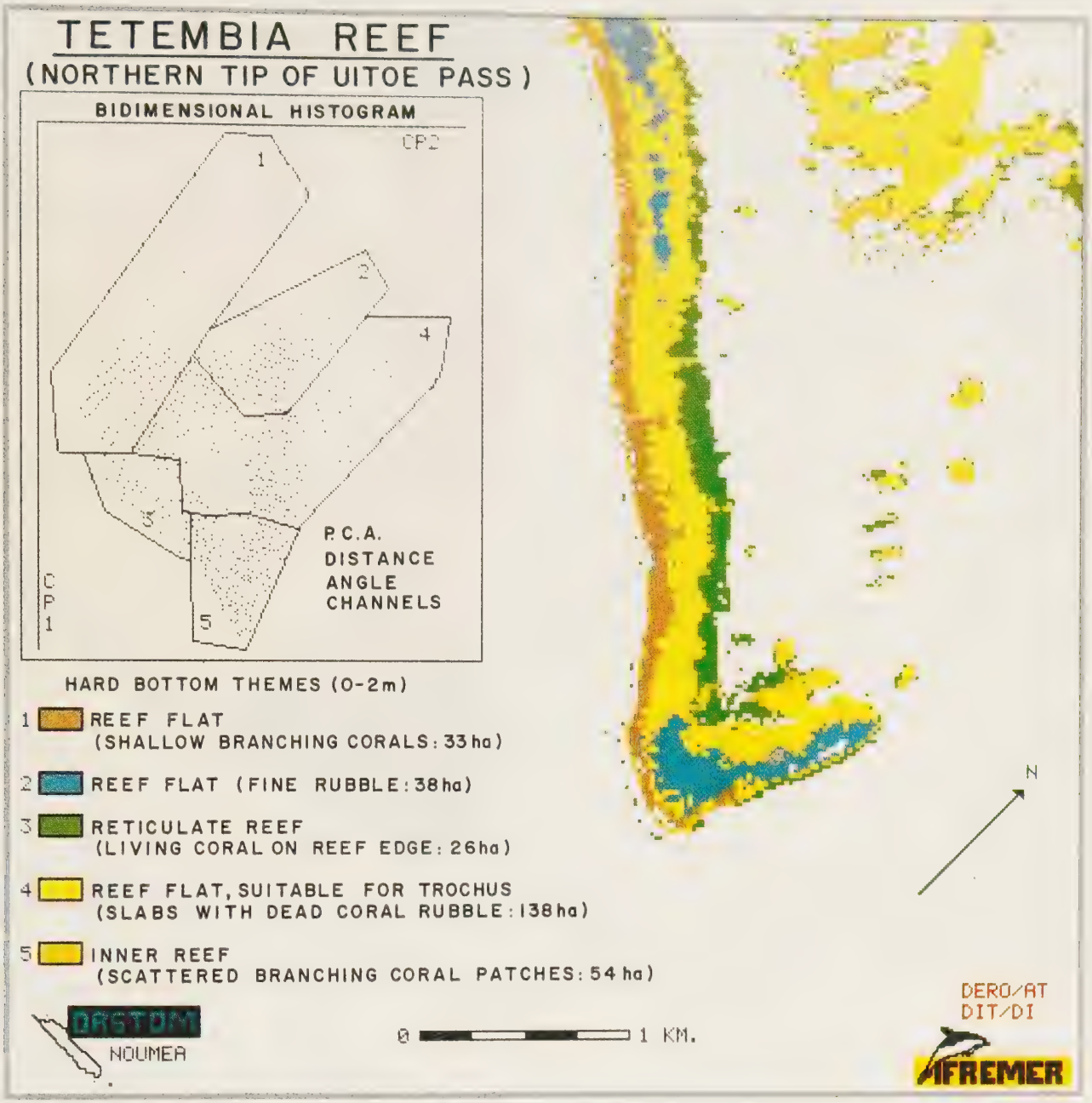

Figure 8.30 Tetembia reef: hard bottom themes.

8.16 Case Study No. 16

Reference: Jensen, J.R. et al., 1980, Remote sensing techniques for kelp surveys. Photogramm.Eng.Remote Sensing, 46(6):743-55.

Remote Sensing Technique: Satellite and Airborne Remote Sensing: Platforms - Aircraft, LANDSAT, SEASAT; Sensors - Aerial Camera, X-Band Radar, LANDSAT MSS, L-Band SEASAT Radar.

Objective: To survey and monitor giant kelp resources off the California coast, with images obtained from LANDSAT, MSS, CIR photography, X-band airborne radar and L-band SEASAT radar.

Experimental Rationale: The spectral signature of healthy Macrocystis pyrifera (kelp) was found to be similar to that of terrestrial orange brown vegetation. In the visible region of the electromagnetic spectrum, chlorophyll absorption in the green band was apparent with slightly greater reflectance in the blue and red. Kelp reflects 60-70% of the incident radiant flux in the region between 0.7-11.0 micrometres. In contrast, water absorbs the majority of infrared radiation flux in this region, thus providing a good contrast between kelp and water.

The sensors which are sensitive to the spectral difference between kelp and water include normal colour and colour infrared (CIR) photography and multispectral scanning systems. Radar can also be used to discriminate kelp beds from the ocean, provided there is a difference in either surface roughness or dielectric constant between the two classes. Kelp normally exhibits a vertical relief of approximately 1 to 2 cm above the water surface while calm glassy ocean attains a surface relief of about 0.1 to 0.3 cm. It is hypothesized that this difference in surface roughness is sufficient to discriminate between kelp and water at certain radar wavelengths.

Method: During the period from 1975 to 1977 a base line inventory of kelp beds was obtained on a quarterly basis with the aid of 70 mm large-scale (1:24,000) colour photography and CIR vertical aerial photography. In this study high altitude CIR photographs (1:125,000) were obtained also from a NASA U-2 aircraft. The dates of the high altitude photography were chosen to coincide as nearly as possible with the dates of the large-scale inventories.

LANDSAT imagery was obtained on a repetitive basis for 18 days and classification procedures were conducted to discriminate kelp areas from water.

An important advantage of microwave remote sensors over other types is their ability to image through fog. An extensive radar survey of the marine target was conducted with X-band horizontally polarized radar at a

height of 6,500 feet. A vertically polarized X-band synthetic aperture radar system, equipped with 16 ft and 8 ft antenna, was also flown simultaneously at 5,500 feet.

SEASAT-A images also were analysed for the detection of kelp beds.

Results:

The kelp bed areas, calculated by means of low altitude photography, showed a very high agreement with those calculated by the high altitude photography. These results suggest that the analysis of high altitude CIR aerial photography can provide accurate measurement of kelp areal extent. The estimate derived from LANDSAT imagery was highly correlated with that of the aerial photography inventory.

The spectral nature of kelp and ocean was remarkably consistent in its clustering for three of the four LANDSAT images. The separation of kelp from ocean was due solely to the water penetration capability of band 4.

Kelp acreage statistics obtained from manual interpretation of X-band radar imagery provided relative accuracy. The synthetic aperture system, however, consistently yielded overestimates while the real aperture system yielded underestimates.

Conventionally derived kelp acreage statistics were not available for comparison with those obtained from SEASAT-A data. It was shown, however, that SEASAT radar signatures could be used for accurate kelp surveys.

The most striking difference between X and L band imagery was the signature reversal between kelp and ocean. In the X-band imagery kelp was bright and the water was dark whereas in the L-band imagery, kelp was dark and water was bright.

Conclusion:

This study showed that high altitude CIR photography (refer to Figure 8.31) and X-band radar imagery can provide areal extent data on kelp at approximately the same level of accuracy as conventional large-scale inventories.

LANDSAT data (refer to Figure 8.32) also provides accurate statistics if the consistent underestimation is corrected by using a simple linear equation. Given these results multispectral sensors in the 1980's offer potential for the operational monitoring of renewable kelp resources.

Figure 8.31 Example of high altitude CIR photography (original scale 1:125,000) and manually interpreted kelp acreage surveys on four dates.

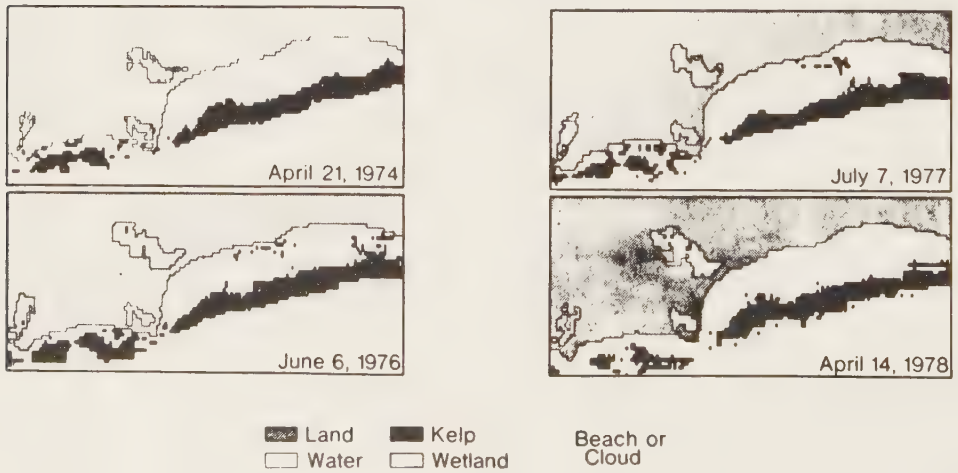

Figure 8.32 Kelp acreage surveys derived from four dates of LANDSAT image processing.

8.17 Case Study No. 17

Reference:

Belsher, T. and M. Viollier, 1984,
Thematic study of the 1982 SPOT simulation of Roscoff and the west coast of the Contentin peninsula (France). In Proceedings of the Eighteenth International Symposium on remote sensing of environment, Paris, France. Ann Arbor, Environment Research Institute, pp.1161-6

Remote Sensing Technique:

Airborne Remote Sensing:
Platform - Aircraft (Simulated SPOT);
Sensor - HRV.

Objective:

To give a quantitative evaluation of the seaweed cover and to determine the reliability of the technique for species differentiation.

Experimental Rationale:

The SPOT HRV (Haute Résolution Visible) sensor is primarily designed for land observation. Seaweed species in the intertidal zone, like land vegetation, may be classified according to their particular spectral reflectances. The spatial resolution of the HRV (20m) permits discrimination of relatively small seaweed patches.

Method:

The interval zone was initially isolated for analysis by the removal of water and land data from the imagery. Water has a very low reflectance in the near-infrared and the corresponding pixels are recognized by simple thresholding on channel 3 (790-890 nm). For land, interactive operations were required to superimpose the shoreline from accurate charts.

A derived image was generated by computing a vegetation index I_V =

$$I_V = \frac{CH_3 - CH_2}{CH_3 + CH_2} \qquad \begin{matrix} CH_2 \ (610 - 680 \text{ nm}) \\ CH3 \ (790 - 890 \text{ nm}) \end{matrix}$$

where CH_2 and CH_3 referred to the raw data of the corresponding channels. Thereafter, thresholding of this image lead to the identification of the algae production zone since non-vegetation pixels were characterized by very low relative values of this index.

A principal component transform was performed on raw data of the seaweed production zone on channel 3 to identify clusters of pixels of similar spectral signature. Then these spectral signatures were linked to individual species or dominant vegetation types by correlation with ground observed data.

Conclusion: The above vegetation index could provide an estimate of seaweed cover for a SPOT pixel area. Principal component analysis permits identification of five to six species. Refer to Figure 8.33 which shows the study areas after digital processing. The colours may be interpreted as follows:

green = Fucus (vesiculosus and serratus)

blue = Ascophyllum nodosum

yellow = Sargassum muticium

orange = Ulva and Enteromorpha

brown = Pelvetia canaliculata

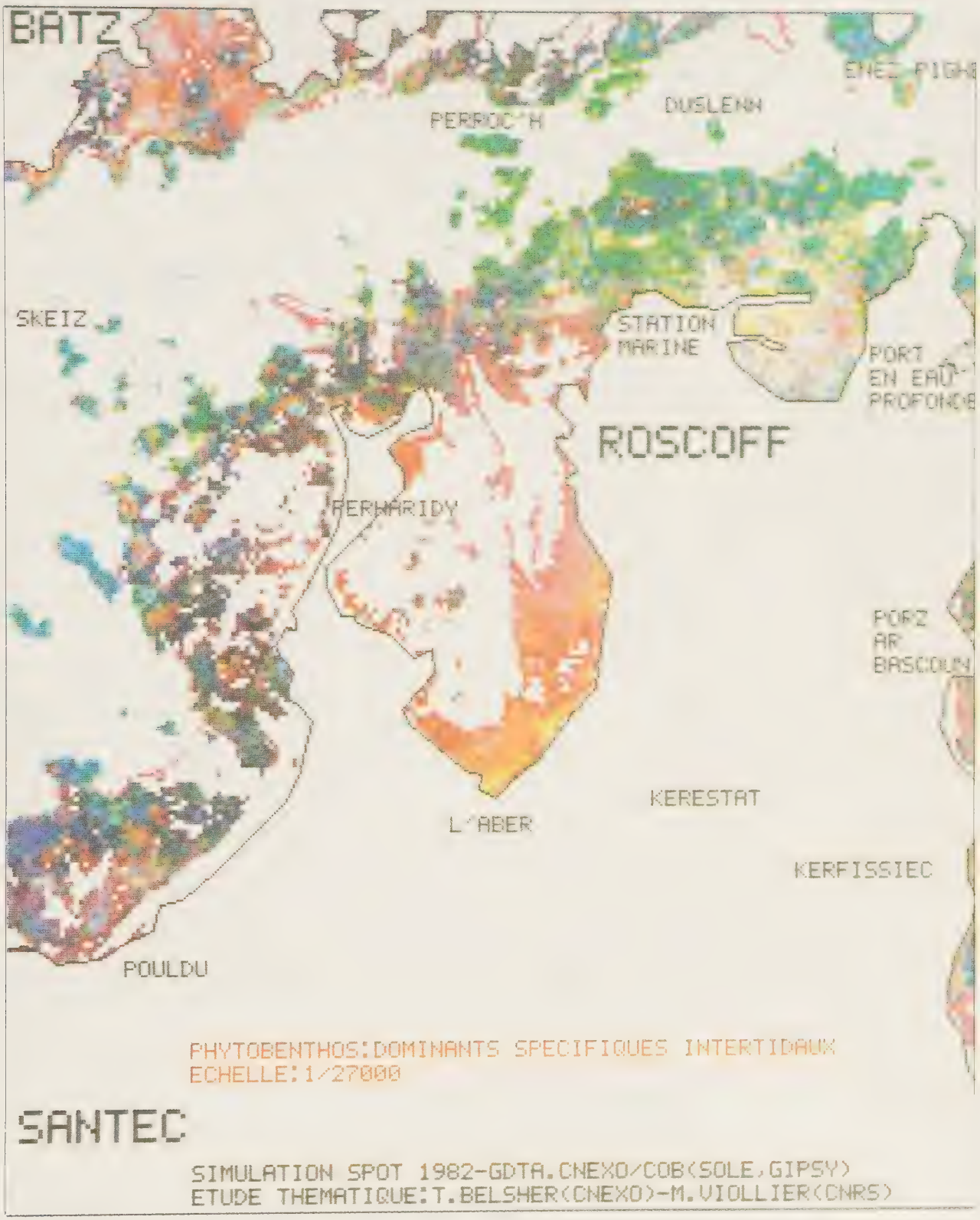

Figure 8.33 Digital processing of SPOT image. Each colour represents a particular type of seaweed.

8.18 Case Study No.18

Reference: Armstrong, R.A., 1983, Marine environments of Puerto Rico and the Virgin Islands: automated mapping and inventory using LANDSAT data. Caribbean Fishery Management Council, 37p.

Remote Sensing Technique: Satellite Remote Sensing:
Platform - LANDSAT;
Sensor - MSS.

Objective: To explore the possibility of discriminating marine communities of Puerto Rico and the Virgin Islands with LANDSAT imagery.

Experimental Rationale: The different spectral signatures associated with submerged plant life and reefs in coastal seas can be utilized to differentiate marine communities.

Method: LANDSAT imagery with less than 30% cloud cover was analyzed to discriminate coral reefs and other large marine communities for Puerto Rico and the Virgin Islands.

It was shown that a change in sensor mode from low gain to high gain caused a 25% increase in water penetration power from 6 m to 8 m.

The digital imagery used in marine community classification was subjected to preprocessing procedures to eliminate the distortions caused by atmospheric attenuation (radiometric distortion) and curvature of the earth (geometric distortions).

Supervised classification with user-defined training areas was carried out for images of St. John where up-to-date bathymetric and topographic maps were available for selection of training areas. The sea around St. John was classified into 6 regions using a digital image analysis system. Utilizing the spectral signatures obtained from the St. John image the sea around Culebra and Vieques was then classified into 5 regions, St. Croix into 7 regions and Puerto Rico east and north into 6 regions each.

Results: The sea around St. John was classified as follows (refer to Figure 8.34):

Water Class 1- deep water 18-31 m;
Water Class 2- 18 m contour;
Water Class 3- 18 m contour with submerged vegetation;
Water Class 4- shallow sand bottom;
Water Class 5- fringing coral reef;
Water Class 6- coral reef at a depth of 4-6 m.

A certain degree of classification error was found in water class 4; although shallow sand bottom was correctly identified in the St. John area, coral reef crests were identified in this water class around St. Thomas, St. Croix, and Culebra.

The land classification was generally not successful although large vegetation areas of mangrove were accurately classified on Puerto Rico using hybrid supervised/unsupervised classification procedures.

Conclusion:

The resolution of LANDSAT MSS imagery was found to be adequate for the discrimination of large marine communities such as coral reefs. With low gain imagery, submerged features to a depth of 6 m could be classified accurately.

Recommendations:

1. Only high gain imagery with high quality band ratings for MSS-4 and MSS-5 should be used for studies of coastal environments and general marine use.

2. The initial classification run should be done in an area that is familiar to the user or with adequate ground truth information.

3. LANDSAT MSS data are useful for the study of large marine communities in the depth range of 0-5 m. Submerged features which are relatively small and submerged features which have deeper bathymetric ranges, however, will remain unclassified. In such cases a high-resolution airborne MSS with several narrow bands in the 0.4-0.7 micrometre range, or the Thematic Mapper which has three bands in the 0.4-0.7 micrometre range (versus only two in LANDSAT MSS) and a higher (30 m) resolution, should be used.

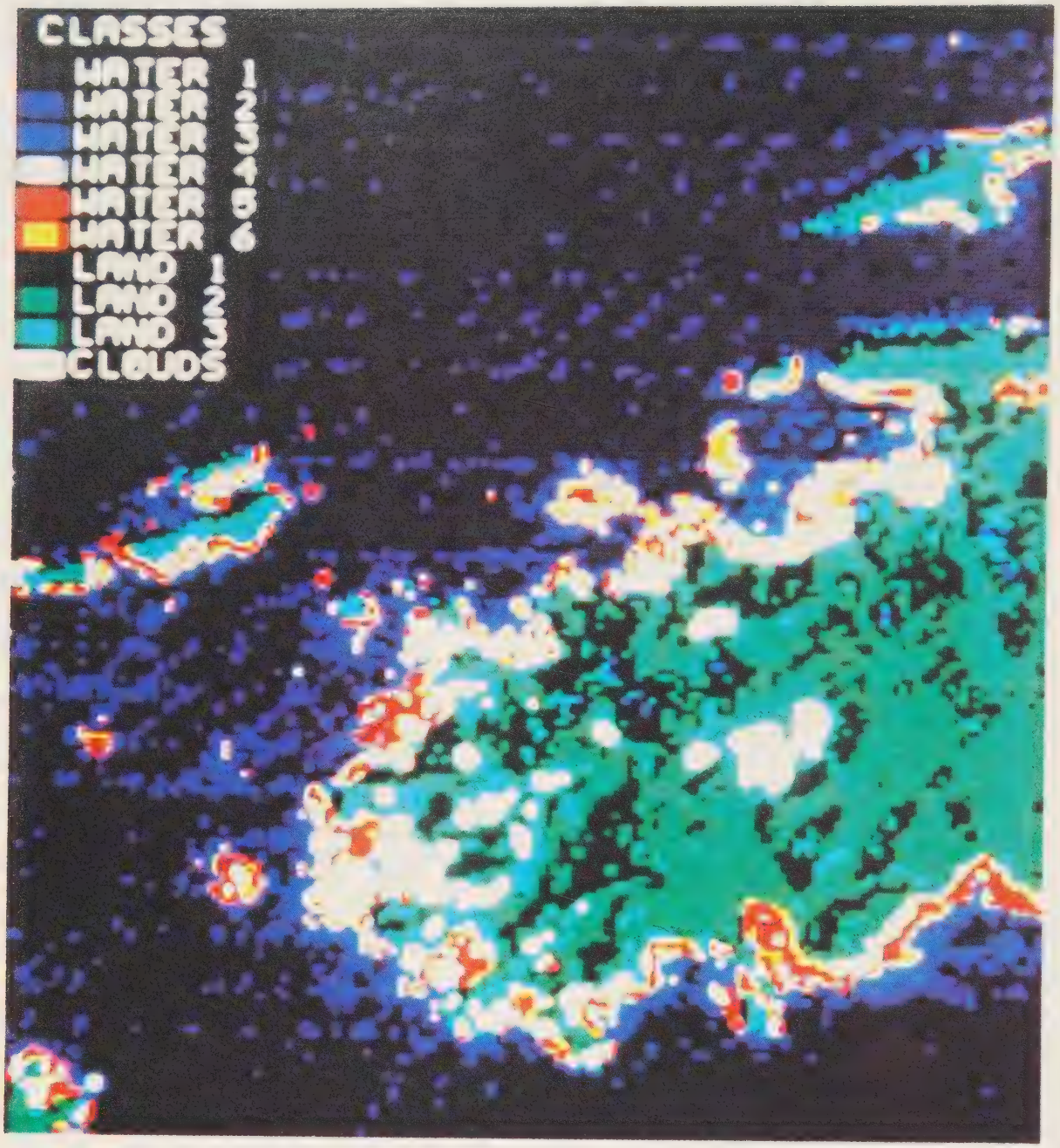

Figure 8.34 Classified image of St. John, US Virgin Islands.

8.19 Case Study No. 19

Reference:

Middleton, E.M. and J.L. Barker, 1976, Hydrographic charting from LANDSAT satellite: a comparison with aircraft imagery. In Oceans '76. Second combined conference, Marine Technology Society/Institute of Electrical and Electronics Engineers. New York, IEEE Inc. and Washington, D.C., MTS, (CH 1118-90 EC):6 p.

Remote Sensing Technique:

Satellite and Airborne Remote Sensing:
Platforms - LANDSAT-2, U-2 Aircraft;
Sensors - MSS, OCS (Ocean Colour Scanner).

Objective:

To identify, quantify and isolate depth information from other factors to permit study of superimposed transient phenomena such as red tide. In pursuit of this objective, an additional application of considerable merit, namely hydrographic mapping of coastal areas, was recognized.

Experimental Rationale:

Analysis of imagery produced by the MSS of LANDSAT-2 and OCS on a U-2 aircraft revealed that depth-related information represents the major contribution to the total recorded radiance in those satellite/aircraft sensor channels that are expected to be of most value for phytoplankton and sediment detection.

Method:

LANDSAT-2 imagery of the Gulf of Mexico and Tampa Bay were analyzed for hydrographic charting. All the images used (except one) were recorded on the high gain mode.

Simultaneous coverage was provided by the Ocean Colour Scanner flown at an altitude of 20 km on a U-2 aircraft. A sub-area of both OCS and MSS imagery along the west coast of Florida was chosen for intensive study. It should be noted that OCS was subsequently renamed Coastal Zone Colour Scanner (CZCS).

Results:

The depth was effectively discriminated with the LANDSAT MSS-4 (channel 4 - 0.5 to 0.6 micrometres) imagery taken in the high gain mode. Contours to a depth of at least 8 metres were recognized with 10% error over a radiance intensity of 42 grey levels. A 26 grey level range of MSS-5 (0.6 to 0.7 micrometres) gave depth information to at least 5 metres with 10% error.

The simultaneous coverage of OCS and MSS on September 19, 1975 provided a good opportunity to compare the performances of the two sensors. The channels 4 and 5 of OCS were found to be the most sensitive for the discrimination of depth or depth related factors. The greatest sensitivity as indicated by a radiance intensity range of 56 grey levels was found in OCS-4 which measured depth to at least 12 metres with 5% error (refer to Figure 8.35).

Conclusions and Recommendations:

The available channels of two remote sensors were analyzed spatially and temporally for their capacity to discern bathymetric information. The OCS-4 provided the greatest depth penetration and discrimination with the smallest error estimate; therefore, it is recommended for small-scale hydrographic mapping of sandy bottom coastal areas.

LANDSAT's MSS-4 in the high gain mode is recommended when mapping at a scale of 1:80,000 or smaller is adequate. Bottom depths and the log of radiance intensities were found to be related by a linear relationship for depths down to 12 metres. This shows the possibility of depth estimation in this range given several radiance values.

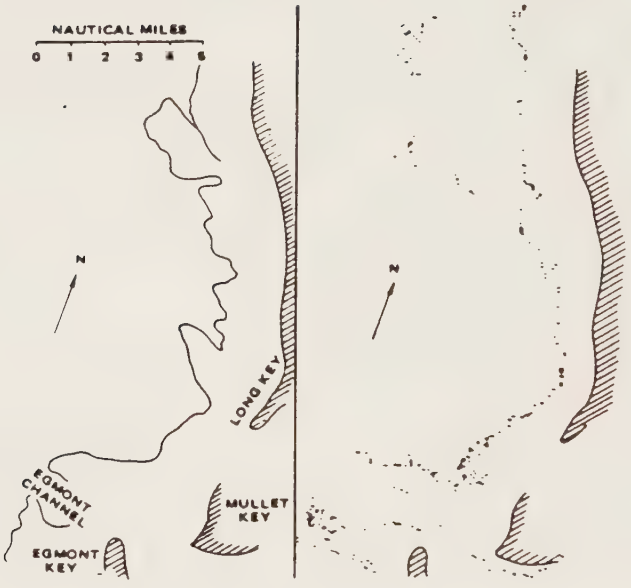

Figure 8.35 The charted depth contour (5 m) in the study site in comparison with the binary print of the OCS-4 radiance-value distribution pattern for a single grey level in this depth range.

8.20 Case Study No. 20

Reference:

Roy, S.E., 1978,
Sea surface temperature and related measurements of the South Caribbean Sea, utilizing GOES, NOAA and GOSSTCOMP data for locating structures. In Proceedings of the Seventh annual remote sensing of earth resources conference. Tullahoma, Tennessee, University of Tennessee, Space Institute, pp.261-87.

Remote Sensing Technique:

Satellite Remote Sensing:
Platforms - GOES, NOAA;
Sensors - VISSR, VTPR, VHRR (Very High Resolution Recorder), SR (Scanning Radiometer).

Objective:

To determine the sea surface temperature (SST) and related measurements associated with ocean currents and structures such as upwelling and eddies by the analysis of images from GOES and NOAA satellites.

Experimental Rationale:

The temperature of an object is related to the IR radiation coming from it. Since the launching of the first NOAA satellite, the National Environmental Satellite Service (NESS) has developed a process to convert IR data into sea surface temperature information. Subsequently, interactive processing of NOAA satellite data using atmospheric attenuation data obtained from a Vertical Temperature Profile Radiometer (VTPR) has led to an improved quality of SST measurements. A further improvement of analytical procedures led to the development of an operational and highly flexible model called Global Operational Sea Surface Temperature Computation (GOSSTCOMP) which permits rapid retrieval and updating.

Method:

The data for this study was obtained from a geo-stationary satellite of the SMS/GOES series and distributed by NESS. The visible and IR Spin Scan Radiometer (VISSR) data recorded on tape and relayed by telephone line for facsimile reception was the chief source of data for the Caribbean Sea study area.

The surface temperature measurements were obtained by a statistical histogram analysis. The corrections for atmospheric attenuation were calculated from the VTPR data.

The quantitative measurements of sea surface and land surface temperatures, however, are still affected by noise, the extent of cloud and haze in the retrieval area and atmospheric moisture content. In addition, sea state condition, surface reflectance, etc. influence the accuracy of sea surface temperature measurements. For accurate temporal monitoring of ocean phenomena, the images had to be geometrically corrected; land markers were used for accurate registration purposes.

Results: The results show that the (GOSSTCOMP) charts obtained weekly were too broad to discern any local structures. Digitally enhanced images, however, clearly showed SST and defined most structures. The digital enhancement program with 12 step increments of 0.5°C over a 6°C range was found to be the most convenient for general use of GOES and NOAA data in the subtropical region.

Conclusion: Thermal IR imagery from SMS/GOES can be used to derive SST on an operational basis over the Caribbean Sea region. NOAA series data, although of higher resolution, could not be acquired and analysed cost effectively in near real time.

However, because of excessive cloudiness, atmospheric moisture content and a high general albedo over the sub-tropics, VTPR data from the NOAA series is essential for the correction of atmospheric attenuation on SMS/GOES imagery.

8.21 Case Study No. 21

Reference:

Mattie, M.G. and D.E. Lichy, 1980, SEASAT detection of waves, currents and inlet discharge. Int.J.Remote Sensing, 1(4):377-98.

Remote Sensing Technique:

Satellite Remote Sensing:
Platform - SEASAT;
Sensor - SAR.

Objective:

To demonstrate the capabilities of SEASAT Synthetic Aperture Radar (SAR) to image certain coastal and nearshore phenomena during specific orbits.

Experimental Rationale:

Because radar wavelengths do not penetrate the sea surface, the backscatter pattern indicates its condition. Surface winds are clearly distinguishable in addition to surface interactions which have little relationship to the wind, such as currents, eddies and ship wakes.

Method:

Duck X was a 2 month experiment conducted during August to October 1978 off the coast of the U.S.A. to test the SEASAT SAR. For the verification of SEASAT SAR images various types of sensors were used including airborne photographic and radar imagery, meteorological satellite imagery, land-based radars and conventional wave gauges.

Results and Conclusion:

The data set obtained by SEASAT SAR (orbit no. 974, 1339), although relatively sparse, contained a great deal of information on a variety of phenomena including ocean currents, ocean surface waves and coastal inlet discharge. Ocean waves with heights as low as 0.1 m and their shoaling were imaged. Hurricane Ella passed 300 km east of the SAR swath at Cape Hatteras and its effects were observed.

The SEASAT SAR images enabled the Gulf Stream boundary and eddy features to be identified. Coastal inlet hydraulics and marshland water levels were also seen in SAR images. The other phenomena identified in SEASAT SAR images included: wave diffraction, bottom sand waves, hydrographic features and internal waves. SEASAT SAR also supplemented information obtained by other instruments which are weather limited, such as IR photography.

Figure 8.36 shows a digitally processed image indicating some of the multitude of phenomena that have been noted in the SAR imagery. The dark regions generally correspond to low surface winds. A low energy swell system with 200 m wavelength is travelling through the area from the south-east.

Figure 8.36 SEASAT SAR image (resolution of 25 metres, horizontal dimension 100 km).

8.22 Case Study No. 22

Reference:

Tanaka, S. et al., 1983,
Accuracy of direct measurement of mean surface water velocity of the Kuroshio using multi-temporal NOAA-6 imageries. In Proceedings of the Seventeenth International Symposium on remote sensing of environment, Ann Arbor, 1983. Ann Arbor, Michigan, Environment Research Institute, pp. 933-44.

Remote Sensing Technique:

Satellite Remote Sensing:
Platform - NOAA-6;
Sensor - AVHRR.

Objective:

To determine the surface water velocity of the Kuroshio current using the "Sea Mark" method in NOAA-6 images. "Sea Mark" is a point pattern on the sea surface, which can be identified in at least 2 consecutive images.

Experimental Rationale:

The movements of "Sea Marks" show the direction of the currents. These "Sea Marks" tend to keep their configuration intact since water drifts as a mass. Tracking the prominent points of the fronts or the centres of eddies gives the necessary current vectors.

Method:

Two NOAA-6/AVHRR images recorded on the same day were used in this study (refer to Figure 8.37). The time difference between these two scenes was 11 hours and 17 minutes. Both scenes were mapped in relation to the earth coordinate system to measure accurately the velocity vectors. Ground control points were used in the mapping procedures.

The maps produced by this method contained a maximum error of 0.2 mm regardless of mapping scale, i.e. an error of only 600 metres in horizontal distance on the 1:3,000,000 map.

Results:

Because of the temperature differences between the Kuroshio and surrounding water, clear fronts could be identified by the imagery. In addition oceanic eddies probably generated on the shallow sea bottom south of Tanegashima Island were recognized and the movement of their prominent points was traced in the consecutive images. The distances these points moved within the 11 hours and 17 minutes time interval were used to calculate the average velocity of the eddy.

Sea current phenomena were found to vary in 12 hour intervals. Measurement accuracy of mean surface water velocity was within 0.1 knots based on an assumed "Sea Mark" orientation accuracy of "2.0 pixels".

Conclusions:

The accuracy of measuring the mean surface velocity of an ocean current such as the Kuroshio depends on the following:

a) the ability to recognize special floating points on both NOAA-6/AVHRR images recorded on the same day;

b) the necessity to integrate (or map) the NOAA-6/AVHRR imagery into the earth coordinate system. The ground control points necessary for this transformation should be taken from uniformly scattered points within the scene.

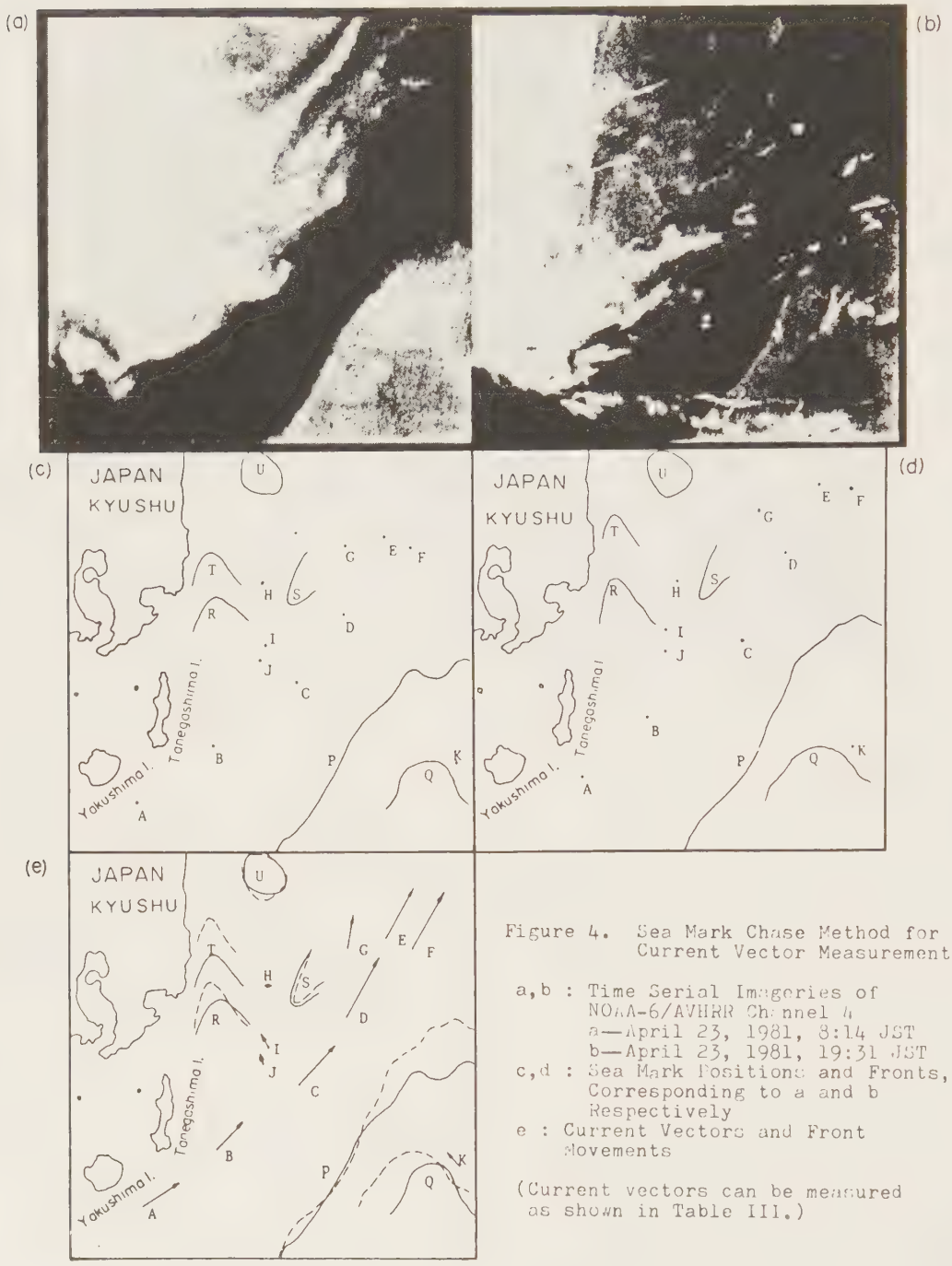

Figure 4. Sea Mark Chase Method for Current Vector Measurement.

a,b : Time Serial Imageries of NOAA-6/AVHRR Channel 4
a—April 23, 1981, 8:14 JST
b—April 23, 1981, 19:31 JST
c,d : Sea Mark Positions and Fronts, Corresponding to a and b Respectively
e : Current Vectors and Front Movements

(Current vectors can be measured as shown in Table III.)

Figure 8.37 "Sea Mark" chase method for current vector measurement.

SECTION 9

BIBLIOGRAPHY

Aird, W.J., 1977 Remote sensing: airborne mission planning. Ottawa, Department of Fisheries and Environment, Environmental Protection Service, Environmental Impact Control Directorate, 94 p.

Allan, T.D., 1982 Satellite microwave remote sensing. Toronto, John Wiley and Sons, 526 p.

Andrews, H.C., 1970 Computer techniques in image processing. New York, Academic Press, 187 p.

_____, 1983 Applying remote sensing techniques to the marine environment. In The ocean and offshore regions, coastal zones, arctic areas, rivers, and lakes. Course no. 947 - April 18-22. Washington, D.C., George Washington University, 2 vols.

Armstrong, R.A., 1983 Marine environments of Puerto Rico and the Virgin Islands: automated mapping and inventory using LANDSAT data. Caribbean Fishery Management Council, 37 p.

Avery, T.E. and G.L. Berlin, 1985 Interpretation of aerial photographs. Minneapolis, Burgess Publishing Co., 554 p.

Barale, V. et al., 1986 Space and time variability of the surface color field in the Northern Adriatic Sea. J.Geophys.Res., 91(C11):12957-74

Barrett, E.C. and L.F. Curtis, 1982 Introduction to environmental remote sensing. London, Chapman and Hall, 352 p.

Bazigos, G.P. et al., 1979 Aerial frame survey along the southwest coast of India. Rome, FAO, UNDP/FAO Pelagic fishery investigation project on the southwest coast of India. FIRM-IND/75/038: 104 p.

Belsher, T. and M. Viollier, 1984 Thematic study of the 1982 SPOT simulation of Roscoff and the west coast of the Cotentin peninsula (France). In Proceedings of the Eighteenth International Symposium on remote sensing of environment, Paris, France. Ann Arbor, Environment Research Institute, pp.1161-6

Blindheim, J., G.H.P. de Bruin and G. Saetersdal, 1979 A survey of the coastal fish resources of Sri Lanka. Report no. 2, April-June 1979. Reports on surveys with R/V DR. FRIDTJOF NANSEN. Bergen, Institute of Marine Research, 63 p.

Bour, W. et al., 1986 Thematic mapping of reefs by processing of simulated SPOT satellite data: application to the Trochus niloticus biotope on Tetembia Reef (New Caledonia). Mar.Ecol.Prog. Ser.), 34:243-9

Bravio, P.A. and E. Zilioli, 1980 Image processing. In Report of the International training course in remote sensing applications for water resources and hydrology, held in Rome, 19 May-6 June 1980. FAO Remote Sensing Cent.Ser., (9):22-41

Butler, M.J.A. et al., 1986 Marine resource mapping: an introductory manual. FAO Fish.Tech.Pap., (274):256 p.

Caraux, D. and R.W. Austin, 1983 Delineation of seasonal changes of chlorophyll frontal boundaries in Mediterranean coastal waters with NIMBUS-7 coastal zone colour scanner data. Remote Sensing Environ., 13(3):239-49

Carter, D.J., 1986 The remote sensing sourcebook: a guide to remote sensing products, services, facilities, publications and other materials. London, McCarta Ltd., 175 p.

Colwell, R.N. (ed.), 1983 Manual of remote sensing. Falls Church, Virginia, American Society of Photogrammetry, 2240 p. 2nd ed.

Cornillon, P. et al., 1986 Sea surface temperature charts for the southern New England fishing community. Mar.TechnolSoc.J., 20(2):57-65

Cracknell, A.P., 1983 Remote sensing applications in marine science and technology. Dordrecht, Netherlands, D. Reidel Publishing Co., NATO AS1 series, 466 p.

Cram, D.L., 1979 A role for the NIMBUS-9 coastal zone colour scanner in the management of a pelagic fishery. Fish.Bull./Visserij-Bull.,Cape Town, (11):1-9

Cushing, D.H, 1973 Detection of fish. London, Pergamon Press, 200 p.

Estes, J.E. and L.W. Senger, 1974 Remote sensing: techniques for environmental analysis. Santa Barbara, California, Hamilton Publishing Co., 340 p.

FAO, 1980 Echo sounding and sonar for fishing. London, Fishing News Books Ltd., FAO fishing manuals, 116 p.

Feldman, G.C., 1986 Variability of the productive habitat in the Eastern Equatorial Pacific. EOS Trans.Am.Geophys.Union, 67(9): 106-8

Gower, J.F.R., 1972 A survey of the uses of remote sensing from aircraft and satellites in oceanography and hydrography. Pac.Mar.Sci.Rep.Inst.Ocean.Sci.,Sidney,B.C.,Can., (72-3)

Hall, E.L., 1979 Computer image processing and recognition. New York, Academic Press, 584 p.

Hara, I., 1985 Moving direction of Japanese sardine school on the basis of aerial surveys. Bull.Japan.Soc.Sci.Fish., 51(12):1939-45

Harper, D., 1983 Eye in the sky: introduction to remote sensing. Montreal, Multiscience Publications Ltd., 164 p.

Holligan, P.M. et al., 1983 Satellite studies on the distribution of chlorophyll and dinoflagellate blooms in the western English Channel. Cont.Shelf.Res., 2(2-3):81-96

Holz, R.K., 1973 The surveillant science: remote sensing of the environment. Boston, Houghton Mifflin Co., 390 p.

Jensen, J.R. et al., 1980 Remote sensing techniques for kelp surveys. Photogramm.Eng.Remote Sensing, 46(6):743-55

Kemmerer, A.J., 1980 Environmental preferences and behavior patterns of Gulf menhaden (Brevoortia patronus) inferred from fishing and remotely sensed data. ICLARM Conf.Proc., (5):345-70

Kim, H.H., 1977 Airborne bathymetric charting using pulsed blue-green lasers. Appl.Optics, 16(1):46-56

Lasker, R. et al., 1981 The use of satellite infrared imagery for describing ocean processes in relation to spawning of the northern anchovy (Engraulis mordax). Remote Sensing Environ., 11:439-53

Laurs, R.M. et al., 1984 Albacore tuna catch distributions relative to environmental features observed from satellites. Deep-Sea Res., 31(9):1085-99

Lillesand, T.M. and R.W. Kiefer, 1979 Remote sensing and image interpretation. New York, John Wiley and Sons, 612 p.

Lyzenga, D.R., 1978 Passive remote sensing techniques for mapping water depth and bottom features. Appl.Optics, 17(3):379-83

Mattie, M.G. and D.E. Lichy, 1980 SEASAT detection of waves, currents and inlet discharge. Int.J.Remote Sensing, 1(4):377-98

Maughan, D. et al., 1973 Application of ERTS imagery to the harvest model of the U.S. menhaden fishery. In Proceedings of the Symposium on significant results obtained from the ERTS-1, NASA, edited by S.C. Freden, E.P. Mercanti and D.E. Witten. Greenbelt, Maryland, NASA, pp.1405-11

Maul, G.A., 1985 Introduction to satellite oceanography. Hingham, Maine, Kluwer Academic Publishers, 606 p.

McLeish, W. et al., 1983 Imaging radar observations of directional properties of ocean waves. J.Geophys.Res., 88(c7):4407-19

Meadows, G.A. et al., 1983 SEASAT synthetic aperture radar observations of wave-current and wave-topographic interactions. J.Geophys.Res., 88(c7):4393-406

Meynen, E., 1968 Orbis geographicus: world directory of geography. Wiesbaden, Franz Steiner Verlag, 309 p.

Middleton, E.M. and J.L. Barker, 1976 Hydrographic charting from LANDSAT satellite: a comparison with aircraft imagery. In Oceans '76. Second combined conference, Marine Technology Society/ Institute of Electrical and Electronics Engineers. New York, IEEE Inc. and Washington, D.C., MTS, (CH 1118-90 EC): 6 p.

Moik, J.G., 1980 Digital processing of remotely sensed images. Washington, D.C., U.S. Government Printing Office, (NASA SP 431):330 p.

Montgomery, D.R. et al., 1986 The applications of satellite-derived ocean color products to commerical fishing operations. Mar.Technol. Soc.J., 20(2):72-86

Munday, J.C. and T.T. Alföldi, 1979 LANDSAT test of diffuse reflectance models for aquatic suspended solids measurement. Remote Sensing Environ., 8(2):169-83

NASA, var.d. Earth observing system reports. Greenbelt, Maryland, NASA, 10 vols

Njoku, E.G. et al., 1985 Advances in satellite sea surface temperature measurements and oceanographic applications. J.Geophys. Res., 90(c6):11573-86

O'Neil, R.A., 1983 Coastal hydrography using the C.C.R.S. lidar bathymeter. In The ocean environment and its interactions with offshore structures. Goteborg, Sweden, Swedish Trade Fair Foundation.

Pierson, W.J. et al., 1984 Synoptic scale wind field properties from the SEASAT-SASS. NASA Contractor Rep.,(3810)

Pringle, J.D. and R.E. Duggan, 1983 A remote sensing technique for quantifying lobster fishing effort. Can.Tech.Rep.Fish.Aquat.Sci., 1217:16 p.

Queffeubu, P., 1983 SEASAT wave height measurement: a comparison with sea-truth data and a wave forecasting model. J.Geophys.Res., 88(c3):1779-88

Richards, J.A., 1986 Remote sensing digital image analysis: an introduction. Berlin, Springer-Verlag, 281 p.

Robinson, I.S., 1985 Satellite oceanography: an introduction for oceanographers and remote sensing scientists. Chichester, England, Ellis Horwood Ltd., 455 p.

Roithmayr, C.M., 1970 Airborne low-light sensor detects luminescing fish schools at night. Commer.Fish.Rev., 32(12): 42-51

Rosenfeld, A. and A.G. Kak, 1976 Digital picture processing. New York, Academic Press, 457 p.

Roy, S.E., 1978 Sea surface temperature and related measurements of the South Caribbean Sea, utilizing GOES, NOAA and GOSSTCOMP data for locating structures. In Proceedings of the Seventh annual remote sensing of earth resources conference. Tullahoma, Tennessee, University of Tennessee, Space Institute, pp.261-87

Ruffenach, C.L. et al., 1983 Interpretation of synthetic aperture radar measurements of ocean currents. J.Geophys.Res., 88(c3):1867-76

Sabins, F.F. Jr., 1978 Remote sensing principles and interpretations. San Francisco, W.H. Freeman

SCOR Working Group 70, 1986 Opportunities and problems in satellite measurements of the sea: report of the SCOR Working Group 70/editor J.F.R. Gower; co-editor J.R. Apel. Paris, UNESCO, 70p. (UNESCO technical papers in marine science, 0503-4299;46).

Smith, J.T., 1968 Manual of color aerial photography. Falls Church, Virginia, American Society of Photogrammetry, 550 p.

Stevenson, W.H. and E.J. Pastula, 1971 Observations on remote sensing in fisheries. Commer.Fish.Rev., 33(9):9-21

Strong, A.E., 1983 El Nino observations by remote sensing. In Proceedings of the Seventeenth International Symposium on remote sensing of environment, Ann Arbor, 1983. Ann Arbor, Michigan, Environment Research Institute, pp.177-84

Swain, P.H and S.M. Davis, Remote sensing: the quantitative approach.
1978 New York, McGraw-Hill, 396 p.

Tanaka, S. et al., Accuracy of direct measurement of mean surface water
1983 velocity of the Kuroshio using multi-temporal NOAA-6 imageries. In Proceedings of the Seventeenth International Symposium on remote sensing of environment, Ann Arbor, 1983. Ann Arbor, Michigan, Environment Research Institute, pp.933-44

Thomas, M.H.B., Coastal and marine applications of remote sensing. In
1980 Physics underlying the remote sensing of the oceans. Reading, England, Remote Sensing Society, 1-2C p.

Tucker, D.G., Sonar in fisheries: a forward look. London, Fishing News
1967 (Books) Ltd., A Buckland Foundation book:136 p.

Van der Piepen, H. et al., The ocean color experiment (OCE) on the second
1983 orbital flight test of the space shuttle. IEEE Trans. Geosci.Remote Sensing, GE 21(3):350-7

Venable, D.V. et al., Sensitivity of airborne fluorosensor measurements
1984 to linear vertical gradients in chlorophyll concentration. Appl.Optics, 23:970-2

Werle, D., Radar remote sensing in tropical environments - a review of
1988 investigations and potential applications for spaceborne SARS. RADARSAT Project Office Report. Ottawa, Canada, Energy, Mines and Resources.

Williamson, E.J. and G.A. Wilkinson, Sea surface temperature from
1980 METEOSAT. In The second METEOSAT scientific user meeting. London, European Space Agency, pp.710-9

APPENDIX A

GLOSSARY OF TERMS AND ACRONYMS

AVHRR	Advanced Very High Resolution Radiometer
AWAR	Area Weighted Average Resolution
ABSORPTION	A process by which radiation is converted to other types of energy (especially heat) by a material.
ACTIVE REMOTE SENSING	Remote sensing methods that provide their own source of electromagnetic radiation, e.g., Radar.
ADDITIVE PRIMARY COLOURS	The colours blue, green and red. Filters of these colours transmit the primary colour of the filter and absorb the other two colours.
ALBEDO	The ratio of the amount of electromagnetic energy reflected by a surface to the amount of energy incident upon it. The symbol is A.
ALTIMETER (ALT)	Instrument which determines the altitude of an object with respect to a fixed level such as sea level.
ANALOG	A form of data display in which values are shown in graphic form such as curves. Also a form of computing in which values are represented by directly measurable quantities such as voltages or resistances. Analog computing methods contrast with digital methods in which values are treated numerically.
ANGLE OF INCIDENCE	(1) The angle between the direction of incoming EMR and the normal to the intercepting surface; (2) In SLAR systems this is the angle between the vertical and a line connecting the antenna and the target.
ANGSTROM (Å)	A measurement of length (10^{-10}m).
ANGULAR FIELD OF VIEW	The angle subtended by lines from a remote sensing system to the outer margins of the strip of terrain that is viewed by the system.
ANTENNA	The device that transmits and/or receives microwave and radio energy.
ASPECT ANGLE	Same as angle of incidence in SLAR.
ATMOSPHERE	The layer of gases that surround some planets.
ATMOSPHERIC WINDOWS	Wavelength intervals at which atmosphere transmits most electromagnetic radiation.
ATTITUDE	The angle of orientation of a remote sensing system with respect to a geographic reference system.

AZIMUTH	The geographic orientation of a line given as an angle measured clockwise from north.
BACKSCATTER	(1) The scattering of radiant energy into the hemisphere of space bounded by a plane normal to the direction of the incident radiation and lying on the same side as the incident ray; (2) In SLAR usage this refers to the portion of the microwave energy scattered by the terrain surface that is directed back towards the antenna.
BAND	A wavelength interval in the electromagnetic spectrum. For example, in LANDSAT the bands designate specific wavelength intervals at which images are required.
BEAM	A focused pulse of energy.
BEAM WIDTH	In SLAR usage this is the angle subtended in the horizontal plane by the radar beam.
BINARY	A numerical system using the base 2.
BIT	In digital computer terminology, this is a binary digit that is an exponent of the base 2.
BLACKBODY	A substance that radiates energy at the maximum possible rate per unit area at each wavelength for any given temperature. A blackbody also absorbs all energy that falls on it.
BRIGHTNESS	Magnitude of the response produced in the eye by light.
BRUTE FORCE RADAR	See Real-aperture Radar.
BYTE	A group of eight bits of digital data.
CCT	See Computer Compatible Tape
CIR	Colour Infrared
CRT	See Cathode Ray Tube
CZCS	Coastal Zone Colour Scanner
CALIBRATION	The process of comparing measurements, made by an instrument, with a standard.
CALORIE	The amount of heat required to raise the temperature of 1 gm of water by $1^{o}C$.
CATHODE RAY TUBE (CRT)	A vacuum tube with a phosphorescent screen upon which images are displayed by an electron beam.
CLASSIFICATION	The process of assigning individual pixels of a digital image to categories, generally on the basis of spectral reflectance or radiometric characteristics.

COLOUR-COMPOSITE IMAGE	A colour image prepared by combining individual band images. Each band (up to a maximum of 3) is assigned one of the three additive primary colours: blue, green and red.
COMPUTER COMPATIBLE TAPE (CCT)	The magnetic tape upon which the digital data for remotely sensed images are distributed.
CONDUCTION	The transfer of electromagnetic energy through a material by molecular interaction.
CONTRAST	The difference between highlights and shadows in a photographic image. The larger the difference in density the greater the contrast.
CONTRAST RATIO	The ratio between the reflectance of the brightest and darkest parts of the image, commonly referred to as contrast.
CONTRAST STRETCHING	Improving the contrast of images by digital processing. The original range of digital values is expanded to utilize the full contrast range of the recording film or display device.
CONVECTION	The transfer of heat through the physical movement of heated matter.
DCS	Data Collecting System
DENSITY OF IMAGES	A measure of the opacity or darkness of an image.
DENSITY OF MATERIALS	The ratio of mass to volume of a material, typically expressed as $gm \cdot cm^{-3}$.
DENSITY SLICING	The process of converting the continuous grey tone of an image into a series of density intervals or slices, each corresponding to a specific digital range.
DEPOLARIZATION	Change in polarization of a radar pulse as a result of multiple reflections from the terrain surface.
DEPRESSION ANGLE	In SLAR usage this is the angle between the horizontal plane passing through the antenna and the line connecting the antenna and the target.
DETECTOR	The component of a remote sensing system that converts the electromagnetic radiation into a signal that is recorded.
DEVELOPMENT	The chemical processing of exposed photographic material to produce an image.
DIAZO FILM	A transparent material on which image transparencies may be reproduced in specific colours.
DICHORIC	A beam-splitting mirror that efficiently reflects certain wavelengths while it efficiently transmits others.

DIELECTRIC	A substance which contains few or no free charges and is consequently a poor electrical conductor.
DIELECTRIC CONSTANT	Electrical property of matter that influences radar returns; also referred to as complex dielectric constant.
DIFFRACTION	The propagation of EMR around the edges of opaque objects into the shadow region.
DIGITAL DATA	Data displayed, recorded or stored in binary notation.
DIGITAL IMAGE PROCESSING	Computer manipulation of the digital values for picture elements of an image.
DIGITIZATION	The process of converting an image into numerical format.
DIGITIZER	A device for scanning an image and converting it into numerical picture elements.
DISPERSION	Separation of EMR into its spectral components.
DISTORTION	On an image, this refers to changes in shape and position of objects with respect to their true shape and position.
DOPPLER PRINCIPLE	Describes the change in observed frequency of electromagnetic or other waves caused by relative movement between the source of waves and the observer.
EM	Electromagnetic
EMR	See Electromagnetic Radiation
ERTS	Earth Resource Technology Satellite
ESA	European Space Agency
EKTACHROME	A Kodak colour-positive film.
ELECTROMAGNETIC RADIATION (EMR)	Energy propagated through space or through material media in the form of an advancing interaction between electric and magnetic fields.
EMISSION	With respect to EMR, the process by which a body emits EMR usually as a consequence of its temperature only.
EMISSIVITY	The ratio of radiant flux from a body to that from a blackbody at the same kinetic temperature.
EMULSION	A suspension of photosensitive silver halide grains in gelatin that constitutes the image-forming layer on photographic materials.
ENHANCEMENT	The process of altering the appearance of an image so that the interpreter can extract more information. Enhancement may be done by digital or photographic methods.

FLIR	Forward Looking Infrared
FALSE COLOUR IMAGE	A colour image in which the dye colour is not the same as the scene colour.
FILM (PHOTOGRAPHIC)	A transparent base having a light-sensitive photographic emulsion.
FILM SPEED	A measure of the sensitivity of photographic film to light. Larger numbers indicate higher sensitivity.
FILTER	Any physical device or mathematical function that is used to modify a spectrum.
FILTER, DIGITAL	A mathematical procedure for removing unwanted values from numerical data.
FILTER, OPTICAL	A material that, by absorption or reflection, selectively modifies the radiation transmitted through an optical system.
FLIGHT PATH	The line on the ground directly beneath a remote sensing aircraft or satellite.
FLUORESCENCE	The emission of light from a substance caused by exposure to radiation from an external source.
FOCAL LENGTH	In cameras, the distance measured along the optical axis from the optical centre of the lens to the plane at which the image of a distant object is brought into focus.
FOCUS	To adjust a remote sensing system to produce a sharp, distinct image.
FOOTPRINT	A definite patch of earth surface illuminated by a radar at any given instant of time.
FORMAT	The size and scale of an image.
FRAMING CAMERA	A camera that observes and records the scene in sections (or frames) in contrast, for example, to a strip camera.
FREQUENCY	The number of wave oscillations per unit time or the number of wavelengths that pass a point per unit time. The symbol is
GOES	Geostationary Operational Environment Satellite
GAIN	An increase in signal power in transmission from one point to another and usually expressed in decibels.
GAMMA RAYS	High energy electromagnetic radiation emitted by radioactive decay. Gamma rays have wavelengths shorter than 1 Angstrom unit.
GEOID	The figure of the earth considered as a sea-level surface extended continuously over the entire earth's surface.

GELBSTOFFE	Dissolved yellow substances which absorb light in natural waters.
GREY BODY	A material that does not display strong absorption and emission features, but has an overall reduced emissivity (in comparison to a blackbody) which is practically constant over all wavelengths.
GREY SCALE	A calibrated sequence of grey tones ranging from black to white.
GROUND RANGE	The distance from the ground track to an object.
GROUND RECEIVING STATION	A facility that records image data transmitted by airborne or spaceborne sensors.
GROUND RESOLUTION CELL	The area on the terrain that is covered by the instantaneous field of view of a detector. Size of the ground resolution cell is usually determined by the altitude of the remote sensing system and the instantaneous field of view of the detector.
h	See Planck's Constant
HCMM	Heat Capacity Mapping Mission
HCMR	Heat Capacity Mapping Radiometer
HRVR	High Resolution Visible Radiometer
HARMONIC	Refers to waves in which the component frequencies are whole number multiples of the fundamental frequency.
HERTZ (Hz)	Cycles per second.
HUE	The attribute of a colour that differentiates it from grey of the same brilliance and that allows it to be classed as blue, green, red or intermediate shades of these colours.
IFOV	See Instantaneous Field of View
IR	See Infrared
IMAGE	The representation of a scene as recorded by a remote sensing system. Although image is a general term, it is commonly restricted to representations acquired by non-photographic methods.
INFRARED(IR)	Portion of the electromagnetic spectrum lying between the red end of the visible spectrum and microwave radiation (0.7 to 1000 micrometres).
INSTANTANEOUS FIELD OF VIEW (IFOV)	The cone angle within which incident energy is focused on the detector. The instantaneous field of view is commonly expressed in milliradians.
INTEGER	Any positive or negative whole number or zero.

INTENSITY	A measure of energy reflected from a surface.
INTERACTIVE PROCESSING	The method of data processing by which the operator views preliminary results and can alter the instructions to the computer to achieve optimum results.
INTERPRETATION	The extraction of information from an image.
INTERPRETATION KEY	A characteristic or combination of characteristics that enable an object or material to be identified on an image.
IR COLOUR FILM	A colour film consisting of three layers in which the red-imaging layer responds to photographic IR radiation ranging in wavelength from 0.7 to 1.3 micrometres. The green-imaging layer responds to red light and the blue-imaging layer responds to green light.
IRRADIANCE	The radiant power density incident on a surface (watts/cm square).
K-BAND	Radar wavelength region from 0.8 to 1.1 cm.
KINETIC ENERGY	The ability of a moving body to do work by virtue of its motion. The molecular motion of matter is a form of kinetic energy.
KINETIC TEMPERATURE	The internal temperature of an object, which is determined by the molecular motion. Kinetic temperature is measured with a contact thermometer and differs from radiant temperature which is a function of emissivity and internal temperature.
KODACHROME	A normal colour-positive film manufactured by Kodak.
LASER	Light Amplification by Stimulated Emission of Radiation
LIDAR	Light Detection and Ranging
LANDSAT	An unmanned earth-orbiting NASA satellite (formerly called ERTS) that transmits multispectral images in the 0.4 to 1.1 micrometre range to earth receiving stations.
L-BAND	Radar wavelengths region from 15 to 30 cm.
LENS	A piece or combination of pieces of glass or other transparent material that enables images to form by refraction of light.
LIGHT	EMR within 0.4 to 0.7 micrometres in wavelength that is detectable by the human eye.
LIGHT METER	A device for measuring the intensity of visible radiation to determine the appropriate exposure for acquiring photographs.

LINEAMENT	A linear topographic or tonal feature on the terrain and on images and maps that may represent a zone of structural weakness.
LINEAR	An adjective that describes the straight line nature of features on the terrain or on images and maps.
LINE-PAIR	A pair of light and dark bars of equal sizes. The number of such line-pairs that can be distinguished per unit distance is used to express resolving power of imaging systems.
LOOK DIRECTION	Direction in which pulses of microwave energy are transmitted by a radar system. Look direction is normal to the azimuth direction. Also called range direction.
LOW-SUN ANGLE PHOTOGRAPHS	Aerial photographs acquired in the morning, evening or winter when the sun is at a low elevation above the horizon.
LUMINANCE	A quantitative measure of the intensity of light from a source, measured with a device called a photometer.
MEIS	Multi-detector Electro Optical Imaging Scanner
MESSR	Multispectral Electronic Self Scanning Radiometer
MOS	Marine Observation Satellite
MSR	Microwave Scanning Radiometer
MSS	See Multispectral Scanner
METEOSAT	A European geostationary satellite used for meteorological observations and communications. The major instrument onboard is a scanning radiometer which has three spectral bands: visible 0.4 to 1.1 micrometres, thermal infrared 10.5 to 12.5 micrometres and infrared water vapour absorption 5.7 to 7.1 micrometres.
MICROWAVE	The region of the electromagnetic spectrum in the wavelength range from 1 mm to beyond 1 m.
MIE SCATTERING	Multiple reflection of light waves by atmospheric particles that have the approximate dimensions of the wavelength of light.
MULTISPECTRAL CAMERA	A system that simultaneously acquires photographs at different wavelengths of the same scene. Also called multiband camera.
MULTISPECTRAL SCANNER (MSS)	A scanner system that simultaneously acquires images of the same scene in various wavelength bands.
NASA	National Aeronautical and Space Administration (U.S.A.)

NOAA	National Oceanic and Atmospheric Administration (U.S.A.)
NADIR	The point on the ground vertically beneath the centre of a remote sensing system.
NEAR RANGE	Refers to the portion of a radar image closest to the flight path.
NEGATIVE PHOTOGRAPH	A photograph on film or paper in which the tones are reversed from the brightness of the features on the terrain.
NOISE	Random or repetitive events that obscure or interfere with the desired information.
NORMAL COLOUR FILM	A film in which the colours are essentially true representations of the colour of the terrain.
OBLIQUE PHOTOGRAPH	A photograph acquired with the camera axis intentionally directed between the horizontal and vertical orientations.
ORBIT	The path of a satellite around a body under the influence of gravity.
OVERLAP	The extent to which adjacent images or photographs cover the same terrain, expressed in percentages.
PANCHROMATIC	Sensitive to entire visible part of EMR spectrum.
PARALLEL POLARIZED	Radar returned pulse in which the polarization is the same as the transmitted pulse. Images recorded with parallel-polarized energy may be HH (horizontal transmit, horizontal return) or VV (vertical transmit, vertical return).
PASS	In digital filters this refers to the spatial frequency of data transmitted by the filter. High-pass filters transmit high-frequency data; low-pass filters transmit low-frequency data.
PASSIVE REMOTE SENSING	Remote sensing of energy naturally reflected or radiated from the terrain.
PATTERN	The regular repetition of tonal variation on an image or photograph.
PHOTODETECTOR	A device for measuring energy in the photographic band.
PHOTOGRAPH	A representation of targets formed by the action of light on silver halide grains of an emulsion.
PHOTON	The elementary quantity of radiant energy.

PICTURE ELEMENT	In a digitized image this is the area on the ground represented by each digital value. Because the analog signal from the detector of a scanner may be sampled at any desired interval, the picture element may be smaller than the ground resolution cell of the detector. Commonly abbreviated as pixel.
PITCH	Rotation of an aircraft about the horizontal axis normal to its longitudinal axis, that causes a nose-up or nose-down attitude.
PIXEL	A contraction of picture element.
PLANCK'S CONSTANT (h)	The ratio of the energy of a photon to its frequency; it is equal to $6.62620 \pm 0.00005 \times 10^{-34}$ Joules-seconds.
PLANCK'S LAW	A fundamental law of quantum theory stating that energy associated with electromagnetic radiation is emitted or absorbed in discrete amounts which are proportional to the frequency of radiation.
POLARIZATION	The direction of vibration of the electrical field vector of electromagnetic radiation. In radar systems polarization is either horizontal or vertical.
PULSE	A short burst of electromagnetic radiation transmitted by a radar antenna.
QUANTIZATION	Division of the range of values of a wave into a finite number of subranges, each of which is represented by an assigned or quantized value within the subrange.
RADAR	Radio Detection and Ranging
RBV	See Return Beam Vidicon
RUFAS	Remote Underwater Fishery Assessment System
RADAR-ROCK UNITS	Rock units characterized by distinctive signatures on radar images. The signatures are determined by surface roughness of the rocks.
RADAR SHADOW	A dark area of no return on a radar image that extends in the far-range direction from an object on the terrain that intercepts the radar beam.
RADIANT TEMPERATURE	Concentration of the radiant flux from a material. Radiant temperature is the product of the kinetic temperature multiplied by the emissivity to the one-fourth power.
RADIATION	The propagation of energy in the form of electromagnetic waves.
RANGE DIRECTION	For radar images, this is the direction in which energy is transmitted from the antenna and is normal to the azimuth direction. Also called look direction.

RASTER LINES	The individual lines swept by an electron beam across the face of a CRT, that constitute the image display.
RATIO IMAGE	An image prepared by processing digital multispectral data. For each pixel the value for one band is divided by that of another. The resulting digital values are displayed as an image.
RAYLEIGH CRITERION	For radar images, this is the relationship between surface roughness, depression angle and wavelength that determines whether a surface will respond in rough or smooth fashion to the radar pulse.
REAL-APERTURE RADAR	SLAR system in which azimuth resolution is determined by the physical length of the antenna and by the wavelength. The radar returns are recorded directly to produce images. Also called brute-force radar.
REAL TIME	Time in which reporting of events or recording of events is simultaneous with the event.
REFLECTANCE	The ratio of the radiant energy reflected by a body to that incident upon it.
REFLECTANCE, SPECTRAL	Reflectance measured at a specific wavelength interval.
REFLECTIVITY	The ability of a surface to reflect incident energy.
REFRACTION	The bending of electromagnetic rays as they pass from one medium into another.
REMOTE SENSING	The collection of information about an object or event without being in physical contact with the object or event. Remote sensing is restricted to methods that record the electromagnetic radiation reflected or radiated from an object, which excludes magnetic and gravity surveys that record force fields.
RESOLUTION	The ability to distinguish closely spaced objects on an image or photograph. Commonly expressed as the spacing, in line-pairs per unit distance, of the most closely spaced lines that can be distinguished.
RESOLVING POWER	A measure of the ability of individual components and of remote sensing systems to define closely spaced targets.
RETURN-BEAM VIDICON (RBV)	A little-used imaging system on LANDSAT that consists of three cameras operating in the green, red and photographic IR spectral regions. Instead of using film, the images are formed on the photosensitive surface of a vacuum tube. The image is scanned with an electron beam and transmitted to an earth receiving station.

REVERSAL FILM	A photographic film in which the negative image is converted to a positive image during the developing process.
ROLL	Rotation of an aircraft about the longitudinal axis to cause a wing-up or wing-down attitude.
SAR	Synthetic Aperture Radar
SASS	SEASAT-A Satellite Scatterometer
SLAR	Side-Looking Airborne Radar
SMMR	Scanning Multichannel Microwave Radiometer
SMS	Synchronous Meteorological Satellite
SPOT	Satellite Pour l'Observation de la Terre
SST	Sea Surface Temperature
SATELLITE	An object in orbit around a celestial body.
SCALE	The ratio of the distance on an image to the equivalent distance on the ground.
SCAN LINE	The narrow strip on the ground that is swept by the instantaneous field of view of a detector in a scanner system.
SCAN SKEW	Distortion of scanner images caused by forward motion of the aircraft or satellite during the time required to complete a scan.
SCANNER	(1) Any device that scans, and thus produces an image; (2) A radar set incorporating a rotatable antenna for directing a searching radar beam through space and imparting target information to an indicator.
SCANNER DISTORTION	The geometric distortion that is characteristic of scanner images. The scale of the image is constant in the direction parallel with the aircraft or spacecraft flight direction. At right angles to this direction, however, the image scale becomes progressively smaller from the nadir line outward toward either margin of the image. Linear features, such as roads, that trend diagonally across a scanner image are distorted into S-shaped curves. Distortion is imperceptible for scanners with a narrow angular field of view but becomes more pronounced with a larger angular field of view. Also called panoramic distortion.
SCATTERING	Multiple reflection of electromagnetic waves by gases or particles in the atmosphere.
SCATTEROMETER	A non-imaging radar device that records backscatter of terrain as a function of incidence angle.
SCENE	The area on the ground that is covered by an image or photograph.

SENSITIVITY	The degree to which a detector responds to electromagnetic energy incident upon it.
SENSOR	A device that receives electromagnetic radiation and converts it into a signal that can be recorded and displayed as numerical data or as an image.
SIGNATURE	A characteristic, or combination of characteristics, by which a material or an object may be identified on an image or photograph.
SILVER HALIDE	Silver salts that are sensitive to electromagnetic radiation and convert to metallic silver when developed.
SKYLAB	The United States' earth-orbiting workshop that housed three crews of three men in 1973 and 1974.
SKYLIGHT	The component of light that is scattered by the atmosphere and consists predominantly of shorter wavelengths of light.
SLANT RANGE	For radar images this term represents the distance measured along a line between the antenna and the target.
SOFTWARE	The programs that control computer operations.
SPECIFIC HEAT	The ratio between thermal capacity of a substance and thermal capacity of water.
SPECTRAL REFLECTANCE	See Reflectance, Spectral
SPECTRAL SENSITIVITY	The response or sensitivity of a film or detector to radiation in different spectral regions.
SPECTROMETER	Device for measuring intensity of radiation absorbed or reflected by a material as a function of wavelength.
SPECTRUM	(1) In physics, any series of energies arranged according to wavelength (or frequency); (2) The series of images produced when a beam of radiant energy is subject to dispersion. A rainbow-coloured band of light is formed when white light is passed through a prism or a diffraction grating. This band of colours results from the fact that the different wavelengths of light are bent in varying degrees by the dispersing medium and is evidence of the fact that white light is composed of coloured light of various wavelengths.
SUBTRACTIVE PRIMARY COLOURS	Yellow, cyan and magenta. When used as filters for white light these colours remove blue, red, and green, respectively.

SUN SYNCHRONOUS	An earth satellite orbit in which the orbit plane is near polar and the altitude such that the satellite passes over all places on earth having the same latitude twice daily at the same local sun time. Also known as heliosynchronous.
SUPERVISED CLASSIFICATION	A computer-implemented process through which each measurement vector is assigned to a class according to a specified decision rule, when the possible classes have been defined on the basis of representative training samples of known identity.
SURFACE PHENOMENON	Interaction between electromagnetic radiation and the surface of a material.
SYNTHETIC-APERTURE RADAR	SLAR system in which high resolution in the azimuth direction is achieved by utilizing the Doppler principle to give the effect of a very long antenna.
SYSTEMATIC DISTORTION	Predictable geometric irregularities on images that are caused by the characteristics of the imaging system.
THIR	Temperature Humidity Infrared Radiometer
TIROS	Television Infrared Observational Satellite
TM	Thematic Mapper
THERMAL CAPACITY	The ability of a material to store heat, expressed in cal $\cdot$ g^{-1} $\cdot$ $^{o}C^{-1}$. The symbol is C.
THERMAL CONDUCTIVITY	The measure of the rate at which heat passes through a material, expressed in cal $\cdot$ cm^{-1} $\cdot$ sec^{-1} $\cdot$ $^{o}C^{-1}$. The symbol is K.
THERMAL INERTIA	A measure of the response of a material to temperature changes, expressed in cal $\cdot$ cm^{-2} $\cdot$ $^{o}C^{-1}$ $\cdot$ $sec^{-1/2}$. The symbol is P.
THERMAL IR	The portion of the IR region from approximately 8 to 14 micrometres that corresponds to heat radiation. This spectral region spans the radiant power peak of the earth.
THERMAL IR IMAGE	An image acquired by a scanner that records radiation within the electromagnetic band that ranges from approximately 8 to 14 micrometres in wavelength.
TRADE OFF	The compensating change that occurs in a remote sensing system as a result of changing one factor elsewhere in the system. For example, an increase in altitude increases the lateral coverage of an imaging system but the trade off is a decrease in scale and resolution of the image.

ULTRAVIOLET (UV) RADIATION	The region of the electromagnetic spectrum consisting of wavelengths from 10 to 4000 Angstroms.
VAS	VISSR Atmospheric Sounder
VIRR	Visible Infrared Radiometer
VISSR	Visible Infrared Spin Scan Radiometer
VTIR	Visible and Thermal Infrared Radiometer
VISIBLE RADIATION	Energy at wavelengths from 0.4 to 0.7 micrometres that is detectable by the eye.
WATT	Unit of electrical power equal to the rate of work done by one ampere under a pressure of one volt. The symbol is W.
WAVELENGTH	The distance between successive wave crests or other equivalent points in a harmonic wave.
WIEN'S DISPLACE-MENT	Describes the shift of the radiant power peak to shorter wavelengths with increasing temperature.
X-BAND	Radar wavelength region from 2.4 to 3.8 cm.
YAW	Rotation of an aircraft about its vertical axis that causes the longitudinal axis to deviate from the flight line.

APPENDIX B

SOURCES OF OCEANOGRAPHIC SATELLITE DATA

ARGENTINA

Comision Nacional de Investigaciones
Espaciales
Centro de Prosesamiento Dorreo 4010
1425 Buenos Aires, Argentina

AUSTRALIA

Australian LANDSAT Station
Data Processing Facility
14-16 Oakley Court
P.O. Box 28
Belconnen, Australia
ACT 2616

BELGIUM

Services de Programmation
de la Politique Scientifique
8 Rue de la Science
1040 Bruxelles, Belgium
Tel 02-511 59 85

BRAZIL

Instituto de Pesquisas Espaciais (INPE)
a/c Direcao
Av. dos Astronautas
1758, Caixa Postal 515 12200
Sao Jose dos Campos, S.P. Brazil

Instituto de Pesquisas Espaciais (INPE)
Departmento de Producas de Imagens
ATUS - Banco de Imagens Terresties
Rodoua Presidente Dutra KM210
Cachoeira Paulista CEP-12-630, Brazil

CANADA

Canada Centre for Remote Sensing
Emerald Plaza
1547 Merivale Road
Ottawa, Ontario, Canada K1A 0Y7
Tel 613-952-0500

CHINA

Academia Sinica
LANDSAT Station
Beijing, China

DENMARK

National Technological Library
Centre for Documentation
Anker Engelundsvej 1
2800 Lyngby, Denmark
Tel 02-88 30 88

EUROPE

European Space Agency (ESA)
8-10 rue Mario Nikis
75738 Paris, Cedex 15, France

FRANCE

Centre National d'Études Spatiales (CNES)
18 Avenue Édouard Belin
31055 Toulouse Cedex, France
Tel 61-53 11 12

GERMANY

DFVLR Hauptabteillung Raumflugtrieb
8031 Oberpfaffenhofen
Post Wessling, West Germany
Tel 08-153 281

INDIA

Indian Space Research Organization
Bangalore, India

National Remote Sensing Agency (NRSA)
Balanagar
Hyderabad, India

INDONESIA

Bakosurtanae
Jln Raya
Jakarta Bogor 46, Indonesia

IRELAND

National Board for Science and Technology
Shelbourne House
Shelbourne Road
Dublin 4, Ireland
Tel Dublin 01-601 797

ITALY

Telespazio
Via Alberto Bergamini, 50
00159 Roma, Italy
Tel 06 49871

JAPAN

Japan Meteorological Agency (JMA)
1-3-4, Ote-machi
Chiyoda-ku
Tokyo, Japan

National Space Development Agency (NASDA)
World Trade Center Building
2-4-1, Hamamatsu-chu
Minato-ku
Tokyo, Japan

Remote Sensing Technology Center of Japan
7-15-7 Uni-Roppongi Building
Miriato-ku
Tokyo 106, Japan

NETHERLANDS

National Aerospace Laboratory
NLR
Anthony Fokkerweg 2
Amsterdam 1071, Netherlands
Tel 020-511 31 13

SOUTH AFRICA	National Institute for Telecommunications Research Satellite Remote Sensing Centre P.O. Box 3718 Johannesburg 2000, South Africa
SPAIN	CONIE Pintor Rosales 34 Madrid 8, Spain Tel 01-247 98 00
SWEDEN	Satimage P.O. Box 816 28 Kiruna Kir. S-981, Sweden Swedish Space Corporation Tritonvagen 27 S-17154 Solna, Sweden Tel 08 980200
SWITZERLAND	Bundesamt fur Landestopographie Sefigenstrasse 264 CH-3084 Wabern, Switzerland Tel 031-541331
THAILAND	Remote Sensing Division National Research Council Bangkok 9, Thailand
UNITED KINGDOM	National Remote Sensing Centre Space Department Royal Aircraft Establishment Farnborough Hants, England GU14 6TD Tel 25224461
UNITED STATES	Office of Space Science and Applications National Aeronautics and Space Administration Washington, District of Columbia 20546 U.S.A. Satellite Data Services Branch National Climate Center Environmental Data Service National Oceanic and Atmospheric Administration World Weather Building Washington, District of Columbia 20233 U.S.A.
U.S.S.R.	The Hydrometeorological Service of the U.S.S.R. 123376, Moscow, U1 Pavlika Morozova, d.12 U.S.S.R.

APPENDIX C

SELECTED LIST OF NATIONAL AND INTERNATIONAL INSTITUTIONS WHICH PROVIDE TRAINING IN REMOTE SENSING TECHNOLOGY

A comprehensive listing of training institutes and programs in remote sensing is currently unavailable. The following is a selection of the numerous and growing list of educational and research establishments which offer training in remote sensing at all levels. Much of the information contained in this Appendix was obtained from: "The remote sensing sourcebook: a guide to remote sensing products, services, facilities, publications and other materials" by D.J. Carter (1986).

AUSTRALIA	CSIRO Division of Land Resources Management Deniliquin, New South Wales, Australia
BRAZIL	Instituto de Pesquisas Espaciais C.P. 515 Sao Jose dos Campos, Brazil
CANADA	Canadian Remote Sensing Training Institute c/o Canada Centre for Remote Sensing 2464 Sheffield Road Ottawa, Canada K1A 0Y7
COLUMBIA	Centro Interamericano de Fotointerpretacion Bogotà, Columbia
COSTA RICA	Institut Interamericano de Ciencias Agricolas Turrialla San Jose, Costa Rica
ETHIOPIA	African Remote Sensing Council Addis Ababa, Ethiopia
EUROPE	NATO Advanced Studies Institute NATO Scientific Affairs Division B-1110 Bruxelles, Belgium Joint Research Centre (JRC) of the Commission of the European Community 21020 Ispra (Varese), Italy
FRANCE	Centre National d'Études Spatiales (CNES) 18 Avenue Édouard Belin 31055 Toulouse Cedex, France
GERMANY	Fachhochschule for Technik Stuttgart, West Germany

INDIA

Indian Institute of Remote Sensing
(National Remote Sensing Agency)
Department of Space
Government of India
4, Kalidas Road, PB 135
Dehra Dun 248001, India

ITALY

United Nations
Food and Agriculture Organization
Remote Sensing Centre
Via delle Terme di Caracalla
00100 Roma, Italy

JAPAN

Remote Sensing Technology Centre of Japan
7-15-17 Roppongi
Minato-ku
Tokyo 106, Japan

KENYA

Regional Remote Sensing Facility
P.O. Box 18332
Nairobi, Kenya

NEW ZEALAND

New Zealand Ministry of Works and Development
Aokautere Science Center
Palmerston North, New Zealand

NETHERLANDS

International Institute for Aerospace Survey and Earth Sciences (ITC)
Student Affairs Office
P.O. Box 6
7500 AA Enschede, Netherlands

NIGERIA

Regional Centre for Training in Aerial Surveys
Ile-Ife, Nigeria

SWITZERLAND

University of Zurich
Department of Geography
P.O. Box CH-8033
Zurich, Switzerland

THAILAND

Asian Institute of Technology
P.O. Box 2754
Bangkok, Thailand

UNITED KINGDOM

Students interested in training in the U.K. should consult the "Report on Full-time Training Facilities in the United Kingdom in Land Survey, Photogrammetry, Remote Sensing, Cartography and Map Reproduction (including printing), Cadastre, Land Resource and Management Studies, and Hydrographic Surveying, which are available to overseas students", Directorate of Overseas Surveys (Revised edition, June 1983). Copies are available from British Council Offices in most countries.

University of Aston
Remote Sensing Unit
Department of Civil Engineering
Gosta Green
Birmingham, England B4 7ET

University of London
University College
Department of Geography
26 Bedford Way
London, England WC1H 0AP

University of Nottingham
Department of Geography
(Remote Sensing Unit)
Nottingham, England NG7 2RD

Silsoe College
Cranfield Institute of Technology
Silsoe, Bedford, England MK45 4DT

Land Resources Development Centre
Overseas Development Administration
Tolworth Tower
Surbiton, Surrey, England KT6 7DY

University of Dundee
Carnegie Laboratory of Physics
Dundee, Scotland DD1 4HN

University of Glasgow
Department of Geography
Glasgow, Scotland G12 8QQ

UNITED STATES

Students interested in advanced training in the U.S.A. should consult the paper by L.D. Nealy in Photogrammetric Engineering and Remote Sensing, 1977, 43(3): 259-84. More up-to-date listings are available from the American Society of Photogrammetry and the Association of American Geographers. Forthcoming training courses in the U.S.A. are listed in the LANDSAT data users notes which can be obtained from:
LANDSAT Customer Services, Mundt Federal Building, Sioux Falls, South Dakota 57198, U.S.A.

Northern Arizona University
Flagstaff, Arizona, U.S.A.

University of California
Department of Earth and Space Sciences
Los Angeles, California 90024, U.S.A.

Yale University
School of Forestry and Environmental Studies
New Haven, Connecticut 06511, U.S.A.

George Washington University
School of Engineering and Applied Science
Washington, District of Columbia 20052
U.S.A.

Laboratory for Applications of Remote Sensing
(LARS)
Purdue University
1220 Potter Drive
W. Lafayette, Indiana 47906, U.S.A.

University of Massachusetts
Remote Sensing Centre
Amherst, Massachusetts 01003, U.S.A.

University of Michigan
Remote Sensing Laboratory
School of Natural Resources
Ann Arbor, Michigan 48109, U.S.A.

Michigan State University
Remote Sensing Project
East Lansing, Michigan 48824, U.S.A.

Remote Sensing Unit
Division of Natural Resources and Energy
(DNRE)
New York, New York, U.S.A.

University of North Dakota
Institute for Remote Sensing
Grand Forks, North Dakota 58202, U.S.A.

Oregon State University
Environmental Remote Sensing
Application Laboratory
Cornvallis, Oregon 97331, U.S.A.

Remote Sensing Institute
South Dakota State University
P.O. Box 507
Brookings, South Dakota 57007, U.S.A.

U.S. Geological Survey
EROS Data Center
Sioux Falls, South Dakota 57198, U.S.A.

Office of International Geology
U.S. Geological Survey, 1917
National Center
Reston, Virginia 22092, U.S.A.

U.S.S.R.

INTERCOSMOS
Council on International Cooperation in the
Study and Utilization of Outer Space
117901 North Moscow
V-71 Leninsky Prospect 14
Moscow, U.S.S.R.

APPENDIX D

CONVERSION TABLES

1 picometre = 1 pm = 10^{-12}m 1 Angstrom = 1 Å = 10^{-10}m 1 nanometre = 1 nm = 10^{-9}m 1 micrometre = 1 μm = 10^{-6}m 1 millimetre = 1 mm = 10^{-3}m 1 centimetre = 1 cm = 10^{-2}m 1 decimetre = 1 dm = 10^{-1}m	WAVELENGTH
1 kilohertz = 1 kHz = 10^{3}Hz 1 megahertz = 1 MHz = 10^{6}Hz 1 gigahertz = 1 GHz = 10^{9}Hz 1 terahertz = 1 THz = 10^{12}Hz	FREQUENCY
1 degree = 1^{o} 1 degree = 60 minutes = 60' 1 minute = 60 seconds = 60" 1 degree = 1.745×10^{-2} rad (radians) 1 circle = 360^{o} = 6.283 rad 1 radian = 57.29^{o}	ANGLE OF VIEW

M-40
ISBN 92-5-102694-7